

Effect of Peroxisome Proliferation on Replication of Emerging RNA Viruses

by

Cheung Pang Wong

A thesis submitted in partial fulfillment of the requirements for the degree of

Doctor of Philosophy

in

Virology

Department of Medical Microbiology and Immunology

University of Alberta

© Cheung Pang Wong, 2022

Abstract

Zika virus (ZIKV) and severe acute respiratory syndrome coronavirus 2 (SARS-CoV-2) are important emerging human pathogens that have disrupted global health. More therapeutic and prophylactic treatments for the diseases caused by the emerging viruses are needed. Expansion of our knowledge on the interplay between host cellular pathways and the viruses during infection will provide insights on how these viruses cause diseases and potentially on the development of antivirals. In this thesis, I used two different approaches to induce peroxisome proliferation in cells and investigated the antiviral effects of peroxisome proliferation on the replication of emerging viruses, including ZIKV and SARS-CoV-2.

A major finding was that both over-expression of PEX11B in cells and inhibition of Wnt/ β -catenin signaling pathway suppress the replication of ZIKV and SARS-CoV-2. This is in large part due to the enhanced induction of interferon (IFN) expression resulting from the expansion of the abundance of peroxisomes. Specifically, pre-infection treatment with the ten Wnt/ β -catenin inhibitors reported in the thesis were shown to greatly reduce SARS-CoV-2 replication. Three of these inhibitors also blocked viral replication when added post infection. Together, this thesis work describes novel roles of Wnt/ β -catenin signaling pathway inhibitors in peroxisome biogenesis and provide new avenues for therapeutic and even non-vaccine prophylactic development.

Preface

Many findings in this thesis are the results of collaborative work.

A version of Chapter 3 was published as Wong CP, Xu Z, Hou S, Limonta D, Kumar A, Power C, Hobman TC. “Interplay between Zika Virus and Peroxisomes during Infection”. *Cells*. 2019 Jul 15;8(7):725. I was responsible for hypotheses development, experimental design and performance, data collection and analyses, as well as manuscript editing. Z. Xu performed the co-immunoprecipitation assays. S. Hou offered intellectual input. C. Power provided primary human fetal astrocytes. D. Limonta prepared and helped with primary cell cultures. T Hobman was the supervisory author and contributed to concept formation and manuscript composition.

In chapter 4, SARS-CoV-2 infections and the subsequent plaque assay analyses were conducted in a biosafety level 3 facility by Dr. Z. Xu.

Dedication

To my family

Acknowledgements

To my supervisor Dr. Tom Hobman, thank you for the opportunity to work and learn in the lab. I am grateful for his insights and guidance on my research, as well as the support for my performance on my doctoral studies. I may not be one of the brightest students in his lab, but his trust has been the cornerstone of my Ph.D. studies.

To my committee members, Dr. Maya Shmulevitz and Dr. Paul LaPointe, thank you for the valuable feedback and continued support. Thank you to Dr. Kevin Coombs and Dr. Chris Power for serving as my PhD defense examiners. Special thanks to Dr. Zaikun Xu for invaluable contributions to Chapter 4. It was a pleasure learning from him while working alongside him throughout my Ph.D. studies. I wish his family the best of luck in the future. Thank you to past and present members of the Hobman lab with special mention to Valeria Mancinelli for experimental support, Eileen Reklow for technical support. Thank you to the Department of MMI and the MMI students for being such a wonderful group. Lastly, thank you to Greg Plummer for helping me with the confocal microscopy and your input into the analyses. I would not have been able to generate beautiful confocal images without your help and support.

To my family, thank you for your unconditional support for my decision to come to Canada for my doctoral studies. I am sure the words in this section of the thesis are not enough to describe how important your support has been to my journey in Canada, but I hope that the results presented in this thesis will make you proud.

Table of Contents

Chapter 1	1
1.1. Overview	2
1.2. Zika virus (ZIKV)	3
1.2.1. Epidemiology and clinical importance of ZIKV	3
1.2.2. Genome and proteins of ZIKV	5
1.2.3. Replication cycle of ZIKV	7
1.2.4. Pathogenesis of severe ZIKV disease.....	10
1.2.5. Development of ZIKV vaccines	11
1.3. Severe acute respiratory syndrome coronavirus 2 (SARS-CoV-2).....	11
1.3.1. Epidemiology and clinical importance of SARS-CoV-2	12
1.3.2. Genome and proteins of SARS-CoV-2	13
1.3.3. Replication cycle of SARS-CoV-2.....	16
1.3.4. Pathogenesis of COVID-19	19
1.3.5. Development of COVID-19 vaccines and antivirals	20
1.4 Interferon system.....	21
1.4.1 Types of Interferons.....	21
1.4.2 Interferon response pathways	22
1.4.3 Suppression of IFN system by ZIKV and SARS-CoV-2	28
1.4.4 IFNs restrict ZIKV and SARS-CoV-2 replication and pathogenesis	30
1.4.4.1 IFNs restrict ZIKV replication and pathogenesis	30
1.4.4.2 IFNs restrict SARS-CoV-2 replication and pathogenesis.....	32
1.4.5 The therapeutic use of IFN β for COVID-19	33
1.4.6 The therapeutic use of IFN λ for COVID-19	34

1.5. Peroxisomes	35
1.5.1. Peroxisome biogenesis	36
1.5.1.1. Matrix protein import.....	36
1.5.1.2. Membrane protein import	37
1.5.1.3. Peroxisome biogenesis by growth and fission	38
1.5.1.4. <i>De Novo</i> synthesis of peroxisomes	39
1.5.1.5. Peroxisome-ER tethering.....	40
1.5.1.6. Pexophagy.....	40
1.5.2. Peroxisomes as antiviral signaling hubs.....	42
1.5.3. The interplay between peroxisomes and viruses during infection	42
1.6 Interplay between IFN system and Wnt/ β -catenin signaling pathway	44
1.7 Objectives of thesis	46
Chapter 2.....	47
2.1 Materials.....	48
2.1.1 Reagents.....	48
2.1.2 Commonly used Buffers and Solutions	53
2.1.3 Oligonucleotides.....	54
2.1.4 Antibodies.....	56
2.1.5 Cell lines and viruses.....	58
2.1.5.1 Cell lines	58
2.1.5.2 Viruses	58
2.2 Methods.....	59
2.2.1 Molecular Biology.....	59
2.2.1.1 Isolation of plasmid DNA from <i>Escherichia coli</i> (E.coli)	59
2.2.1.2 Polymerase chain reaction (PCR).....	60

2.2.1.3 Restriction endonuclease digestion.....	60
2.2.1.4 Agarose gel electrophoresis	60
2.2.1.5 Purification of DNA fragments.....	60
2.2.1.6 Ligation of DNA	61
2.2.1.7 Transformation of E. coli.....	61
2.2.2 Construction of AcGFP plus myc-tagged PEX11B expression	61
2.2.3 Cell culture and transfection.....	62
2.2.3.1 Cell culture maintenance.....	62
2.2.3.2 Transient transfection of cell lines	63
2.2.3.3 RNA interference	63
2.2.4 Virology techniques.....	64
2.2.4.1 Virus infection	64
2.2.4.2 DENV-2, ZIKV and MAYV plaque assays.....	64
2.2.4.3 Production and use of recombinant lentiviruses	65
2.2.5 Microscopy	65
2.2.5.1 Indirect Immunofluorescence	65
2.2.5.2 Quantification of peroxisomes and cell volume	66
2.2.6 Protein gel electrophoresis and detection	67
2.2.6.1 Preparation of protein samples.....	67
2.2.6.2 Sodium dodecyl-sulphate polyacrylamide gel electrophoresis (SDS-PAGE)	67
2.2.6.3 Western Blot analysis	68
2.2.6.4 Detection of fluorophore-conjugated secondary antibodies	68
2.2.7 Biochemical analysis of protein-protein interactions	69
2.2.7.1 Co-immunoprecipitation	69
2.2.8 RNA techniques.....	70

2.2.8.1 RNA isolation	70
2.2.8.2 cDNA synthesis	70
2.2.8.3 Quantitative reverse-transcriptase PCR (qRT-PCR)	70
2.2.9 EC50 and CC50 determination.....	71
Chapter 3.....	73
3.1 Rationale.....	74
3.2 Results.....	76
3.2.1 ZIKV infection reduces number of peroxisomes in primary human fetal astrocytes (HFAs) and U251 cells.....	76
3.2.2 ZIKV capsid protein forms a stable complex with PEX19 and causes loss of peroxisomes.....	83
3.2.3 Over-expression of PEX11B suppresses ZIKV replication	86
3.2.4 Over-expression of PEX11B up-regulates the innate immune response.....	89
3.2.5 Summary.....	94
Chapter 4.....	95
4.1 Rationale.....	96
4.2. Results	100
4.2.1. Wnt/ β -catenin signaling inhibitors reduce SARS-CoV-2 titer and replication	100
4.2.2. Wnt/ β -catenin inhibitors increase peroxisome density and potentiate the interferon response	116
4.2.3. Reducing β -catenin levels induces peroxisome proliferation and reduces SARS-CoV-2 infection	130
4.2.4. Wnt/ β -catenin inhibitors have broad-spectrum antiviral activity	136
4.2.6. Summary.....	139
Chapter 5.....	141
5.1 Synopsis	142

5.2 Peroxisomes are antiviral organelles.....	142
5.3 Elimination of peroxisomes by ZIKV capsid protein	145
5.4 Potentials use of Wnt/ β -catenin inhibitors in treating COVID-19	148
5.5 Induction of peroxisome proliferation by inhibiting Wnt/ β -catenin signaling pathway ...	150
5.6 IFN-independent antiviral effects of Wnt/ β -catenin signaling pathway inhibitors.....	152
5.7 Peroxisome-independent antiviral effects of Wnt/ β -catenin signaling pathway inhibitors	153
5.8 Concluding remarks	154
Appendices.....	155
References.....	161

List of Tables

Table 2.1 Commercial sources of materials, chemicals, and reagents.....	48
Table 2.2 Molecular size standards.....	51
Table 2.3 DNA/RNA modifying enzymes.....	51
Table 2.4 Multi-component systems.....	52
Table 2.5 Detection systems	52
Table 2.6 Buffers and Solutions.....	53
Table 2.7 Oligonucleotides	54
Table 2.8 siRNA sequences	55
Table 2.9 Plasmid vectors	56
Table 2.10 Primary antibodies	56
Table 2.11 Secondary antibodies	57
Table 4.1 A summary of the action of the 10 Wnt/ β -catenin inhibitors reported in the study	99

List of Figures

Figure 1.1. Schematic representation of ZIKV genome organization	6
Figure 1.2. The replication cycle of ZIKV	8
Figure 1.3. Schematic representation of SARS-CoV-2 genome organization.....	15
Figure 1.4. The replication cycle of SARS-CoV-2.....	17
Figure 1.5. IFN response pathway	23
Figure 3.2. ZIKV infection reduces number of peroxisomes in U251 cells	82
Figure 3.3. Expression of ZIKV capsid protein causes loss of peroxisomes.....	85
Figure 3.4. Over-expression of PEX11B suppresses ZIKV replication	88
Figure 3.5. Over-expression of PEX11B up-regulates the innate immune response.....	93
Figure 4.1. Wnt inhibitors significantly reduce SARS-CoV-2 infection in Calu3 cells.....	103
Figure 4.2. The Wnt/ β -catenin inhibitors IWP-O1, KYA1797K and Pyrvinium reduce SARS-CoV-2 replication when added 6-hours post-infection.....	107
Figure 4.3. The Wnt/ β -catenin inhibitors IWP-O1, KYA1797K and Pyrvinium reduce SARS-CoV-2 replication when added 12-hours post-infection.....	109
Figure 4.4. Wnt inhibitors significantly reduce SARS-CoV-2 virus titer in normal human bronchial epithelial (NHBE) lung cells.....	110
Figure 4.5. Effect of Wnt/ β -catenin inhibitors on cell viability.....	112
Figure 4.6. Wnt inhibitors inhibit replication of SARS-CoV-2 variants of concern	115
Figure 4.7. Inhibitors of the Wnt/ β -catenin pathway increase peroxisome density in human cells	119
Figure 4.8. Wnt/ β -catenin pathway inhibitors enhance production of type I and III interferons in response to viral infection.....	122

Figure 4.9. Wnt/ β -catenin pathway inhibitors do not induce expression of interferon in the absence of viral infection123

Figure 4.10. Wnt inhibitors do not increase MAVS protein levels124

Figure 4.11. Wnt inhibitors increase the colocalization between MAVS and peroxisomes.....127

Figure 4.12. Inhibition of the Wnt/ β -catenin pathway increases peroxisome density in Vero cells129

Figure 4.13. Wnt/ β -catenin inhibitors do not reduce SARS-CoV-2 replication in Vero cells ...132

Figure 4.14. Reducing β -catenin expression increases peroxisome density and inhibits replication of SARS-CoV-2.....135

Figure 4.15. Wnt/ β -catenin inhibitors reduce replication of other RNA viruses.....138

List of Nomenclature and Abbreviations

°C	degrees Celsius
ACE2	angiotensin-converting enzyme 2
AcGFP	<i>Aquorea corelescens</i> Green Fluorescent Protein
ADP	adenosine diphosphate
APS	ammonium persulfate
ATF	activating transcription factor
ATP	adenosine triphosphate
ATPase	adenosine triphosphatase
BSA	bovine serum albumin
C	capsid
CARD	caspase activation and recruitment domain
cDNA	complementary deoxyribonucleic acid
cGAS	cyclic GMP-AMP synthase
CT	threshold cycle
DAPI	4',6-diamidino-2-phenylindole
DENV	Dengue virus
DMEM	Dulbecco's modified Eagle's medium
DMSO	dimethyl sulphoxide
DNA	deoxyribonucleic acid
DNase	deoxyribonuclease
dNTP	deoxyribonucleotide triphosphate
DRP	dynamamin-related protein
dsRNA	double-stranded ribonucleic acid
E	Envelope
EDTA	ethylenediaminetetraacetic acid

eGFP	enhanced green fluorescent protein
ER	endoplasmic reticulum
ERGIC	endoplasmic reticulum–Golgi intermediate compartment
FBS	fetal bovine serum
Fis1	Fission 1 protein 1
<i>g</i>	gravitational force
GAS	IFN-gamma-activated sequence
GBS	Guillain-Barré syndrome
GTPases	guanosine triphosphate hydrolase
h.p.i	hour-post infection
HCMV	human cytomegalovirus
HCV	hepatitis C virus
HEK293T	human embryonic kidney 293T cells
HEPES	4-(2-hydroxyethyl)-1-piperazineethanesulphonic acid
HFA	human fetal astrocyte
HIV-1	human immunodeficiency virus-1
hr	hour
IF	Immunofluorescence
IFIT	IFN-induced protein with tetratricopeptide repeats
IFITM	IFN-inducible transmembrane
IFN	Interferon
IFNAR	IFN-alpha receptor
IFNLR	IFN-lambda receptor
IgG	immunoglobulin G
IP	immunoprecipitation
IRF	interferon regulatory factor

ISGs	interferon-stimulated genes
ISRE	IFN-stimulated response element
JAK	Janus kinase
JEV	Japanese encephalitis virus
kb	kilo ($\times 10^3$) base-pairs
kDa	kilo Daltons
L	liter
m	milli ($\times 10^{-3}$)
M	moles per liter
M	membrane
MAM	mitochondrion-associated-endoplasmic reticulum membranes
MAYV	Mayaro virus
MAVS	mitochondrial antiviral signalling
MDA5	differentiation-antigen 5
MEM	minimal essential media
MERS	Middle East respiratory syndrome coronavirus
Mff	mitochondria fission factor
min	minute
MOI	multiplicity of infection
mRNA	messenger RNA
mPTS	membrane PTSs
MYD88	myeloid differentiation factor 88
n	nano (10^{-9})
N	nucleocapsid
NF κ B	nuclear factor-B
NP40	nonidet-P40

NS	non-structural
nt	nucleotide
NTPase	nucleoside triphosphatase
ORF	open reading frame
PAMP	pathogen-associated molecular pattern
PBS	phosphate buffered saline
PBS-T	phosphate buffered saline, tween 20
PCR	polymerase chain reaction
PEX	peroxin
pH	power hydrogenii
PMP	peroxisome membrane protein
PTS	peroxisomal targeting signal
poly(I:C)	polyinosinic-polycytidylic acid
PPAR α	peroxisome proliferative activated-receptor α
PPAR γ	peroxisome proliferative activated-receptor γ
prM	precursor membrane
PRR	pattern recognition receptor
PVDF	polyvinylidene difluoride
RdRP	RNA-dependent RNA polymerase
RIG-I	retinoic acid inducible gene-1
RLR	RIG-I-like receptor
S	spike
SARS-CoV	Severe acute respiratory syndrome coronavirus
SARS-CoV-2	Severe acute respiratory syndrome coronavirus 2
SDS	sodium dodecyl-sulphate
SDS-PAGE	SDS-polyacrylamide gel electrophoresis

sec	second
siRNA	short interfering RNA
ssRNA	single-stranded RNA
STAT	signal transducers and activators of transcription
STING	stimulator of interferon genes
sg	sub-genomic
TAK1	transforming growth factor- β -activated kinase 1
TAM	TYRO3, AXL and MER
TBK1	TANK-binding kinase 1
TBS	Tris-buffered saline
TEMED	N,N,N',N'-tetramethylenediamine
TIM	T-cell Immunoglobulin and Mucin domain
TLR	Toll-like receptor
TM	transmembrane
TMPRSS2	transmembrane serine protease 2
TRIF	TIR-domain-containing adaptor inducing interferon
TYK	tyrosine kinase
U	enzymatic units
UTR	Untranslated Region
V	volt
WB	Western blot
WHO	World Health Organization
WNV	West Nile virus
ZIKV	Zika virus
μ	micro ($\times 10^{-6}$)

Chapter 1

Introduction

1.1. Overview

An emerging disease is a disease that appears in a population for the first time, or one that existed previously but is now rapidly increasing in incidence or geographical range. Over the years, multiple novel pathogenic viruses continue to emerge in human and animal populations. Given their high adaptability to current and new hosts and rapidly evolving strategies to escape antiviral measures, emerging and re-emerging viruses will continue to pose a threat to public health.

Recent examples of emerging diseases include Zika virus (ZIKV) disease which rapidly spread to more than 50 countries between 2014 and 2017 and COVID-19, caused by a novel coronavirus, severe acute respiratory syndrome coronavirus 2 (SARS-CoV-2), which became a pandemic in 2020. Since then, COVID-19 has afflicted more than 500 million people resulting in more than 6 million deaths. The rapid spread of COVID-19 caused unprecedented social, economic, and healthcare disruption. Clearly, there is a pressing need to better understand re-emerging and emerging viruses so that we may develop effective therapeutics in a more timely manner.

1.2. Zika virus (ZIKV)

Flaviviruses are arboviruses belonging to the family *Flaviviridae*. The genus consists of mosquito-transmitted viruses, including Zika virus (ZIKV), Dengue virus (DENV), and Japanese encephalitis virus (JEV) and others which cause disease in humans through sporadic and epidemic transmission. The following sections discuss the epidemiology and clinical importance of ZIKV (section 1.2.1), ZIKV biology (section 1.2.2-1.2.3), pathogenesis of ZIKV disease (section 1.2.4) as well as the development of ZIKV vaccines (section 1.2.5).

1.2.1. Epidemiology and clinical importance of ZIKV

ZIKV was discovered in 1947 by scientists conducting routine surveillance for yellow fever in the Zika forest located in Uganda (Dick et al., 1952). They isolated ZIKV from samples obtained from a captive sentinel rhesus monkey in the canopy of the forest and then again the following year from a *Aedes africanus* mosquito caught on a tree platform in the Zika forest. In less than a decade, the first human infections were reported in Uganda and the United Republic of Tanzania in 1952 (Macnamara, 1954). The virus was also detected in mosquitos in countries in Asia including India, Indonesia, Malaysia and Pakistan. No significant outbreaks had been described until 2007 during which 49 human cases were reported on the Pacific Island of Yap (Duffy et al., 2009). Between 2013 and 2014 the virus caused much larger outbreaks in other Pacific Islands including French Polynesia (Cao-Lormeau et al., 2014). Shortly afterward, ZIKV was detected in Brazil after which it spread rapidly to other countries in South and Central America (Fauci and Morens, 2016). In early 2016, the World Health Organization declared the ZIKV epidemic as a public health emergency of international concern. This was due to the large

number of human infections and the prevalence of congenital brain abnormalities, such as microcephaly, in fetuses borne to women who contracted the virus during pregnancy (Parra et al., 2016; Roos, 2016; Rubin et al., 2016). By 2017, there were more than 800,000 cases reported in more than 50 countries (PAHO, 2018). ZIKV strains can be divided into the African and Asian lineages (Haddock et al., 2012). The contemporary strains circulating in the Americas appear to have evolved from the Asian lineage (Faria et al., 2016).

Modes of ZIKV transmission can be vector-borne and non-vector-borne. *Aedes aegypti*, *Aedes polynesiensis* and *Aedes albopictus* mosquitoes are the major vectors responsible for ZIKV transmission to humans. These mosquitoes are usually found in tropical and subtropical regions, and as such, the spread of the virus is closely related to the prevalence of the vectors (Sikka et al., 2016). In humans, transmission of ZIKV can also occur through sexual contact. A male American scientist who was bitten often by wild *Aedes* spp. mosquitoes during his work in Senegal in 2008 contracted ZIKV (Foy et al., 2011). His wife who did not travel to Africa, developed similar clinical symptoms days after having vaginal sexual intercourse and also tested positive for ZIKV. The possibility of ZIKV sexual transmission was further supported by a report showing isolation of ZIKV RNA from the semen of a patient during the ZIKV outbreak in French Polynesia in 2013 (Musso et al., 2015). Later, ZIKV was found to be able to cross the placenta barrier resulting in maternal to fetal transmission and teratogenesis (Brasil et al., 2016; Calvet et al., 2016).

The incubation period of ZIKV disease is 2 -7 days but only 20% of infected patients are symptomatic, exhibiting mild influenza-like illness including fever, headache, dizziness and stomach ache (Saxena et al., 2016). ZIKV infection is rarely fatal in adults but development of Guillain–Barré syndrome, which is an acute inflammatory immune-mediated polyneuropathy, has been linked to this virus (Cao-Lormeau et al., 2016).

1.2.2. Genome and proteins of ZIKV

ZIKV is an enveloped virus which possesses a non-segmented positive-sense single-stranded RNA genome of ~11kb. The genome encodes a single open reading frame (ORF) flanked by two structured untranslated regions (UTRs) (reviewed in (Hasan et al., 2018)). The long ORF encodes a single polyprotein: 5'-C-prM-E-NS1-NS2A-NS2B-NS3-NS4A-NS4B-NS5-3' which is threaded back and forth through the ER membrane, exposing different viral proteins to either the cytoplasm or ER lumen. The polyprotein is processed by host cell and viral proteases into three structural proteins (capsid (C), precursor of membrane (prM) and envelope (E)) and seven non-structural (NS) proteins (NS1, NS2A, NS2B, NS3, NS4A, NS4B and NS5). The three structural proteins are responsible for the assembly of ZIKV virions, whereas the non-structural proteins function in replication of viral RNA, viral polyprotein processing and modulation of the host response (Figure 1.1)

ZIKV capsid protein (122 amino acid (aa) residues) is the first viral protein translated in the viral polypeptide chain. It shares a similar tertiary structure with West Nile virus (WNV) and Dengue virus (DENV) capsid proteins and forms a homodimer that has two distinct surfaces (Tan et al., 2020). The hydrophobic side of the homodimer interacts with the viral envelope, whereas the positively charged side binds the viral RNA to form the nucleocapsid core (Shang et al., 2018). Formation of infectious mature flavivirus virions is promoted by the cleavage of the pr peptide (~75 aa) from M protein by the host serine protease furin (Stadler et al., 1997). On the virion surface, the E protein contains cellular receptor binding sites and a fusion peptide for mediating membrane fusion during viral entry. NS3 is the second largest viral protein and contains protease and helicase activities. The protease activity of NS3 requires interaction with NS2B to mediate the cleavage of the capsid protein (Amberg and Rice, 1999).

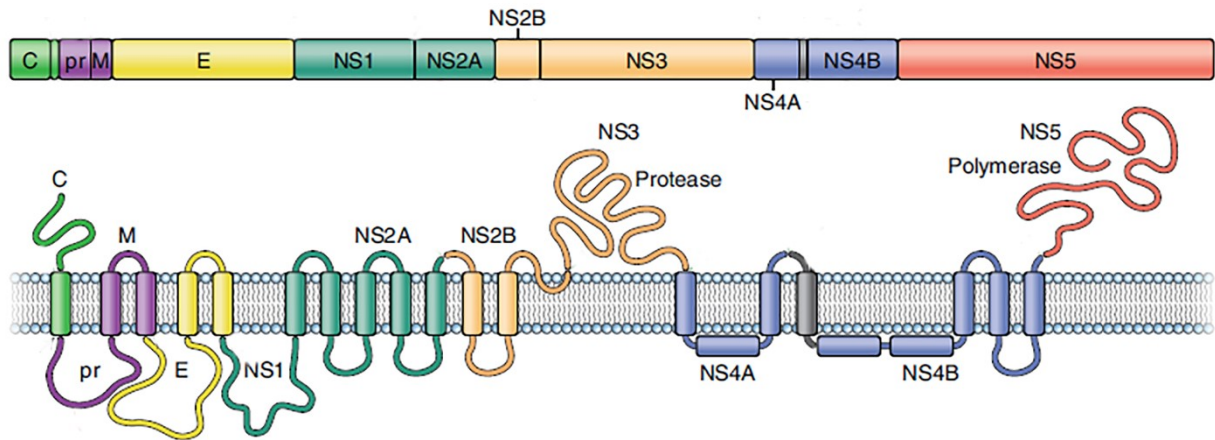


Figure 1.1. Schematic representation of ZIKV genome organization. The ZIKV genome, which is ~11 kb in length, contains one open reading frame encoding three structural proteins (capsid (C), precursor membrane (prM) and envelope (E)) and 7 non-structural proteins (NS1, NS2A, NS2B, NS3, NS4A, NS4B and NS5). The predicted topologies of viral proteins with respect to the ER membrane are presented. (Modified from (Pierson and Diamond, 2020)).

The NS3 helicase possesses intrinsic nucleoside triphosphatase (NTPase) activity, which is modulated by the cofactor NS4A that increases the rate of NTP hydrolysis (Kumar et al., 2020). NS5 is the largest ZIKV protein (~900 aa) and is critical for RNA synthesis, and therefore viral replication. The C-terminal 620 aa of NS5 form the RNA-dependent RNA polymerase (RdRp) (Upadhyay et al., 2017). Viral RNA replication also requires helicase activity though. ZIKV NS5 interacts with NS3 to stimulate the helicase activity of NS3, a process that is for RNA unwinding during RNA replication (Xu et al., 2019).

1.2.3. Replication cycle of ZIKV

The life cycle of ZIKV (Figure 1.2) involves multiple steps including viral attachment and entry, viral genome translation and replication, virion assembly and egress. The multi-step process requires the engagement of an array of host and viral proteins, and the steps usually happen concurrently, suggesting that it is a highly coordinated process.

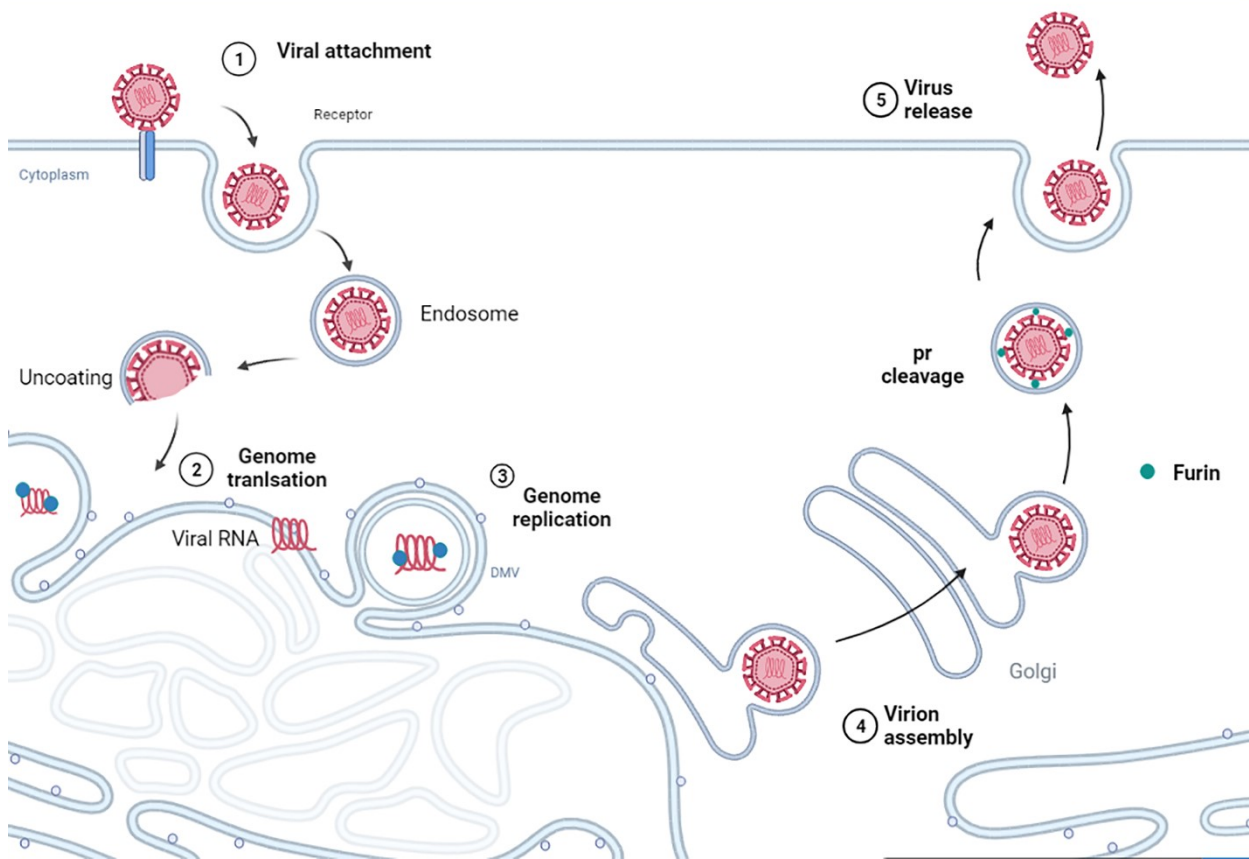


Figure 1.2. The replication cycle of ZIKV. Virions attach to a host cell receptor and subsequently enter the cell by receptor-mediated endocytosis (step 1). Acidification of the endosomes triggers the release of nucleocapsid into the cytoplasm. The viral RNA is translated into a single polyprotein on the rough endoplasmic reticulum (ER) (step 2). The viral proteins induce the formation of replication complexes at the ER membrane where genomic replication takes place (step 3). The virion is assembled on the surface of the ER and buds into the ER lumen (step 4). Immature viral particles are transported through the Golgi and the trans-Golgi network where the host protease furin cleaves the prM protein, promoting the maturation of virions which are released by exocytosis (step 5). Created in BioRender.com

ZIKV infects a wide range of cell types, a process that requires interaction of virion components with multiple host proteins on the plasma membrane. Examples include binding of charged surfaces on the E protein to glycosaminoglycans (Chen et al., 1997) and interactions between the viral lipid envelope and proteins of the T-cell immunoglobulin domain and mucin domain (TIM) and Tyro3, Axl and Mertk (TAM) family (Meertens et al., 2012). After attachment, ZIKV enters host cells through receptor-mediated clathrin-dependent endocytosis (Owczarek et al., 2019). Fusion of the viral envelope and endosome membranes is triggered by a low pH-induced conformational change in the E protein (Stiasny et al., 2011). The positive-sense RNA genome is then released into the cytoplasm where it serves as an mRNA for translation of the viral polyprotein (reviewed in (Mazeaud et al., 2018)).

Like other flaviviruses, ZIKV replication occurs in association with membrane structures formed by host and viral factors during infection. The ultrastructure of these replication complexes as revealed by cryo-EM tomography show invaginations of the ER and the presence of viral proteins NS1, NS2A, NS3, NS4A and NS5 (Aktepe and Mackenzie, 2018). This architecture facilitates the replication of viral RNA while allowing exchange of the contents of the complexes including viral RNA to take place between the invaginations and the sites of viral translation. The replication of viral RNA begins with the *de novo* synthesis of negative-sense RNA by the viral polymerase NS5 using the viral positive-sense RNA as a template. The negative-sense RNA then serves as a template for the synthesis of positive-sense genomic RNA which is used as mRNA for viral polyprotein synthesis or are packaged into immature virions (Lindenbach and Charles, 2007). Finally, flavivirus replication complexes are thought to shield the viral RNA from cytosolic innate immune sensors like RIG-I and MDA5 to prevent the activation of antiviral signaling pathways (Overby et al., 2010; Welsch et al., 2009)

E, prM, a host-derived lipid membrane and the nucleocapsid are the components of the immature ZIKV particles in the ER. The immature particles are transported from the ER through the *trans*-Golgi network to the cell surface, during which the E proteins undergo conformational changes and the prM protein is cleaved by furin (Stadler *et al.*, 1997), a process which results in the generation of the mature virion-associated M protein (Yu *et al.*, 2009) and shedding of the pr fragment during release. Mature virions are released from the cell by exocytosis.

1.2.4. Pathogenesis of severe ZIKV disease

The majority of ZIKV infections in humans are asymptomatic or involve a mild flu-like illness (Saxena *et al.*, 2016). In newborns who were infected *in utero*, ZIKV is associated with congenital diseases including microcephaly and intracranial calcifications. The condition may occur in combination with other abnormalities including intellectual and motor disabilities. Investigation of fetal ZIKV infection has focused on the placenta which is the barrier between the maternal decidua and the fetus during pregnancy (Calvet *et al.*, 2016; de Araújo *et al.*, 2016). The interface consists of cytotrophoblasts derived from the fetus and terminally differentiated syncytiotrophoblasts both of which are susceptible to ZIKV infection (Sheridan *et al.*, 2017). In addition, ZIKV was shown to infect primary human placental macrophages (Quicke *et al.*, 2016) and fetal endothelial cells (Richard *et al.*, 2017), suggesting the possibility of an intra-uterine transmission of ZIKV.

1.2.5. Development of ZIKV vaccines

Research and development of therapeutics against ZIKV commenced soon after the recent epidemics in the Americas. The main focus has been development of vaccines to protect against congenital disease. Multiple vaccines platforms have been under investigation in preclinical and clinical studies including DNA vaccines, mRNA vaccines, and inactivated vaccines. Examples of ZIKV prM-E DNA vaccines candidates include VRC5283 which was shown to elicit neutralizing antibodies in all subjects in a phase I study (Gaudinski et al., 2018). Phase II study was completed (NCT number: NCT03110770), but the data including ZIKV-specific neutralizing antibody activity is currently not available as the testing is anticipated to be completed in 2022. An mRNA vaccine candidate expressing prM-E induced potent neutralizing antibodies in mice and non-human primates, thereby protecting them against ZIKV challenge (Pardi et al., 2017). An inactivated ZIKV vaccine by formalin-inactivation of a Puerto Rican (PR) ZIKV isolate induced ZIKV-specific neutralizing antibodies and protected rhesus monkeys against the challenge of ZIKV PR strain (Abbink et al., 2016).

1.3. Severe acute respiratory syndrome coronavirus 2 (SARS-CoV-2)

Coronaviruses are RNA viruses belonging to the family *Coronaviridae* which is subdivided into four genera - Alphacoronavirus, Betacoronavirus, Gammacoronavirus and Deltacoronavirus. The emergence of two highly pathogenic betacoronaviruses; severe acute respiratory syndrome coronavirus (SARS-CoV) and Middle East respiratory syndrome coronavirus (MERS-CoV) in 2002 and 2012 respectively highlighted the potential of these viruses to cause large outbreaks of disease in humans. The following sections discuss the epidemiology

and clinical importance of SARS-CoV-2 (section 1.3.1), SARS-CoV-2 biology (section 1.3.2-1.3.3), pathogenesis of COVID-19 (section 1.3.4) as well as the development of COVID-19 vaccines and antivirals (section 1.3.5).

1.3.1. Epidemiology and clinical importance of SARS-CoV-2

In late December 2019, the capital city of Hubei province in central China, Wuhan, reported patients exhibiting symptoms of viral pneumonia similar to those of SARS and MERS, including fever, cough and chest discomfort (Gralinski and Menachery, 2020; Zhu et al., 2020). Many of the first 27 hospitalized patients were linked to a wet market in the city that sold seafood and live animals (Deng and Peng, 2020). In early January 2020, Chinese scientists identified the causative agent of the emerging disease as a new betacoronavirus which was closely related to SARS-CoV (Wu et al., 2020a; Zhu *et al.*, 2020). Later, patients who were not exposed to the wet market, also became infected with this new virus, indicating person-to-person transmission of this pathogen (Chan et al., 2020; Deng and Peng, 2020). The spread of the virus was fuelled by the social gathering during Chinese New Year, resulting in an exponential increase in the number of confirmed cases in just a month. In early February 2020, The International Committee on Taxonomy of Viruses named the novel coronavirus “SARS-CoV-2” (Viruses, 2020). The virus continued to spread rapidly across countries in the rest of the world, leading to a sharp jump of confirmed cases and number of deaths. The World Health Organization (WHO) officially declared the global COVID-19 outbreak as a pandemic in March 2020 (WHO, 2020). As of April 13, 2022, the virus has infected over 500 million people resulting in more than 6.1 million deaths.

Understanding how and when infected people transmit the virus in different settings is critical for developing prevention and control strategies to stop virus circulation. We now know that SARS-CoV-2 can be transmitted by close contact with infected persons through saliva and respiratory secretions or droplets (Chan *et al.*, 2020; Ghinai *et al.*, 2020; Hamner *et al.*, 2020), which are between 5 and 10µm in diameter (WHO, 2014). Most patients infected with SARS-CoV-2 develop signs of disease 3-6 days after exposure (Cevik *et al.*, 2020). Young adults and children often exhibit mild symptoms including fever, fatigue, and dry cough whereas people who are aged 65 or above are more likely to develop severe respiratory disease which may require hospitalization.

1.3.2. Genome and proteins of SARS-CoV-2

SARS-CoV-2 is an enveloped virus which possesses a positive-sense single-stranded RNA genome of ~30kb (Zhu *et al.*, 2020). The capped and polyadenylated genome contains 2 large ORFs, ORF1a and ORF1b, flanked by two structured UTRs. The translation of ORF1a produces polyprotein 1a, and polyprotein 1b is produced by continuous translation of ORF1a and ORF1b through a programmed -1 ribosomal frameshift upstream of the ORF1a termination codon (Perlman and Netland, 2009). The polyproteins are processed by viral proteases that are encoded by papain-like protease (PL^{pro}) in nsp3 and the main protease (M^{pro}) in nsp5, which yields the 16 non-structural protein (nsp) 1–16 that are involved in replication. Polyprotein 1a is cleaved into nsp1-11, and pp1ab is cleaved into nsp1-10 and nsp12-16 (Zhou *et al.*, 2020). In addition, the genome also encodes structural proteins (spike (S), envelope (E), membrane (M) and nucleocapsid (N)) and a set of accessory proteins (ORF3a, ORF3b, ORF6, ORF7a, ORF7b, ORF8 and ORF9b)

from the sub-genomic (sg) mRNA (Zhou *et al.*, 2020). Accessory proteins such as ORF6 and ORF7 are involved in the antagonism of the interferon system to establish infection (Figure 1.3).

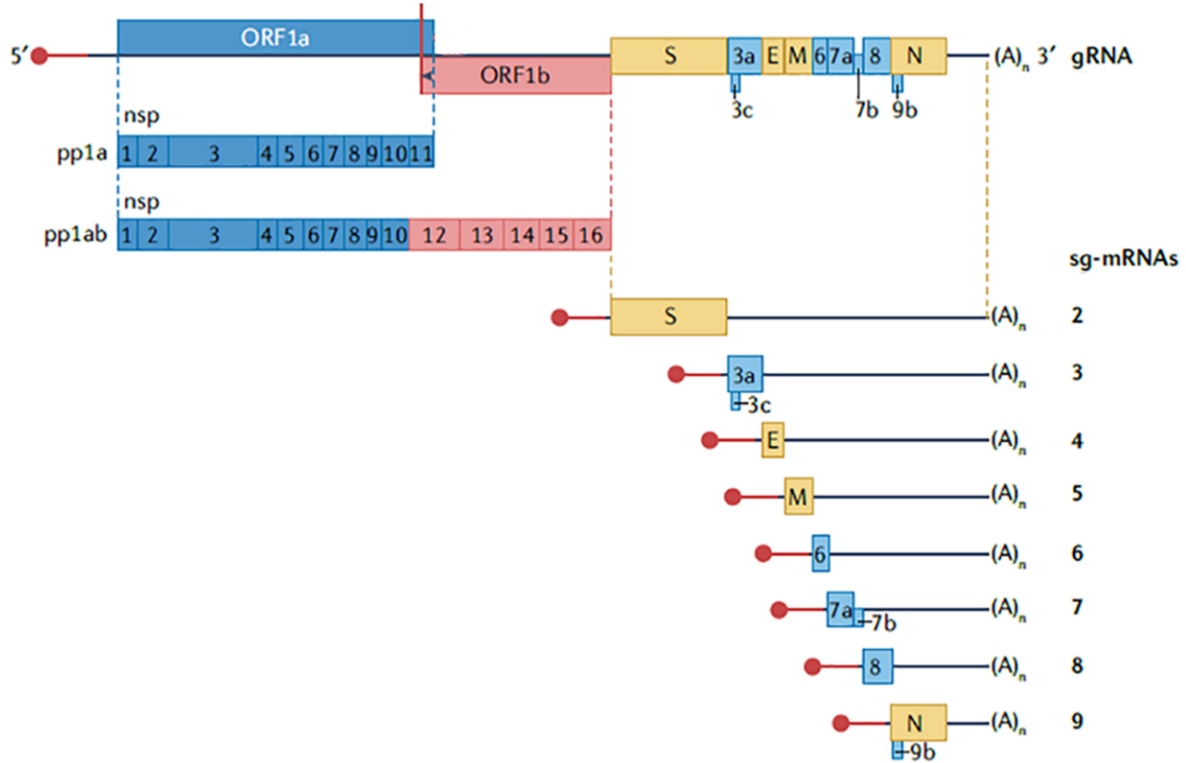


Figure 1.3. Schematic representation of SARS-CoV-2 genome organization. The SARS-CoV-2 genome, which is ~30 kb in length, contains multiple open reading frames (ORFs) encoding 16 non-structural proteins (nsp), 4 structural proteins and multiple accessory proteins. The 5' end of the genome encodes the polyproteins pp1a, which yields nsp1-nsp11; and pp1ab, which yields nsp1-nsp16. The 3's ends of the genome encode the structural proteins (S, E, M, and N) and the accessory proteins. Structural and accessory proteins are expressed from a set of sub-genomic (sg) mRNAs. Modified from (Malone et al., 2022).

The structural proteins are responsible for the assembly of SARS-CoV-2 virions. S protein mediates cell binding and entry by interacting with membrane-bound angiotensin-converting enzyme 2 (ACE2) receptors (Jackson et al., 2022). M protein is present as a dimer in the virion and interacts with S and N proteins. It adopts two conformations in the ER, long and compact (MLONG and MCOMPACT), which together induce membrane curvature as revealed by cryo-electron microscopy (Neuman et al., 2011). N protein possesses an RNA binding domain and based on analogy with other coronaviruses it is involved in RNA packaging and virion assembly (McBride et al., 2014). The non-structural proteins function in replication of viral RNA. Nsp1 protein mediates host cell translational shut-off by targeting ribosomes (Thoms et al., 2020). Triple transfection of transmembrane proteins nsp3, nsp4 and nsp6 induces formation of double-membrane vesicles which are very similar to those observed in SARS-CoV-infected cells. In those double-membrane vesicles, nsp3-containing pore complexes that span both membranes of the vesicles and allow the export of RNA to the cytosol suggesting that these structures are the sites for viral RNA replication (Angelini et al., 2013; Wolff et al., 2020). Viral RNA synthesis is catalysed by nsp12, which has RNA-dependent RNA polymerase activity, with the support of nsp7 and nsp8 (Wilamowski et al., 2021). Nsp14 possesses a unique RNA proofreading function and is also involved in viral RNA synthesis (reviewed in (V'kovski et al., 2021)).

1.3.3. Replication cycle of SARS-CoV-2

During entry, SARS-CoV-2 S protein engages with the surface receptor ACE2 to mediate binding and attachment of viral particles with host cells (Figure 1.4). Cell surface proteases such as transmembrane serine protease 2 (TMPRSS2) promote the cleavage of S protein to trigger the fusion with the host plasma membrane (Hoffmann et al., 2020).

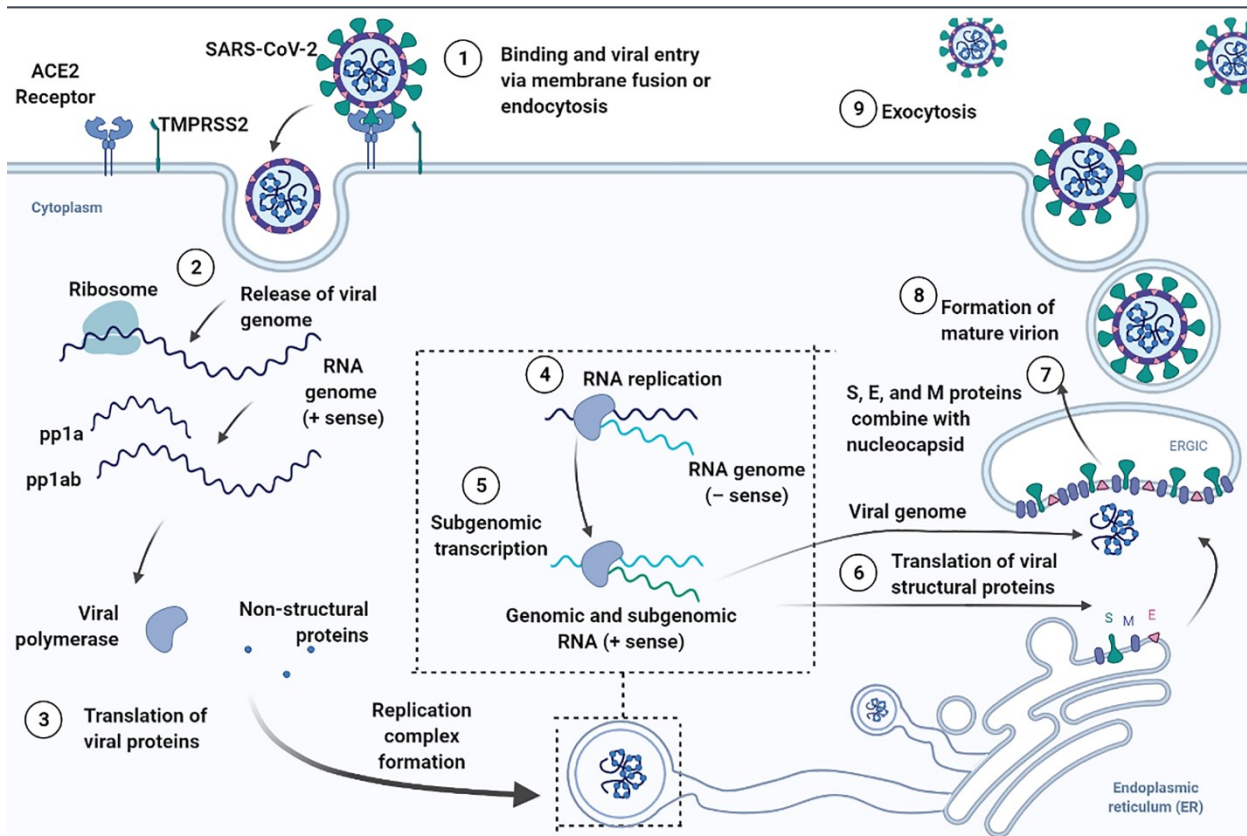


Figure 1.4. The replication cycle of SARS-CoV-2. SARS-CoV-2 S protein interacts with the cellular surface protein ACE2 and is cleaved by the cellular protease TMPRSS2 to activate its membrane fusion activity. The genomic RNA (gRNA) is released from the viral particle into the cytoplasm and is translated into two polyproteins, pp1a and pp1ab. The non-structural proteins induce the formation of replication complexes in which viral RNA synthesis occurs. In the replication complexes, new gRNAs and a sub-genomic mRNAs (sg-mRNAs) which encode the structural S, M, E and N proteins and some accessory proteins, are produced. Newly made gRNAs can be translated to yield additional non-structural proteins, serve as a template for further RNA synthesis or be packaged into new virions. Immature virion assembly starts with binding gRNAs to N proteins and budding into the endoplasmic reticulum–Golgi intermediate compartment (ERGIC), thereby associating with the viral S, M and E proteins. Finally, enveloped progeny virions egress by exocytosis. Created in BioRender.com

The positive-sense genomic RNA is then released from the viral particle and translated to form two replicase polyproteins, pp1a and pp1ab, which are cleaved by the protease activities of nsp3 and nsp5 into non-structural (ns) proteins 1-16. The ns proteins form replication–transcription complexes associated with the ER to provide an optimal environment for viral RNA replication (Hackstadt et al., 2021). In the replication complexes, the RNA-dependent RNA polymerase complex formed by nsp12, nsp7 and nsp8 uses the positive-sense genomic RNA as a template to generate a negative-strand genomic RNA that serves as a template for the synthesis of more positive-strand RNA genomes as well as subgenomic mRNAs that encode structural and accessory proteins (Hartenian et al., 2020; Wilamowski *et al.*, 2021).

The genomic RNA interacts with N proteins to form nucleocapsids that bud into endoplasmic reticulum–Golgi intermediate compartment (ERGIC) where it they associate with structural proteins S, M and E to form new virions, which are thought to exit the infected cell by exocytosis (Klein et al., 2020; Stertz et al., 2007). Recently, β -coronaviruses including mouse hepatitis virus (MHV) and SARS-CoV-2 progeny virions were reported to traffic to lysosomes and egress by lysosomal trafficking pathway (Ghosh et al., 2020). By treating the cells with a Rab7 inhibitor which reduces lysosome numbers, the authors reported that the extracellular MHV RNA was lower than that of the non-treated infected cells. However, many experiments described in the study did not focus on SARS-CoV-2, and the effects of lysosome numbers on SARS-CoV-2 egress was not investigated. Furthermore, the study does not explain how β -coronaviruses deacidify the lysosomes to exit the cells by lysosome trafficking pathway.

1.3.4. Pathogenesis of COVID-19

Entry of SARS-CoV-2 is initiated by the binding of S protein with the host cell receptor ACE2 which is present on epithelial and other cell types (Hoffmann *et al.*, 2020). The expression of ACE2 receptors in tissues may also explain the sites of SARS-CoV-2 replication and COVID-19 symptoms. For example, ACE2 receptors are highly expressed in multi-ciliated epithelial cells in the human respiratory tract (Lee *et al.*, 2020), supporting the infection of SARS-CoV-2 in the bronchial epithelial cells as well as capillary endothelial cells in alveoli. Furthermore, the high ACE2 expression in epithelial cells of the nasal cavity supports the initial site of viral replication (Hou *et al.*, 2020). The most common symptoms of acute COVID-19 are fever, myalgia, headache, and respiratory symptoms (Cevik *et al.*, 2020). COVID-19 patients infected with early variants of SARS-CoV-2 may also exhibit non-respiratory symptoms including taste or olfactory disorders (Giacomelli *et al.*, 2020; Sbrana *et al.*, 2021). Some hospitalized patients with COVID-19 may demonstrate symptoms of pneumonia, the hypoxaemia which can worsen and progress to various stages of the impairment of oxygenation. COVID-19 pneumonia in adults is characterised by clinical signs including fever, cough, and a respiratory rate of more than 30 breaths per minute (reviewed in (Osuchowski *et al.*, 2021)). In addition to respiratory failure, hospitalized patients may develop acute kidney injury and liver dysfunction (Chen *et al.*, 2020; Mao *et al.*, 2020). Data also suggests an association between COVID-19 and myocarditis (Boehmer *et al.*, 2021; Daugherty *et al.*, 2021; Rathore *et al.*, 2021). Specifically, CDC analysed U.S. hospital-based database of healthcare encounters from more than 900 hospitals and reported that patients with COVID-19 during March 2020 to January 2021 had 15 times the risk for myocarditis compared with those without COVID-19 (Boehmer *et al.*, 2021). Furthermore, the risk of thrombotic

complications is higher in patients with COVID-19 admitted to intensive care (Helms et al., 2020; Klok et al., 2020; Llitjos et al., 2020).

1.3.5. Development of COVID-19 vaccines and antivirals

The massive disruption of the global economy and healthcare systems caused by the rapid spread of COVID-19 spurred the development of vaccines and new antivirals at an unprecedented rate. As of January 2022, at least 140 vaccine candidates based on different platforms were in clinical trials, and 194 candidates were in preclinical testing (WHO, 2022b). RNA vaccines (e.g. mRNA-1273 and BNT162b2) and vectored vaccines (e.g. ChAdOx1 nCoV-19 and Ad26.COV2.S) depend on the expression of S protein in the host cells (reviewed in (Nagy and Alhatlani, 2021)). However, the emerging SARS-CoV-2 variants of concern (VOC) including alpha (B.1.1.7), beta (B.1.351), gamma (P.1), delta (B.1.617.2) and now omicron (B.1.1.529) have shown mutations in the receptor binding domain of the S protein, which has raised concerns about the efficacy of the vaccines (Dong et al., 2021). For example, the neutralizing antibody titers of the sera collected from BNT162b2-vaccinated individuals against a gamma variant pseudovirus was reduced by 6.7-fold in comparison to wild-type SARS-CoV-2 pseudovirus (Garcia-Beltran et al., 2021).

Direct-acting antivirals against SARS-CoV-2 such as Merck's molnupiravir (EIDD-2801) and Pfizer's PAXLOVID (PF-07321332) have recently been licensed for use in humans. EIDD-2801 (β -d-N⁴-hydroxycytidine) is an inhibitor that is very similar in structure to the ribonucleoside cytidine. It targets the viral RNA polymerase resulting in increased numbers of mutations in the viral RNA following replication (Wahl et al., 2021). In turn, this leads results in mutant viruses that do not replicate as well. PF-07321332 is a cysteine protease inhibitor that blocks SARS-CoV-2 replication by targeting the viral chymotrypsin-like (CL) cysteine protease (Owen et al., 2021). However, because hydroxycytidine is mutagenic to mammalian cells, there

may be significant side effects for this medication (Zhou et al., 2021). As with many direct-acting antivirals that target viral proteins such as proteases or RNA polymerases, emergence of drug-resistant variants of SARS-CoV-2 is always a concern. Therefore, the development of new antivirals that leverage the host-mediated immune response is a strategy that is worth exploring.

1.4 Interferon system

1.4.1 Types of Interferons

Interferons (IFNs) are class II cytokines that share a conserved α -helical pattern and their receptors, known as class II cytokine receptors, also share sequence homologies in their extracellular domains (reviewed in (Renauld, 2003)). Three types of IFNs have been identified: Type-I, -II, and -III IFNs. The type I IFN family includes 13 IFN- α subtypes and a single IFN β , and several poorly defined single gene products (IFN ϵ , IFN τ , IFN κ , IFN ω , IFN δ and IFN ζ). Type-I IFNs are produced by a wide variety of cell types including immune cells, fibroblasts, endothelial cells and epithelial cells and they influence the development of innate and adaptive immune responses. Type I IFNs bind to their cognate receptors known as type I IFN receptor complexes (Pestka et al., 2004). The type II IFN consists of a single gene product, IFN γ , whose expression is limited to a subset of immune cells including T lymphocytes, macrophages and nature killer cells (Schoenborn and Wilson, 2007). It acts on cell types that express the IFN γ receptor (IFN γ R). IFN γ is an essential regulator of several immune process including macrophage activation, improving antigen recognition in antigen presenting cells, and generating cytokines and inflammatory factors to sustain inflammation (Green et al., 2017). The type III IFN family includes IFN λ 1, IFN λ 2 and IFN λ 3, and the recently identified IFN λ 4. Even though they have similar functions to the type I

IFN family, they signal through type III IFN receptors (O'Brien et al., 2014; Prokunina-Olsson et al., 2013).

1.4.2 Interferon response pathways

The IFN response consists of two phases: an induction phase in which detection of pathogens leads to expression of IFNs that function in autocrine and paracrine manners; and a signaling phase that is initiated by binding of IFNs to their cognate receptors followed by a signaling cascade that leads to expression of interferon-stimulated genes (ISGs) promoting a cellular antiviral state (Figure 1.5).

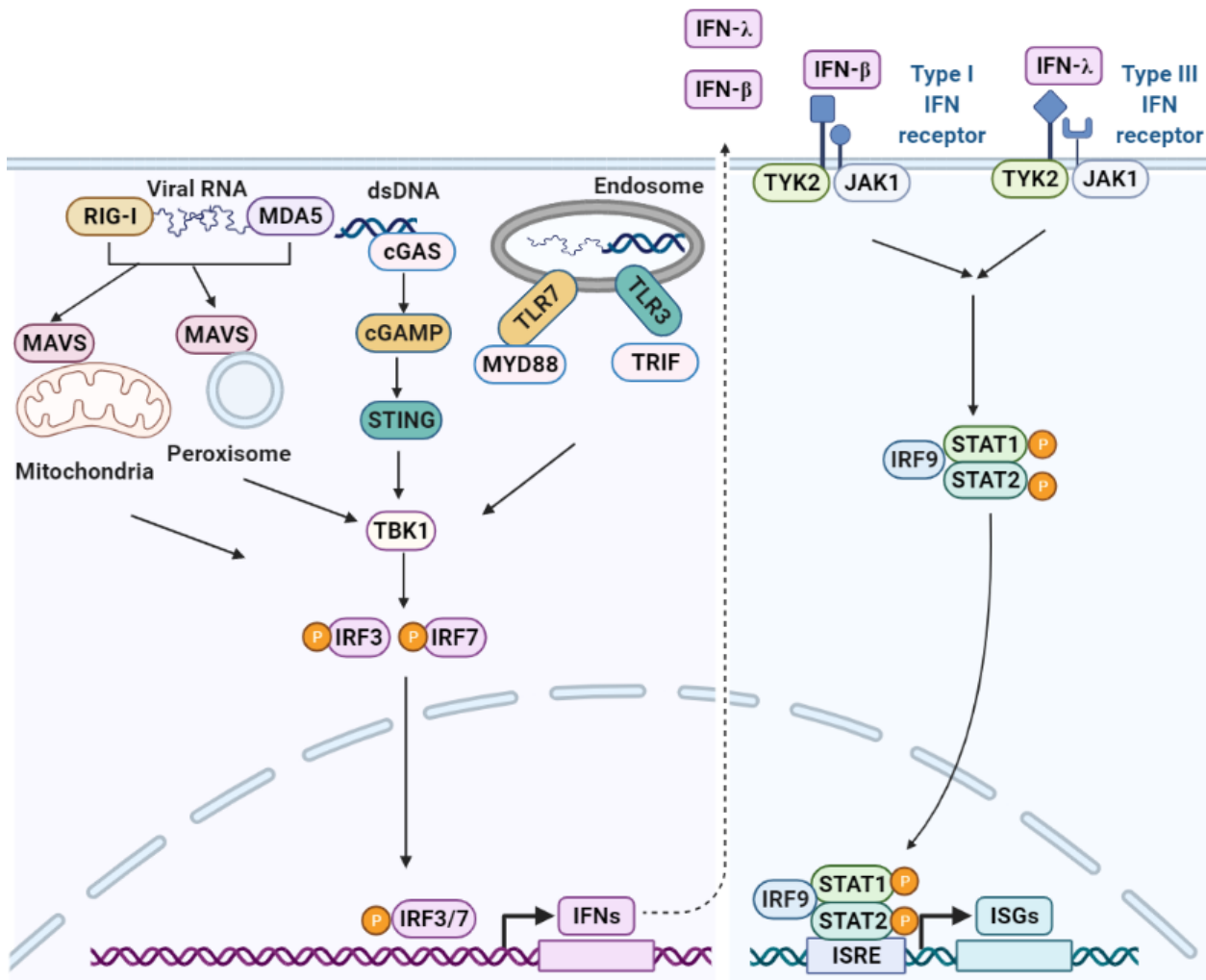


Figure 1.5. IFN response pathway. The IFN induction phase begins with the detection of viral ssRNA or dsRNA. Cytoplasmic helicase receptors (RIG-I and MDA5) detect RNAs while endosomal sensors TLR7 and TLR3 detect viral ssRNA and dsRNA respectively. Viral dsRNA can also be detected by cGAS. Activated RIG-I and MDA-5 activate MAVS on the mitochondria and peroxisomes. Activation of cGAS stimulates the formation of cGAMP and promotes the oligomerization of STING. Activation of TLR3/7 results in the interaction with the adaptor proteins TRIF and MYD88 respectively. The pathways converge on the activation of kinase TBK1 followed by subsequent phosphorylation of the transcription factors IRF-3/7. Phosphorylated IRF-3/7 translocate into nucleus and initiate induction of IFN β and IFN λ expression. The IFN signaling pathway begins with the binding of IFN β and IFN λ to their receptors respectively, which triggers the phosphorylation of STAT1 and STAT2 which then interact with IRF9 to form the IFN-stimulated gene factor. The activated complex translocates to the nucleus where the complex binds to the IFN-stimulated response element (ISRE) resulting in transcription of IFN-stimulated genes (ISGs). Created in BioRender.com.

The induction phase of the IFN response begins with detection of pathogen-associated molecular patterns (PAMPs) by pattern-recognition receptors (PRRs). Cytosolic RIG-I-like receptors (RLRs) such as retinoic acid-inducible gene I (RIG-I) and melanoma differentiation-associated gene 5 (MDA5) are responsible for the recognition of RNAs (Goubau et al., 2013; Hartmann, 2017). Double-stranded DNA (dsDNA) can also be detected by cyclic GMP-AMP synthase (cGAS). The Toll-like receptor (TLR) family including TLR3 and TLR7, which reside in endosomes, detect viral dsRNA and single-stranded RNA (ssRNA) respectively (reviewed in (Kato et al., 2011)).

Activation of RIG-I is stimulated by RNAs with 5' triphosphate (PPP) moieties which are characteristic of genomic RNAs from many RNA viruses (Baum et al., 2010; Hornung et al., 2006). This requirement for 5' PPP distinguishes host RNA transcripts from viral genomes and replication intermediates because the 5' phosphates on host mRNAs are either masked by a cap structure or removed before the host RNA transcripts are exported from the nucleus (reviewed in (Goubau *et al.*, 2013)). Furthermore, dsRNAs are also shown to bind with and activate RIG-I but with lower affinities than 5' PPP based-paired RNAs (Jiang et al., 2011). MDA5, which detects both short and long dsRNAs, can also be activated by poly(I:C), a dsRNA mimic (Takeuchi and Akira, 2010; Wu et al., 2013). The precise mechanism by which MDA5 distinguishes host and viral RNAs is not fully understood, but the 2'-O-methylation of the 5' cap structure, which is a conserved feature of host RNA mRNA transcripts, is important in preventing the detection by MDA5 (Züst et al., 2011). Activation of RIG-I and MDA5 occurs following recognition of 5'PPP by their C-terminal domains (CTDs), resulting in the exposure of N-terminal caspase recruitment domains (CARDs) (Kawai et al., 2005; Seth et al., 2005; Xu et al., 2005), a process that is promoted by the ubiquitylation activity of TRIM25.

The exposed CARDs of activated RIG-I and MDA5 bind to the CARDs of mitochondrial adapter protein MAVS (mitochondrial antiviral signaling), which is also known as IPS-1 [IFN- β promoter stimulator 1], CARDIF [CARD-adapter-inducing IFN- β], or VISA [virus-induced signaling adaptor]) (Kawai *et al.*, 2005; Takeuchi and Akira, 2010; Xu *et al.*, 2005). MAVS contains a C-terminal transmembrane domain that anchors it to the mitochondrial outer membrane (Seth *et al.*, 2005). The CARD-CARD interaction between RIG-I/MDA5 and MAVS induces a conformational change in the MAVS CARD, which converts other MAVS on the mitochondrial outer membrane into prion-like aggregates (Hou *et al.*, 2011). IKK and TANK-binding kinase 1 (TBK1) phosphorylate the C-terminal serine rich region of MAVS at its consensus motif, pLxIS (p, hydrophilic residue; x, any residue; S, phosphorylation site). As an adaptor protein, the C-terminus of phosphorylated MAVS also interacts with the positively charged C-terminus of IFN regulatory factor 3 (IRF3), which is then phosphorylated by TBK1 once they are in proximity. IRF-7 is activated in a similar manner (Dalskov *et al.*, 2020; Liu *et al.*, 2015). Phosphorylation of IRF-3 and IRF7 induces their dissociation from the adaptors and subsequent homodimerization, which is then followed by translocation into the nucleus where phosphorylated IRF-3 and IRF7 binds to IFN-stimulated response elements and induces the transcription of type I and type III IFN genes (Liu *et al.*, 2015; McNab *et al.*, 2015).

Binding of dsDNA with the C-terminus of cGAS results in the synthesis of 2'3' cyclic GMP-AMP (cGAMP), which binds to stimulator of interferon genes (STING) dimers at the ER membrane, a process that promotes the formation of STING tetramers. On the ERGIC, STING tetramer recruits and promotes *trans*-autophosphorylation of TBK1, which in turns, phosphorylates STING, leading to the recruitment of IRF-3. The phosphorylation of IRF-3 by TBK1 enables IRF-3 dimerization and translocation to the nucleus to induce transcription of type

I IFN genes (reviewed at (Decout et al., 2021)). In case of TLRs, the adaptors TRIF (TIR-domain-containing adaptor inducing interferon) and MyD88 (myeloid differentiation factor 88) interact with TLR3 and TLR7 respectively. This results in the activation of the kinases including TBK1, which in turn causes phosphorylation of IRF-3/7 (reviewed in (Kawasaki and Kawai, 2014)).

The signaling phase of the IFN response is initiated by binding of type I and type III IFNs with their cognate heterodimeric receptors at the cell surface. IFN- α R1 and IFN- α R2 form the type I IFN receptor complex, and type III IFN receptor consists of two subunits, IFN- λ R1 and IL-10R2 (Lazear et al., 2019). After binding IFN, the receptor complexes activate Janus activated kinase 1 (JAK1) and tyrosine kinase 2 (TYK2) which leads to recruitment of the transcription factors of the signal transducer and activator of transcription (STAT) family. Phosphorylation of tyrosine residues in STAT1 and STAT2 induces their heterodimerization after which they interact with another transcription factor, IRF9, to form the transcription complex known as IFN-stimulated gene factor 3 (ISGF3). ISGF3 translocates into the nucleus where it binds to IFN-specific response elements (ISRE) which are present in the promoter regions of IFN-stimulated genes (ISGs) (reviewed in (Schneider et al., 2014) and (Lazear *et al.*, 2019)). This leads to transcription of ISGs whose gene products establish an antiviral state in the host cell.

A number of ISGs that specifically restrict replication of ZIKV and SARS-CoV-2 have been reported. For example, viperin was shown to inhibit replication of multiple flaviviruses including ZIKV, DENV, WNV and HCV *in vitro* (Helbig et al., 2013; Helbig et al., 2011; Panayiotou et al., 2018; Szretter et al., 2011; Van der Hoek et al., 2017). Viperin may suppress ZIKV infection by promoting proteasome-mediated degradation of ZIKV NS3 (Panayiotou *et al.*, 2018; Van der Hoek *et al.*, 2017). Mice lacking viperin are more susceptible to WNV-induced pathogenesis as evidenced by increased lethality and viral load in central nervous system tissues

(Szretter *et al.*, 2011). C19orf66 also targets ZIKV NS3 to reduce viral titre and RNA replication, possibly by inducing NS3 degradation via a lysosomal-dependent pathway (Wu *et al.*, 2020b). ZIKV titre was also negatively affected in the serum and spleen of mice when treated with recombinant ISG20 (rISG20). This ISG also restricts ZIKV replication in the brains of the fetuses born to IFNAR1^{-/-} pregnant mice, suggesting ISG20 may protect the fetuses from ZIKV infection (Ding *et al.*, 2021). Reduction in the expression of ISGs including MX1 and IFIT1 in primary human Sertoli cells resulted in enhanced ZIKV titre and viral RNA levels, suggesting MX1 and IFIT1 restrict ZIKV replication in the male reproductive tract (Strange *et al.*, 2021).

SARS-CoV-2 replication is inhibited by several ISGs which block viral entry (Martin-Sancho *et al.*, 2021; Pfaender *et al.*, 2020; Zang *et al.*, 2020). Examples include IFN-inducible lymphocyte antigen 6 complex, locus E (LY6E), which inhibits the replication of multiple coronaviruses, including SARS-CoV, SARS-CoV-2, and MERS-CoV, by blocking fusion of viral and cellular membranes. Twenty-five-hydroxycholesterol (25HC) also has antiviral effects against SARS-CoV-2. It is generated from cholesterol by the ISG cholesterol 25-hydroxylase, and blocks SARS-CoV-2 replication by restricting spike protein mediated membrane fusion (Zang *et al.*, 2020). A more comprehensive study on ISGs that affect SARS-CoV-2 replication was also reported (Martin-Sancho *et al.*, 2021). RNAseq revealed that 399 ISGs were up-regulated in response to activation of type I IFN in human cells such as tracheobronchial epithelial cells and A549 cells. Individual ectopic expression of each of the 399 ISGs showed that 65 of these genes specifically inhibited SARS-CoV-2 replication in human cells at different steps. *LY6E*, *CLEC4D*, *UBD*, *ELF1*, *FAM46C*, and *REC8* inhibited viral entry whereas three members of IFIT family, IFIT1, IFIT3, and IFIT5, were shown to inhibit viral RNA replication. In contrast, bone marrow stromal antigen 2 (*BST2*) inhibited release of virions and silencing of *BST2* resulted in increased

SARS-CoV-2 titres. All these results further demonstrated that ISGs are crucial for restricting replication of ZIKV and SARS-CoV-2.

1.4.3 Suppression of IFN system by ZIKV and SARS-CoV-2

In order to establish infection, viruses have evolved strategies to evade and antagonize the host IFN system. ZIKV and SARS-CoV-2 are known to encode multiple proteins that affect IFN production and signaling by targeting host proteins.

ZIKV NS4A interacts with the CARD-like domain of MAVS and reduces the binding between RIG-I and MAVS, resulting in suppression of IFN expression (Hu et al., 2019). NS1 and NS4B block TBK1 phosphorylation in response to Sendai virus infection, but the precise mechanism is unknown (Wu et al., 2017). Both NS4A and NS5 bind to IRF-3 preventing its phosphorylation and ability to stimulate IFN- β induction (Xia et al., 2018). NS5 protein also interacts with the kinase IKK ϵ to reduce the phosphorylation of IRF-3, resulting in lower activation of the IFN λ promoter (Lundberg et al., 2019). For SARS-CoV-2, M protein was shown to inhibit the phosphorylation of IRF-3 in response to Sendai virus infection and poly(I:C) induction, resulting in the inhibition of IFN β expression (Fu et al., 2021; Sui et al., 2021; Zheng et al., 2020), but different mechanisms of M protein inhibiting IFN β induction were described. M protein was shown to induce the proteasomal degradation of TBK1, leading to the inhibition of dimerization and phosphorylation of IRF-3 (Sui *et al.*, 2021). However, reduction of TBK1 protein level in M protein expressing cells was not demonstrated in other studies (Fu *et al.*, 2021; Zheng *et al.*, 2020). Instead, M protein was shown to interact with the transmembrane domain of MAVS and inhibit its aggregation, disrupting the recruitment of downstream components TBK1 and IRF3

(Fu *et al.*, 2021). However, the analysis of the cellular localization of M protein by confocal microscopy showed that M protein resided on the ER, Golgi and MAVS but not on mitochondria (Zheng *et al.*, 2020). The non-puncta-like structures displayed in M protein expressing cells are less likely to colocalize with the MAVS on peroxisomes. Even though all these studies revealed that M protein impaired the activation of IRF-3, the precise mechanisms of the inhibition remain to be elucidated. NSP-1 protein suppresses IFN induction largely by shutting down host translational machinery and nuclear transport of IRF-3 (Kumar *et al.*, 2021). ORF3 protein was also shown to inhibit induction of IFN β by blocking the nuclear translocation of IRF-3. This viral protein can also inhibit IFN- β promoter activity, even in the presence of a constitutively active form of IRF-3, suggesting that it prevents IFN- β production downstream of IRF-3 activation (Konno *et al.*, 2020; Lei *et al.*, 2020).

ZIKV and SARS-CoV-2 infection also inhibit the signaling phase of the IFN response. Overexpression of ZIKV NS2B reduces levels of Jak1 protein by inducing its proteasomal degradation (Wu *et al.*, 2017). Similarly, ZIKV NS5 binds to and induces degradation of STAT2 thereby blocking IFN signaling (Grant *et al.*, 2016; Kumar *et al.*, 2016). Over-expression of SARS-CoV-2 NSP1 also appears to reduce STAT2 levels and consequently ISRE reporter activity is reduced (Kumar *et al.*, 2021). ORF6 protein of SARS-CoV-2 inhibits nuclear translocation of STAT1 without affecting its phosphorylation, resulting in lower ISRE promoter activity and reduced ISG expression (Lei *et al.*, 2020). Another study showed that SARS-CoV-2 ORF6 protein directly binds the nuclear pore protein Nup98 and inhibits IFN signaling by preventing nuclear translocation of STAT1 and STAT2 (Miorin *et al.*, 2020). Type I IFN signaling is also antagonized by SARS-CoV-2 N protein. The overexpression of this viral protein suppresses phosphorylation and nuclear translocation of STAT1 and STAT2 in response to Sendai virus infection or treatment

with recombinant IFN- β (Lei *et al.*, 2020; Mu *et al.*, 2020). Finally, the papain-like protease (PLpro) domain of NSP3 was shown to cleave the ubiquitin-like interferon-stimulated gene 15 protein (ISG15) to attenuate the IFN response (Shin *et al.*, 2020).

The effects of ZIKV on the IFN system were also studied using samples obtained from infected patients. Flow-cytometry analyses revealed that ZIKV infection was associated with reduced IFN- γ production by CD4 T-cells suggesting that the IFN system is likely impaired in ZIKV infected patients (Cimini *et al.*, 2017).

Proof of SARS-CoV-2 restricting IFN system was also documented in clinical studies on COVID-19 patients. Analyses of transcriptomes of SARS-CoV-2-infected bronchial epithelial cells and lung tissues from patients with COVID-19 showed that SARS-CoV-2 infection reduces type I and type III IFN levels and ISGs (Blanco-Melo *et al.*, 2020). A more recent study that examined immune cells from blood samples obtained from patients with COVID-19 also showed that type I IFN production and ISGs induction were impaired in COVID-19 patients (Hadjadj *et al.*, 2020).

1.4.4 IFNs restrict ZIKV and SARS-CoV-2 replication and pathogenesis

Recombinant IFNs have been investigated as potential treatments for ZIKV and COVID-19. The action of IFNs on restricting ZIKV and SARS-CoV-2 replication and pathogenesis is discussed below.

1.4.4.1 IFNs restrict ZIKV replication and pathogenesis

Type I and type III IFNs have been shown to restrict ZIKV replication in various types of human cells. Addition of IFN β to A549 cells prior to infection inhibited replication of ZIKV

strains from both African and Asian lineages by up to 400-fold (Gobillot et al., 2020). Inhibitory effects of IFNs were also studied in human primary cells. Pre-infection administration of recombinant IFN β and IFN λ to human primary human vaginal epithelial cells (HVECs) and primary human cervical epithelial cells (HCECs) inhibited replication of ZIKV by nearly 40-fold in HVECs and 700-fold in HCECs (Caine et al., 2019). Transcriptional profiling of ZIKV-infected HVECs revealed that IFN β and IFN λ treatment resulted in differential up-regulation of ISGs. These results indicate that type I and type III IFNs enhance the innate immune response in the female reproductive tract which dramatically suppresses replication of ZIKV (Caine *et al.*, 2019). Human placenta cells were also studied to investigate the importance of IFN in reducing ZIKV replication. Primary human trophoblasts (PHTs), which are the barrier cells of the placenta, constitutively produced IFN λ to restrict the infection of ZIKV, and furthermore, the media isolated from PHT cells protected non-trophoblast cells from ZIKV infection, suggesting that IFN λ secreted from PHT cells is likely to protect other non-placental cells (Bayer et al., 2016). Constitutive secretion of IFN λ was also observed in human syncytiotrophoblasts, which are cells that are in direct contact with maternal blood, and they were shown to be resistant to ZIKV infection (Corry et al., 2017). These results suggest that ZIKV has to overcome the robust IFN system in these cells in order to establish infection in fetuses.

The restriction of ZIKV replication by IFNs was also demonstrated in a human explant model. Jagger et al. studied the restriction of IFN λ signaling on ZIKV infection in explant models of maternal and fetal tissues derived from healthy human samples (Jagger et al., 2017). Post-infection treatment of IFN λ and IFN β in fetal amniotic and chorionic membrane was found to reduce ZIKV infection.

Studies which investigated ZIKV disease in pregnant dams showed that pregnant dams lacking a functional IFN λ receptor were more susceptible to ZIKV infection, leading to complications including reduced placental thickness, placental length and diameter. Their fetuses with dysfunctional IFN λ receptors showed demise and impaired head growth. (Jagger *et al.*, 2017). Lazear et al. reported that while adult immunocompetent WT mice are resistant to ZIKV infection, mice lacking type I IFN receptors are more susceptible to ZIKV infection and developing neurological disease and death (Lazear et al., 2016). These studies indicate the importance of the IFN system in restricting ZIKV replication.

1.4.4.2 IFNs restrict SARS-CoV-2 replication and pathogenesis

Several *in vitro* studies have demonstrated that SARS-CoV-2 replication is limited by type I and III IFNs (Busnadiago et al., 2020; Lokugamage et al., 2020; Mantlo et al., 2020; Stanifer et al., 2020). Pre-infection treatment of IFN β and IFN λ resulted in dramatic reduction in SARS-CoV-2 replication in primary human bronchial epithelial cells (Busnadiago *et al.*, 2020), and also induced an efficient antiviral state in human intestinal epithelial cells (hIECs) to control the infection of SARS-CoV-2 (Stanifer *et al.*, 2020). Post-infection treatment of type-I IFN greatly reduced SARS-CoV-2 titer in both Calu-3 cells and Vero cells (Lokugamage *et al.*, 2020; Mantlo *et al.*, 2020), suggesting that Vero cells are able to mount IFN signaling in response to exogenous IFN treatment even though they lack the capacity to produce type-I IFN (Desmyter et al., 1968). The high sensitivity of SARS-CoV-2 to both type I and type III IFNs highlights the possible use of IFNs in the treatment or prevention of COVID-19.

In vivo studies were conducted to study the effects of IFNs on SARS-CoV-2 replication (Hoagland et al., 2021; Humphries et al., 2021). Intranasal administration of IFN α greatly reduced the viral load in hamsters challenged by SARS-CoV-2 by intranasal inoculation (Hoagland *et al.*, 2021). Post-infection IFN α administration was also studied in hamsters to determine whether intranasal IFN α could provide therapeutic benefits. Plaque assay and qRT-PCR analyses showed no infectious virions in the lungs 6 days after infection and demonstrated reduced viral mRNA levels respectively. These support the possibility of using intranasal administration of type I IFNs for therapeutic use against COVID-19 (Hoagland *et al.*, 2021).

The diamidobenzimidazole compound, diABZI-4, which activates STING, was also found to suppress SARS-CoV-2 replication *in vitro* and *in vivo* (Humphries *et al.*, 2021). Pre-infection treatment with diABZI-4 resulted in reduction in SARS-CoV-2 titers and replication in human lung epithelial cells. Intranasal administration of diABZI-4 in ACE2-transgenic mice pre- and post-infection protected the mice from severe respiratory disease induced by SARS-CoV-2 infection. Blocking IFN signaling with an anti-IFNAR neutralizing antibody partially inhibited the protective effects of diABZI-4. Pre-infection treatment with diABZI-4 also reduced titres and replication of influenza A virus (IAV) in the lung and protected mice from lethality. These results suggest that diAZBI-4 activates the host-directed immune response to restrict replication of SARS-CoV-2 infection, and possibly other respiratory viruses.

1.4.5 The therapeutic use of IFN β for COVID-19

Promising results from clinical trials which evaluated IFN β as a single or combination therapy in COVID-19 have been reported. These include a phase 2 clinical trial that compared

subcutaneous injection of IFN β in combination with an oral protease inhibitor (lopinavir-ritonavir) and an oral nucleoside analogue (ribavirin) versus the control group which consisted of lopinavir and ritonavir for COVID-19 patients. Results showed that the triple combination given within 7 days of symptom onset is more effective in reducing the shedding of SARS-CoV-2 in a nasopharyngeal swab compared with the treatment in the control group. In addition, only mild and self-limiting side-effects were observed and there are also great reductions in hospital stay (Hung et al., 2020). Another study of a phase 2 clinical trial reported the use of IFN β as a single therapy in treating patients with COVID-19. Results demonstrated that daily administration of inhaled nebulized IFN β shortened the hospital stay of patients with COVID-19 admitted to the hospital. Those patients also experienced more rapid recovery in comparison to those who received placebo. The results of phase 2 clinical trials suggest high safety and efficacy of the use of IFN β as a single or combination therapy in patients with COVID-19, and also provide strong rationales for more advanced clinical trials (Monk et al., 2020).

1.4.6 The therapeutic use of IFN λ for COVID-19

Even though type I and type III IFNs initiate similar signaling pathways, differential IFN receptor expression in tissues can affect the antiviral response. IFNAR1 and IFNAR2 are present in all nucleated cells, whereas IFNLR1 is expressed preferentially on epithelial cells particularly in the respiratory, intestinal and reproductive tracts (Kotenko and Durbin, 2017; Kotenko et al., 2019). As such, type III IFN responsiveness at epithelial surfaces is associated with the relatively high expression of IFNLR1 (Kotenko and Durbin, 2017; Lazear et al., 2015), and therefore, respiratory epithelial cells respond to the stimulation by both type I and type III IFNs, possibly leading to enhanced antiviral activities and restriction of viral replication. The responsiveness of

epithelial cells on the respiratory tract to type I and type III IFNs provides grounds to initiate studies to explore the use of IFN λ in limiting viral infections.

A phase 2 clinical study evaluated the efficacy of a single subcutaneous injection of peg-IFN λ versus placebo for treating outpatients with COVID-19. Results showed that a greater proportion of patients treated with peg-IFN λ showed an undetectable viral load in nasal swab than the placebo group at day 7 of symptom onset. In addition, peg-IFN λ was safe and well tolerated in outpatients with mild-to-moderate COVID-19 as they showed a similar side-effect profile to those treated with placebo (Feld et al., 2021). As of February 5, 2022, a phase 3 clinical study is still underway in Canada to evaluate the effects of peg-IFN λ in patients with mild to moderate COVID-19 (NCT number: NCT04967430). Together, the promising results of the advanced clinical studies evaluating the efficacies of IFN β and IFN λ for treating COVID-19 suggest that antivirals boosting the host-mediated IFN response are worth investigating.

1.5. Peroxisomes

Peroxisomes have long been known for their critical roles in multiple metabolic pathways, including β -oxidation of carboxylates and synthesis of ether-phospholipids (reviewed in (Van Veldhoven, 2010)). Many of the pathways generate reactive oxygen or nitrogen species (ROS or RNS) (Fransen et al., 2012) such as H₂O₂, which is subsequently converted to H₂O and O₂ by the antioxidant enzyme catalase as a counteract measure to mediate the effects of the reactive species (Bonekamp et al., 2009). Recent studies have shown that beyond their roles in cellular metabolism, peroxisomes function in parallel with mitochondria as antiviral signaling platforms (Dixit et al.,

2010). The following section reviews the important facets of peroxisome biogenesis and pexophagy, and the interplay between peroxisomes and viruses.

1.5.1. Peroxisome biogenesis

1.5.1.1. Matrix protein import

Peroxisomes are membrane-bound organelles that employ ATP-dependent mechanisms for import of matrix proteins and membrane proteins synthesized on free polyribosomes in the cytosol (Lazarow and Fujiki, 1985). The import mechanisms of matrix proteins and membrane proteins are different and will be discussed separately. For matrix proteins, the import process consists of four steps: 1) recognition by the corresponding receptors, 2) docking of receptor-cargo complex at the membrane of peroxisomes, 3) cargo translocation, and 4) recycling of receptors (Kim and Hettema, 2015). Peroxisome matrix proteins are classified into two groups according to their evolutionary conserved peroxisomal targeting signal (PTS). The carboxy-terminal PTS1s conform to the consensus -(SAC)-(KHR)-(LM)- (Gould et al., 1989) and are recognized by the receptor PEX5 (Gatto et al., 2000). The amino-terminal PTS2s fit the consensus -R-(LIVQ)-X-X-(LIVQH)-(LSGA)-X-(HQ)-(LA)- and they bind to the receptor PEX7 (Petřiv et al., 2004). The docking complex on the peroxisomal membranes, which consists of PEX13 and PEX14, interacts with the PTS receptors during the import process (Lanyon-Hogg et al., 2010). Cargo-loaded PTS1 and PTS2 receptors interact with PEX14 and then PEX13 to facilitate docking, after which the cargo is translocated across the membrane and released into the matrix of peroxisomes by a poorly understood process that requires the monoubiquitylation of PTS1 and PTS2 receptors (Kim and Hettema, 2015). The monoubiquitylation of PEX5 and PEX7 not only promotes the release of

cargo, but also facilitates their ATP-dependent recycling process to continue the recognition of target protein in the cytosol (Grou et al., 2008; Rodrigues et al., 2014).

1.5.1.2. Membrane protein import

Similar to peroxisomal matrix proteins, peroxisome membrane proteins (PMPs) are also synthesized on free polyribosomes before insertion into peroxisomal membranes (Fujiki et al., 1984; Imanaka et al., 1996). There are two types of membrane PTSs (mPTS) on PMPs. Class I PMPs possess mPTSs that are recognized by the chaperone and import receptor PEX19, while the import of class II PMPs is independent of PEX19 (Jones et al., 2004).

Newly synthesized class I PMPs are recognized by PEX19 in the cytosol which then guides the PMPs to peroxisomal membranes (Jones *et al.*, 2004). Functional domains of PEX19 in PMP insertion have been characterized. Its N-terminal docking domain interacts with the conserved motif (NH₂-YSTCMLVLLRVQLNII-COOH) in the docking protein PEX3 (Fang et al., 2004), and the C-terminal domain (amino acid residues 88–272) binds to the mPTS of PMPs (Fransen et al., 2005). In addition, the amphipathic segment that lies between its N-terminal segment and C-terminal domain was reported to be essential for PMP insertion (Chen et al., 2014). The docking protein PEX3 also plays a role in PMP insertion. Its cytosolic domain is inserted with the lipid bilayer, and the hydrophobicity of this domain likely allows the cargo to breach the hydrophilic surface of the bilayer to facilitate PMP-membrane insertion. The import of class II PMPs by a PEX19 independent pathway will be discussed in section 1.5.1.4.

1.5.1.3. Peroxisome biogenesis by growth and fission

Peroxisome growth and fission regulates the size and numbers of peroxisomes (Schrader et al., 2012) and is regulated by PEX11 family, dynamin-like protein 1 (DLP1), and membrane receptor proteins Mff and human Fis1 (hFis1). There are three PEX11 isoforms in mammals: PEX11 α , PEX11 β , and PEX11 γ (Abe and Fujiki, 1998; Tanaka et al., 2003). Results of the over-expression of human PEX11 β for 48 hours showed that the abundance of PMP70- and PEX14-positive structures increased in human hepatoma cells and wild-type human skin fibroblasts respectively. The results suggest that over-expression of PEX11 β induces peroxisome proliferation in human cells (Li and Gould, 2002; Schrader et al., 1998b). Conversion of peroxisome morphology was also observed in cells throughout the course of PEX11 β over-expression. At 6 hours after transfection, peroxisomes in the cells became elongated and tubular, which were then gradually replaced by more numerous and smaller vesicles over the following 72 hours. Proteins involved in this multi-step process of PEX11 β -mediated peroxisome proliferation had not been known until Koch et al. reported the roles of mitochondrial fission factors Mff and hFis1 in peroxisomal division. They bind to peroxisomes and recruit another mitochondrial fission factor DLP1 to this organelle (Koch et al., 2005; Koch and Brocard, 2012). PEX11 β interacts with the proteins of fission machinery to form a complex and promote the formation of constriction sites, resulting in increased peroxisome numbers (Delille et al., 2011; Kobayashi et al., 2007; Koch and Brocard, 2012). The functions of DLP1 in peroxisomal fission not only include the binding with the constriction sites, but also self-assembly on the membranes to stabilize the membrane tubules before the final GTP hydrolysis dependent membrane scission (Kamerkar et al., 2018). The functions of PEX11 α and PEX11 γ in peroxisome growth and fission are still not clear, but it

was shown that PEX11 γ is involved in both membrane elongation and interaction with PEX11 β and hFis1.

1.5.1.4. *De Novo* synthesis of peroxisomes

Using live cell fluorescence microscopy, a new route of PMP insertion into pre-existing peroxisomes was identified in which two PMPs, PEX3 and PMP34, were transported from the ER to pre-existing peroxisomes by a process that is dependent on PEX16 (Aranovich et al., 2014; Kim et al., 2006). Other PMPs are known to be recruited via the ER by PEX16, including PEX26, PEX10, PEX11 β and FIS1, a PMP that also localizes to mitochondria (Hua et al., 2015). The functional domains of PEX16 in targeting PMP from the ER to peroxisomes are characterized: ER targeting (transmembrane (TM) domain 1), PMP targeting (amino acid (aa) residues 66-103 and TM domain), and ER-to-peroxisome targeting (aa residues 71-81) (Hua *et al.*, 2015). However, the precise mechanisms in which PEX16 recruits other PMPs to the ER in the absence of PEX19, and how other PMPs target pre-existing peroxisomes from the ER are still unknown. Nonetheless, these findings indicate that the ER and PEX16 are part of an PEX19-independent PMP import pathway which may be important for maintenance of pre-existing peroxisomes.

Involvement of the ER in the biogenesis of peroxisomes has also been described in yeast (Knoblach et al., 2013; Mast et al., 2016; Tam et al., 2005). For example, PEX3p was shown to reside on both peroxisomes and the ER, and interact with the inheritance factor Inp1p which mediates a linkage of ER-bound PEX3p with peroxisomal PEX3p (Knoblach *et al.*, 2013; Tam *et al.*, 2005). PEX29 and PEX30 reside on the ER and associate with other ER-resident proteins, including Rtn1 and Yop1, which play a role in ER membrane curvature (Mast *et al.*, 2016). A model for peroxisome biogenesis was proposed in a study which reported the insertion of PMP into the ER via the Sec61 translocon, and PMPs assemble into two types of sub-complexes on the

ER membrane. Fusion of two classes of ER-derived pre-peroxisomal vesicles in the cytosol is critical for the maturation of peroxisomes (van der Zand et al., 2012).

1.5.1.5. Peroxisome-ER tethering

Peroxisomes and ER form a close-knit network as they are in constant and essential communication with other organelles. Peroxisomes rely on the ER for lipids and also receive PMPs from this organelle ((Knoblach *et al.*, 2013; Mast *et al.*, 2016; Tam *et al.*, 2005), and reviewed in (van den Bosch et al., 1992)) Moreover, the synthesis of plasmalogens and cholesterol initiated in peroxisomes is completed in the ER. The peroxisomal biogenesis factor PEX16 is involved in the recruiting PMPs to the ER before targeting existing peroxisomes as discussed above. However, other proteins involved in this process were not known until Hua et al. reported that VAMP-associated proteins A and B (VAPA and VAPB) are responsible for peroxisomes tethering to the ER through their interaction with the peroxisomal membrane acyl-CoA binding domain containing 5 (ACBD5) (Hua et al., 2017). Disrupting the VAP-ACBD5 interaction reduces the surface area of peroxisomes in cells as well as the plasmalogens and total cholesterol levels, suggesting that the VAP-ACBD5 interaction is required for growth of peroxisomes and lipid synthesis.

1.5.1.6. Pexophagy

Peroxisome abundance in cells is regulated by *de novo* biosynthesis and/or fission and growth as well as the turnover rate of this organelle. Similar to other organelles, peroxisomes are

also subject to a selective quality control process known as autophagy, which involves a specific receptor targeting the substrates to autophagosomes.

Attachment of a ubiquitin chain to PMP34 leads to a reduction of catalase-containing structures, and those peroxisomes modified with ubiquitin showed colocalization with the autophagosome maker protein LC3, suggesting the ubiquitinated peroxisomes became sequestered in autophagosomes (Kim et al., 2008). The role of autophagy in depleting the number of ubiquitinated peroxisomes in cells was further demonstrated through experiments which showed that loss of peroxisomes was dependent on p62, an adaptor scaffold protein which binds to polyubiquitinated proteins in aggregates and LC3. Reduction in peroxisome numbers could be rescued by an autophagy inhibitor 3-MA, suggesting that autophagy was involved in the degradation of ubiquitinated peroxisomes in cells.

The role of autophagy in depleting peroxisomes was further elaborated in a study of a specific autophagy receptor that targets peroxisomes. Increased peroxisome aggregation and targeting to lysosomes in cells over-expressing with NBR1 revealed that this protein does not only work together with p62 in targeting polyubiquitylated protein aggregates to autophagosomes for degradation (Deosaran et al., 2013), but also as an autophagy receptor for peroxisome degradation. In addition, the ubiquitin domain of NBR1 was shown to be required for peroxisome degradation. The results suggested that one or more ubiquitinated PMPs are likely to be targeted by p62 and NBR1 to initiate pexophagy.

The E3 ubiquitin ligase PEX2 is responsible for pexophagy (Sargent et al., 2016). PEX2 not only causes ubiquitination of PEX5 and PMP70, but overexpression of this protein significantly reduces peroxisome density in NBR1 over-expressing cells during amino acid starvation

conditions. Interestingly, only PEX2, but not the other peroxisomal E3 ubiquitin ligases PEX10 or PEX12, mediates ubiquitination of the PMPs PEX5 and PMP70 to recruit the autophagy receptors NBR1 for pexophagy.

1.5.2. Peroxisomes as antiviral signaling hubs

Several mitochondrial proteins including the outer membrane proteins Fis1 and Mff are found on peroxisomes (Gandre-Babbe and van der Blik, 2008; Koch *et al.*, 2005). They share similar domain structures, which include an N-terminal effector domain and a C-terminal localization motif that consists of a transmembrane domain and a short tail that anchors them to the mitochondrial outer membrane. The observation that the antiviral protein MAVS resides on peroxisomes as well as mitochondria suggested peroxisomes may also function in antiviral signaling (Dixit *et al.*, 2010). Indeed, MAVS signaling from peroxisomes, which can be triggered by multiple viruses including Sendai virus and DENV, was found to induce production of type III IFNs, creating a cellular antiviral state dependent on Jak-STAT-1 activities (Dixit *et al.*, 2010; Odendall *et al.*, 2014). Furthermore, the MAVS-dependent induction of type I and type III IFN in response to Sendai virus infection is similar in cells exclusively expressing MAVS on peroxisomes only or mitochondria only suggesting that MAVS-induced IFN expression is not dependent upon a single subcellular localization (Bender *et al.*, 2015).

1.5.3. The interplay between peroxisomes and viruses during infection

Given their roles in antiviral defense, it is not unexpected to find that viruses have evolved different strategies to counteract the IFN system by impairing peroxisome biosynthesis. Both flaviviruses and coronaviruses encode proteins that impair peroxisome biogenesis through

different mechanisms. The first study to document this phenomenon was done by the Hobman lab who showed that in cells infected with DENV or WNV, peroxisome numbers were reduced by more than 40% (You et al., 2015). Further analysis revealed that expression of flavivirus capsid proteins reduced peroxisome numbers by targeting PEX19, which is essential for *de novo* peroxisome biogenesis, for degradation. Later, it was shown that SARS-CoV-2 infection causes the redistribution of peroxisomal matrix proteins to the cytosol and the formation of fragmented peroxisomal membranes, suggesting a loss of integrity of the peroxisome compartment observed during viral infection (Knoblach et al., 2021). Furthermore, SARS-CoV-2 ORF14 protein was shown to interact with PEX14, suggesting the peroxisomal matrix protein import machinery is likely to be disrupted.

Prior to the studies with SARS-CoV-2, the alphacoronavirus porcine diarrhea epidemic virus (PEDV) was reported to reduce peroxisome numbers by more than 60% (Zhang et al., 2018). Expression of the viral protein NSP1 was sufficient for this process as well as blocking nuclear translocation of IRF1 and suppression of type III IFN. Even though the precise mechanisms were not reported in the study, it is possible that PEDV NSP1 reduces peroxisome numbers by inhibiting the translation of mRNAs encoding peroxisomal proteins (Shen et al., 2018). Hepatitis C virus (HCV) infection reduces expression of peroxisomal genes in Huh7.5.1 cells and liver tissue of patients (Lupberger et al., 2019). In addition, peroxisomal MAVS is cleaved by the HCV NS3/4A protease thereby inhibiting IFN induction (Ferreira et al., 2016). Human immunodeficiency virus (HIV) impairs peroxisome biogenesis by 50% in part by upregulation of multiple miRNAs (miR500a-5p, miR-34c-3p, miR-93-3p and miR-381-3p) that target the peroxisome biogenesis factors PEX2, PEX7, PEX11B and PEX13 respectively (Xu et al., 2017).

Intriguingly, some viruses have been shown to induce peroxisome proliferation during infection and/or require peroxisomes for replication. Human cytomegalovirus (HCMV) and herpes simplex virus type 1 (HSV-1) reportedly increase expression of peroxisome biogenesis factors involved in peroxisome membrane assembly (PEX3 and PEX16) and those involved in matrix protein import (PEX13 and PEX14) (Jean Beltran et al., 2018). Quantitative indirect immunofluorescence revealed that infection of cells with HCMV or HSV-1 increased the peroxisome pool by 3.6-fold. Conversely, replication of HCMV was reduced in cells that lack peroxisomes due to knockout of genes encoding PEX3 or PEX19. It was suggested that HCMV induces peroxisome proliferation in part to enhance synthesis of plasmalogens in order to facilitate virus replication, as plasmalogens were shown to be enriched in HCMV viral membranes (Liu et al., 2011). Latent infection of Kaposi's Sarcoma associated Herpesvirus (KSHV) increases expression of PEX3 and PEX19, resulting in ~50% increase in the peroxisome pool (Sychev et al., 2017). Levels of the ATP Binding Cassette Subfamily D Member 3 (ABCD3) protein, a peroxisome resident lipid transporter that transports very long chain fatty acids to peroxisomes for oxidation, is also increased by KSHV infection.

1.6 Interplay between IFN system and Wnt/ β -catenin signaling pathway

In the absence of Wnt ligands, β -catenin in the cytoplasm is processed by the ubiquitin-proteasome system that involves a destruction complex containing glycogen synthase kinase (GSK)-3 α/β , casein kinase 1 (CK1), axin, adenomatous polyposis coli (APC), and the E3-ubiquitin ligase beta-transducin repeats-containing proteins (β -TrCP). The engagement of Wnt ligands to frizzled/LRP receptors results in the destabilization of the destruction complex, thus allowing for the cytoplasmic β -catenin to translocate into the nucleus and bind to lymphoid

enhancer factor/T-cell factor (LEF/TCF) to induce the expression of Wnt target genes (reviewed in (Kimelman and Xu, 2006)).

The IFN system has been reported to be negatively regulated by Wnt/ β -catenin signaling pathway ((Baril et al., 2013)). Baril M *et al.* reported that normal human brachial epithelial (NHBE) cells transduced with lentiviruses encoding shRNA targeting β -catenin demonstrated upregulated expression of IFN β in response to Sendai virus infection. Knockdown of β -catenin by shRNA in HEK 293T cells increased IFN β promoter-driven luciferase activity, as well as secretion of IFN β protein in response to Sendai virus infection. Moreover, HEK 293T cells transfected with siRNA targeting β -catenin not only showed higher IFIT1 and RIG-I protein levels, but also exhibited upregulated expression of IFN β and RIG-I mRNAs in response to Sendai virus infection. Conversely, pharmacological inhibition of GSK3, which results in stabilization of β -catenin, reduced the IFN β promoter-driven luciferase activity in response to Sendai virus infection. Together, these data suggest that Wnt/ β -catenin signaling acts as a negative regulator of IFN induction and signaling in multiple human cell types. In contrast, other studies demonstrated an antiviral role of β -catenin in enhancing the expression of IFN β ((Marcato et al., 2016; Wang et al., 2008)). Marcato V *et al.* showed that inhibition of GSK3 by LiCl not only increased β -catenin protein levels, but also increased in the interaction of β -catenin/TCF with the IFN β promoter region in mouse cells, consequently increasing IFN β mRNA level. Another study reported that siRNA mediated knockdown of GSK3 β increased secretion of IFN β in LPS-stimulated mouse macrophages. In addition, pharmacological inhibition of GSK3 β by SB216763 increased c-jun protein levels as well as secretion of IFN β in mouse macrophages in response to LPS stimulation

((Wang *et al.*, 2008)). These contrasting results may be in part to the fact that different cell types were used in the studies.

1.7 Objectives of thesis

Peroxisomes are now known as signaling platforms that function in the IFN induction pathway. Understanding the interplay between viruses and peroxisomes during infection will provide novel insights into how viruses evade antiviral pathways and possibly reveal novel targets for antiviral therapy. The main research aim is to investigate if and how peroxisome proliferation enhances the IFN response and restricts replication of emerging pathogens such as ZIKV and SARS-CoV-2. In Chapters 3 and 4, I focused on two approaches to manipulate peroxisome abundance in cells. The focus of Chapter 3 was to understand if and how the over-expression of PEX11B boosts IFN response and consequently reduces ZIKV replication. In Chapter 4, I investigated if Wnt/ β -catenin pathway inhibitors can be used to pharmacologically modulate peroxisome biogenesis; and determined if and how the inhibitors enhance IFN response and consequently reduce replication of viruses including SARS-CoV-2 and ZIKV.

Chapter 2

Materials and Methods

2.1 Materials

2.1.1 Reagents

The following reagents were purchased from the indicated suppliers and utilized according to the manufacturers' recommendations unless otherwise stated.

Table 2.1 Commercial sources of materials, chemicals, and reagents

<i>Name</i>	<i>Source</i>
1-Bromo 3-chloropropane	Sigma-Aldrich
4', 6-diamidino-2-phenylindole (DAPI)	Sigma-Aldrich
Acetone (Certified ACS)	Thermo Fisher Scientific
Acrylamide/Bis-acrylamide solution 40%	Bio-Rad
Adavivint (SM04690)	Selleckchem
Agar	Difco
Agarose ultrapure electrophoresis grade	Invitrogen
Ammonium acetate	Invitrogen
Ammonium chloride	Sigma-Aldrich
Ammonium persulphate (APS)	Sigma-Aldrich
Ammonium sulfate	Thermo Fisher Scientific
Ampicillin	Sigma-Aldrich
BEGM TM Bronchial Epithelial Cell Growth Medium	Lonza
BEGM TM Bronchial Epithelial Cell Growth Basal Medium	Lonza
BEGM TM Bronchial Epithelial Cell Growth Medium SingleQuots TM Supplements and Growth Factors	Lonza
Bovine serum albumin (BSA)	Sigma-Aldrich
Bromophenol blue	Sigma-Aldrich
CellMask Deep Red	Invitrogen

Chloroform	Thermo Fisher Scientific
Collagen I	Thermo Fisher Scientific
Complete TM EDTA-free protease inhibitors	Roche
Crystal violet	Sigma-Aldrich
Dimethyl sulphoxide (DMSO)	Sigma-Aldrich
Dithiothreitol (DTT)	Sigma-Aldrich
Dulbecco's modified Eagle's medium (DMEM)	Invitrogen
E7449	Selleckchem
ETC-159	Selleckchem
Ethanol	Commercial Alcohols
Ethidium bromide solution	Sigma-Aldrich
Ethylenediaminetetraacetic acid (EDTA)	EMD Chemicals
Fetal bovine serum (FBS)	Invitrogen
Formaldehyde 40% (v/v)	Sigma-Aldrich
Glacial acetic acid	Thermo Fisher
Glucose	Thermo Fisher Scientific
Glycerol	Thermo Fisher Scientific
Glycine	EM Science
Glycylglycine	Sigma Aldrich
Guanidine hydrochloride	Thermo Fisher Scientific
HCS CellMask™ Deep Red Stain	Invitrogen
Hydrochloric acid	Thermo Fisher Scientific
iCRT14	Selleckchem
Isopropanol	Commercial Alcohols
Isopropanol molecular biology grade	Sigma-Aldrich
IWP-O1	Selleckchem
KYA1797K	Selleckchem
LB agar	Invitrogen
L-Glutamine	Invitrogen
L-Histidine	Sigma-Aldrich
L-Leucine	Sigma-Aldrich

LGK-974	Selleckchem
Lipofectamine 2000	Invitrogen
Magnesium chloride (MgCl ₂)	EMD Chemicals
Magnesium phosphate (MgSO ₄)	BDH Inc.
Methanol	Thermo Fisher Scientific
Methylcellulose	Sigma-Aldrich
Minimal essential media (MEM)	Sigma-Aldrich
NCB-0846	Selleckchem
N, N, N', N'-tetramethylethylenediamine (TEMED)	Sigma-Aldrich
Non-essential amino acids (NEAA)	Gibco
Nonidet P-40 (NP-40)/IGEPAL	Sigma-Aldrich
Nuclease-free water	Thermo Fisher
OptiMEM	Invitrogen
Paraformaldehyde EM-grade (16%)	Electron microscopy sciences
Penicillin-streptomycin solution (100X)	Invitrogen
Polyinosinic-polycytidylic acid (poly(I:C))	Sigma Aldrich
Poly-L-lysine	Sigma-Aldrich
pyrvinium	Selleckchem
Halt phosphatase inhibitor cocktail (100x)	Thermofisher
Potassium acetate	Anachemia
Potassium chloride (KCl)	Becton Dickinson & Company
Potassium phosphate (K ₂ PO ₄)	BDH Inc.
ProLong Gold Antifade reagent without DAPI	Life Technologies
Protein A-sepharose	GE Healthcare
Protein G-sepharose	GE Healthcare
Puromycin	Sigma-Aldrich
Random oligonucleotide primers	Invitrogen
Restore™ Western Blot Stripping Buffer	Pierce
Rutaecarpine	Sigma-Aldrich
Sodium chloride (NaCl)	Sigma-Aldrich
Sodium dodecyl sulphate (SDS)	Bio-Rad

Sodium hydroxide	Sigma-Aldrich
Sodium pyruvate	Gibco
Sucrose	EMD Chemicals
TPCK trypsin	Sigma Aldrich
Tris base	VWR
Triton X-100	Invitrogen
Trypsin-EDTA (0.25%)	Invitrogen
Tween 20 (polyoxyethylenesorbitan monolaureate)	Thermo Fisher Scientific
Wnt-C59	Selleckchem.com
UltraPure distilled water	Invitrogen
β -Mercaptoethanol	Thermo Fisher Scientific

Table 2.2 Molecular size standards

<i>Marker</i>	<i>Source</i>
GeneRuler 1 kb DNA Ladder	Fermentas
PageRuler Pre-stained Protein Ladder (10-170 kDa)	Fermentas

Table 2.3 DNA/RNA modifying enzymes

<i>Enzyme</i>	<i>Source</i>
Benzonase	Millipore
Calf intestinal alkaline phosphatase	Antarctica/ Invitrogen
Restriction endonucleases	New England BioLabs/ Invitrogen
RNase A	Invitrogen
T4 DNA ligase	Invitrogen

Table 2.4 Multi-component systems

<i>System</i>	<i>Source</i>
CellTiter-Glo® Luminescent Cell Viability Assay	Promega
Improm-II Reverse Transcriptase system	Promega
Lipofectamine 2000 Transfection reagent	Invitrogen
Lipofectamine RNAiMAX Transfection reagent	Invitrogen
NucleoBond® Xtra Maxi	Macherey-Nagel
NucleoBond® Xtra Mini	Macherey-Nagel
NucleoSpin® RNA isolation kit	Macherey-Nagel
PerfeCTa SYBR Green SuperMix Low Rox	Quanta Biosciences
Platinum Taq PCR System	Invitrogen
QIAEX II gel extraction kit	QIAGEN
QIAGEN plasmid maxi kit	QIAGEN
QIAprep spin miniprep kit	QIAGEN
QIAquick PCR Purification kit	QIAGEN
RNeasy mini kit	QIAGEN
TransIT-LT1 Transfection reagent	Invitrogen

Table 2.5 Detection systems

<i>System</i>	<i>Source</i>
BIO-RAD C1000 Touch™ thermocycler	BIO-RAD
Molecular Imager GelDoc™ XR+ imaging system	BIO-RAD
NanoDrop ND-000 Spectrometer	Thermo Scientific
IX-81 spinning-disk confocal microscope	Olympus
Odyseeey Infrared Imaging System	LiCor
T100 Thermal cycler	BIO-RAD
PVDF membrane (0.45 uM)	Millipore
Ultraviolet gel transilluminator	Thermo Fisher Scientific

2.1.2 Commonly used Buffers and Solutions

Table 2.6 Buffers and Solutions

<i>Name</i>	<i>Ingredients</i>
5x Protein sample buffer	62.5mM Tris-HCl (pH 6.8), 2% (w/v) SDS, 25% (v/v) glycerol, 0.01 % (w/v) bromophenol blue, 5% (v/v) β -mercaptoethanol
6x DNA gel loading buffer	40% (w/v) sucrose, 0.25% (w/v) bromophenol blue, 0.25% (w/v) xylene cyanol FF
Alkaline lysis buffer	200 mM NaOH, 1% (w/v) SDS
Bacteria resuspension buffer	50 mM Tris-HCl (pH 8.0), 10 mM EDTA, 100 μ g/mL RNase A
HEPES-buffered saline (HEBS)	137 mM NaCl, 5 mM KCl, 6 mM dextrose, 0.7 mM Na ₂ HPO ₄ , 20 mM Hepes pH 7.0
LB growth media	1% (w/v) Bacto-tryptone, 0.5% (w/v) Bacto-yeast extract, 0.5% (w/v) NaCl, 0.1% (v/v) 1 M NaOH
Neutralization buffer	3.0 M Potassium acetate (pH 5.5)
NP-40 lysis buffer	50 mM Tris-HCl (pH 7.2), 150 mM NaCl, 2 mM EDTA, 1% (v/v) NP-40, 1 mM fresh DTT
Phosphate buffered saline (PBS)	137 mM NaCl, 2.7 mM KCl, 8 mM Na ₂ HPO ₄ (pH 7.4)
PBS-T	137 mM NaCl, 2.7 mM KCl, 8 mM Na ₂ HPO ₄ (pH 7.4), 0.05% (v/v) Tween-20
RIPA buffer	50 mM Tris-HCl (pH 7.5), 150 mM NaCl, 0.1% (w/v) SDS, 1% (v/v) Triton X-100 1% (w/v) sodium deoxycholate, 5 mM EDTA
SDS-PAGE resolving gel buffer	0.1% SDS, 374 mM Tris-HCl (pH 8.8)

SDS-PAGE running buffer	250 mM glycine, 0.1% SDS, 100 mM Tris Base (pH 8.3)
SDS-PAGE stacking gel buffer	0.1% SDS, 250 mM Tris-HCl (pH 6.8)
TAE	40 mM Tris acetate, 1 mM EDTA (pH 8.0)
Tris-buffered saline (TBS)	137 mM NaCl, 2.7 mM KCl, 24 mM Tris-HCl (pH 7.4)
TBS-T	137 mM NaCl, 2.7 mM KCl, 24 mM Tris-HCl (pH 7.4), 0.05% (v/v) Tween-20
TE	1 mM EDTA, 10 mM Tris-HCl pH 7.5
Transfer buffer	200 mM glycine, 25 mM Tris base (pH 8.3), 20% (v/v) methanol, 0.1% (w/v) SDS

2.1.3 Oligonucleotides

Table 2.7 Oligonucleotides

Primer name	Sequence (5'-3')	Engineered sites*	Usage
PEX11B-myc Forward	TAGCACTAGTATG GGGAAACTG	Sall	Cloning
PEX11B-myc Reverse	GTACGTCGACTTACAGATCCTCTTC TGAGATGAGTTTTTGTTCGGGCTTG AGTCG	SpeI	Cloning
IFIT1 Forward	AGAAGCAGGCAATCACAGAAAA		qRT-PCR
IFIT1 Reverse	CTGAAACCGACCATAGTGGAAAT		qRT-PCR
IFN-β Forward	TAGCACTGGCTGGAATGAGA		qRT-PCR
IFN-β Reverse	TCCTTGGCCTTCAGGTAATG		qRT-PCR
IFN-λ2 Forward	AGTTCCGGGCCTGTATCCAG		qRT-PCR
IFN-λ2 Reverse	GAACCGGTACAGCCAATGGT		qRT-PCR
Mayaro virus Forward	TTCCGAACCAAGTGGGATTC		qRT-PCR

Mayaro virus Reverse	CACTTTACGTAYGGKGATGG	qRT-PCR
MDA5 Forward	GAGCAACTTCTTTCAACCACAG	qRT-PCR
MDA5 Reverse	CACTTCCTTCTGCCAAACTTG	qRT-PCR
Mx2 Forward	CAGCCACCACCAGGAAACA	qRT-PCR
Mx2 Reverse	TTCTGCTCGTACTGGCTGTACAG	qRT-PCR
RIG-I Forward	AGTGAGCATGCACGAATGAA	qRT-PCR
RIG-I Reverse	GGGATCCCTGGAAACACTTT	qRT-PCR
SARS-CoV-2 Forward	CCTACTAAATTAATGATCTCTGCT TTACT	qRT-PCR
SARS-CoV-2 Reverse	CAAGCTATAACGCAGCCTGTA	qRT-PCR
Viperin Forward	CTTTTGCTGGGAAGCTCTTG	qRT-PCR
Viperin Reverse	CAGCTGCTGCTTTCTCCTCT	
Zika virus Forward	CCTTGGATTCTTGAACGAGGA	qRT-PCR
Zika virus Reverse	AGAGCTTCATTCTCCAGATCAA	qRT-PCR
β -actin Forward	CCTGGCACCCAGCACAAT	qRT-PCR
β -actin Reverse	GCCGATCCACACGGAGTAC	qRT-PCR

*Restriction sites in the sequences are underlined

Table 2.8 siRNA sequences

siRNA	Strand	Sequence (5'-3')	Source
siControl	Antisense	rArUrArCrGrCrGrUrArUrUrArUrArCrGrCrGrArUrUrArA rCrGrArC	IDT
	Sense	rCrGrUrUrArArUrCrGrCrGrUrArUrArArUrArCrGrCrGrU AT	IDT
si- β	Antisense	rCrArCrArArCrCrUrUrUrUrArUrUrArCrArUrCrArArGrA AG	IDT
catenin	Sense	rCrUrUrCrUrUrGrArUrGrUrArArUrArArArArGrGrUrUrG rUrGrGrA	IDT

Table 2.9 Plasmid vectors

Plasmid	Source
pCMV-VSV.G	Charles Rice (Rockefeller University)
pGag-Pol	Charles Rice (Rockefeller University)
pTRIP-IRES-AcGFP	Constructed by M. Urbanowski
pTRIP-IRES-AcGFP- myc-PEX11B	Constructed in this study

2.1.4 Antibodies**Table 2.10 Primary antibodies**

Antibody	Catalog number	Dilution	Application	Source
Goat anti-GFP	ab5450	1: 2000	WB	Abcam
Goat anti-ZIKV NS5		1:500	IF, WB	ProSci Inc.
Mouse anti-FLAG epitope (M2)	F3165	1:1000	IF, WB	Sigma Aldrich
Mouse anti-MAVS	Sc-166583	1:1000	WB	Santa Cruz Biotechnology
Mouse anti-myc (4A6)	05-724	1:1000, 1:1000	IF, WB	Millipore
Mouse anti-PMP70	SAB42001	1:1000, 1:1000	WB, IF	Sigma Aldrich
	81			
Mouse anti-SARS-CoV / SARS-CoV-2 (COVID-19) spike antibody [1A9]	GTX6326 04	1:1000	WB, IF	GeneTex
Mouse anti- β -actin	a3853	1:1000	WB	Sigma Adrich
Rabbit anti-Catalase	ab1877	1:1000	WB	Abcam
Rabbit anti-PEX3	ab74505	1:1000	WB	Abcam
Rabbit anti-PEX7	ab133754	1: 500	WB	Abcam
Rabbit anti-PEX11B	ab74507	1:1000	WB	Abcam

Rabbit anti-PEX13	ab190213	1: 500	WB	Abcam
Rabbit anti-PEX14	NBP-71841	1:300	IF	Novus Biologicals
Rabbit anti-PEX19	ab137072	1:1000, 1:5000 1:20	WB, IF, IP	Abcam
Rabbit anti-ZIKV capsid	GTX1333 17	1:1000, 1:20	WB, IP	Genetex
Rabbit anti- β -catenin	ab32572	1:1000	WB, IF	Abcam

*WB: Western blot; IP: immunoprecipitation; IF: immunofluorescence

Table 2.11 Secondary antibodies

Antibody: Conjugate	Catalog Number	Dilution	Application*	Source
Chicken anti-goat::Alexa647	A21469	1: 1000	IF	Invitrogen
Donkey anti-goat::Alexa680	A21084	1:10000	WB	Invitrogen
Donkey anti-mouse::Alexa488	A10038	1: 1000	IF	Invitrogen
Donkey anti-mouse::Alexa680	A10038	1:10000	WB	Invitrogen
Donkey anti-rabbit::Alexa546	A10040	1: 1000	IF	Invitrogen
Donkey anti-rabbit::Alexa800	926-32213	1:10000	WB	Li-COR
Goat anti-rabbit::Alexa680	A21076	1:10000	WB	Invitrogen

*WB: Western blot; IP: immunoprecipitation; IF: immunofluorescence

2.1.5 Cell lines and viruses

2.1.5.1 Cell lines

A549 (human alveolar basal epithelial), U251 (human glioblastoma), HEK293T (human embryonic kidney), Vero cells (Green monkey kidney), Vero-E6 cells (a clone of Vero 76, which is a derivative of Vero cells), Calu-3 cells (human bronchial epithelial), C6/36 (*Aedes albopictus* clone) were purchased from the American Type Culture Collection (Manassas, VA). Primary human fetal astrocytes (HFAs) were prepared as previously described from 15–19 week aborted fetuses (Vivithanaporn et al., 2016) with written consent approved under the protocol 1420 by the University of Alberta Human Research Ethics Board (Biomedical). Primary normal human bronchial epithelial (NHBE) lung cells from lung brush samples were cultured in Collagen I (Thermo Fisher, Catalog #: A1064401) coated flasks or dishes with commercial BEGMTM Bronchial Epithelial Cell Growth Medium (Catalog #: CC-3170, LONZA, Walkersville MD). Lung brushes were obtained from bronchoscopy patients with written consent approved under the protocol 99685 by the University of Alberta Human Research Ethics Board (Biomedical). This culture system consists of BEGMTM Bronchial Epithelial Cell Growth Basal Medium (Catalog #: CC-3171), BEGMTM Bronchial Epithelial Cell Growth Medium SingleQuotsTMSupplements and Growth Factors (Catalog #: CC-4175).

2.1.5.2 Viruses

DENV-2 (New Guinea strain) was provided by Dr. Mike Drebot (Public Health Agency of Canada, Winnipeg, MB). PLCal and PRVABC59 strains of Zika virus were kindly provided by Dr. David Safronetz (Public Health Agency of Canada). The Zika virus (strain H/PF/2013, French Polynesia) was kindly provided by Dr. Michael Diamond (Washington University School of Medicine, St. Louis, MO, USA). The Zika virus (strain MR766) was generated from a

molecular clone kindly provided by Dr. Matthew J. Evans (Icahn School of Medicine at Mount Sinai, New York, NY, USA). DENV and ZIKV manipulations were performed under level-2 containment procedures. DENV-2 stock was generated using Vero cells while ZIKV stock was generated using C6/36 cells. Zika virus and DENV-2 stocks were titered by plaque assay (as described in Section 2.2.4.2). Sendai virus (SeV) Cantell strain was purchased from Charles River Laboratories (Wilmington, MA). Virus manipulations were performed according to level-2 containment procedures. The CANADA/ON-VIDO-01/2020 isolate of SARS-CoV-2 was kindly provided by Dr. Darryl Falzarano, Vaccine and Infectious Disease Organization, University of Saskatchewan. Clinical isolates representing D614G (72B/CA/CALG), Alpha, Beta and Gamma, Delta and Omicron variants of SARS-CoV-2 were kindly provided by Dr. Lorne Tyrrell (University of Alberta). The alphavirus mayaro virus (MAYV) serotype D (strain 07-18066-99) was kindly gifted by Brandy Russell at Centre for Disease Control and Prevention (Fort Collins, CO, USA). SARS-CoV-2 infection studies were performed according to biosafety level 3 containment procedures.

2.2 Methods

2.2.1 Molecular Biology

2.2.1.1 Isolation of plasmid DNA from *Escherichia coli* (E.coli)

Small- and large-scale isolations of plasmid DNA were performed using QIAprep spin miniprep and QIAGEN plasmid maxi or NucleoBond® Xtra Maxi kit respectively (Table 2.4). The concentrations of plasmid DNAs were determined using a NanoDrop ND-1000 Spectrophotometer (Table 2.5). DNA samples were kept at -20 °C for long-term storage.

2.2.1.2 Polymerase chain reaction (PCR)

Platinum High fidelity Taq (Table 2.4) was used for amplification of DNA. A 50 μ L typical reaction contained 100 ng of DNA template, 200 nM of forward and reverse primers, 200 nM of each dNTP, 1 mM MgSO₄, and 2.5-5 U of DNA polymerase. Reactions were performed for 35 cycles in a T100 Thermal cycler (Bio-Rad; Table 2.5).

2.2.1.3 Restriction endonuclease digestion

DNA digestions were carried out in a reaction volume of 20 μ L containing 2 μ g of DNA and 2-10 U of restriction endonuclease in the appropriate digestion buffer. Where indicated, vector DNA was dephosphorylated using calf intestinal alkaline phosphatase (Table 2.3) according to manufacturer's recommendations.

2.2.1.4 Agarose gel electrophoresis

Electrophoresis grade agarose (0.8%-2.5% [w/v]) was dissolved in the TAE buffer by heating (Table 2.6). Ethidium bromide (Table 2.6) was then added to the agarose solution at a final concentration of 0.5 μ g/mL. The agarose gels were kept at room temperature for solidification, after which they were immersed in a TAE buffer. DNA samples were mixed with 6x DNA gel loading dye (Table 2.6), loaded into gels and which were then subjected to ~100 volts (V). Images of DNA fragments were captured using a Molecular Imager GelDoc XR+ imaging system (Table 2.5), the DNA fragments were visualized using an ultraviolet Transilluminator (Table 2.5).

2.2.1.5 Purification of DNA fragments

PCR products were purified using QIAquick PCR purification kits (Table 2.4) prior to restriction endonuclease digestion. Following endonuclease digestion, DNA fragments were

separated by agarose gel electrophoresis. Bands of interest were excised with a clean razor blade. DNA fragments were subsequently extracted from the gel using a QIAEX gel extraction kit (Table 2.4).

2.2.1.6 Ligation of DNA

Inserts and vectors were combined in molar ratios ranging from 3:1-6:1, using no more than 150 ng of DNA in total with a minimum of 1–5 U of T4 DNA ligase (Table 2.3). Negative controls containing only the vector, but no insert were also used. Reaction volumes were kept at 20 μ L and ligations were performed overnight at 16 °C in a thermocycler. To reduce vector self-ligation, vector DNA was dephosphorylated using calf intestinal alkaline phosphatase (Table 2.3).

2.2.1.7 Transformation of *E. coli*.

SubCloning Efficiency chemically-competent DH5 α *E. coli* (Invitrogen) and MAX Efficiency DH5 α *E. coli* (Invitrogen) were used for plasmid DNA transformation. The cells were thawed on ice, then ~40ng of plasmid was added to the thawed cells followed by a 30 min incubation on ice. The bacterial cells were transformed by heat-shock at 42 °C for 45 sec and cooled on ice for 2 min. Transformed cells were cultured in the appropriate antibiotics following the manufacturer's recommendations. Sixteen-hours later, individual colonies were selected and cultured for plasmid isolation the next day.

2.2.2 Construction of AcGFP plus myc-tagged PEX11B expression

Oligonucleotide primers were designed to amplify the desired PEX11B sequence in the pCMV3-PEX11B construct purchased from Sino Biological Inc, and to introduce a myc epitope cassette into the 5' end of the cDNA. To construct the lentiviral plasmid encoding myc-tagged PEX11B, a PCR generated myc-tagged PEX11B cDNA was subcloned into the SpeI and XhoI

sites of the plasmid pTRIP-MCS-IRES-AcGFP. The resulting plasmid pTRIP-MCS-IRES-AcGFP-myc-PEX11B directs independent expression of AcGFP and myc-tagged PEX11B. All primers used for construction of plasmids are listed in Table 2.7. The authenticity of each plasmid construct was verified by DNA sequencing at The Applied Genomics Centre (University of Alberta).

2.2.3 Cell culture and transfection

2.2.3.1 Cell culture maintenance

A549, HEK293T, U251, Vero and Vero E6 cells were cultured in Dulbecco's modified Eagle's medium (DMEM; Table 2.1) containing 10% (v/v) heat-inactivated FBS (Table 2.1), 4.5 g/L D-glucose (Table 2.1), 2 mM glutamine (Table 2.1), 25 mM HEPES (pH 7.4; Table 2.1), 110 mg/L sodium pyruvate (Table 2.1), 100 units/mL penicillin and 100 µg/mL streptomycin (Table 2.1). HFAs were grown in Minimum Essential Media (Table 2.1) supplemented with 10% FBS, L-glutamine, MEM non-essential amino acids (Table 2.1), sodium pyruvate (Table 2.1), and 1 g/mL glucose (Table 2.1). Calu-3 cells were cultured in Minimum Essential Media supplemented with 100 U/mL penicillin and streptomycin, 1 mM HEPES, 20% heat-inactivated FBS, L-glutamine, MEM non-essential amino acids, and sodium pyruvate. Cells were incubated at 37 °C in a humidified atmosphere with 5% CO₂. Primary normal human bronchial epithelial (NHBE) lung cells were cultured in Collagen I (Table 2.1) coated flasks or dishes with commercial BEGM™ Bronchial Epithelial Cell Growth Medium (Table 2.1). This culture system contains BEGM™ Bronchial Epithelial Cell Growth Basal Medium (Table 2.1) and BEGM™ Bronchial Epithelial Cell Growth Medium SingleQuots™ Supplements and Growth Factors (Table 2.1).

2.2.3.2 Transient transfection of cell lines

HEK293T and U251 cells were transiently transfected with plasmids using Lipofectamine 2000 or TransIT-LT1 transfection reagent (Table 2.4). Twenty-four hours prior to transfection, HEK293T (3×10^5 per well), were seeded into 12-well plates. Cells were then transfected with 1 μ g of plasmid DNAs mixed with 2 μ L of Lipofectamine 2000 in Opti-MEM media (Table 2.1). Transfected cells were processed for experimental analysis 48-hr post-transfection as indicated. For transfection of poly(I:C) (Table 2.1) into U251 cells, 1 μ g of the dsRNA were mixed with 3 μ L of TransIT-LT1 in OptiMEM media (Table 2.1). Transfected cells were processed for experimental analysis 8- or 16-hr post-transfection as indicated. When other culture dish formats were used, the number of cells, DNA plasmids and transfection reagents were scaled up or down according to the surface area of the dish/well.

2.2.3.3 RNA interference

Small interfering RNAs (siRNAs) were used to transiently knockdown expression of β -catenin in transfected cells (Table 2.8). A549 cells (1×10^5 per well) were seeded into 12-well plates 24 hr before transfection. Cells were then transfected with 30 pmol of non-targeting control siRNA (siControl) or siRNAs specific for human β -catenin mRNA. The siRNAs (200 nM, final concentration) were mixed with 4 μ L of Lipofectamine RNAiMAX reagent (Table 2.4) in Opti-MEM media prior to addition to cells according to manufacturer's recommendations. Cells were incubated at 37 °C for another 48 hr before processed for further analyses.

2.2.4 Virology techniques

2.2.4.1 Virus infection

DENV-2, ZIKV and MAYV infection: Experiments with DENV-2, ZIKV and MAYV were conducted under CL-2 conditions. Virus stocks were diluted in DMEM lacking FBS and antibiotics and then added to cells that had been washed with PBS. Cells were infected with viruses at multiplicities of infection (MOIs) of 0.5-5, depending on the experimental objectives. Cells were incubated with the virus for 2 hours at 37°C, after which the inoculum was replaced with normal growth media. Infected cultures were kept at 37°C until experimental analyses.

Sendai virus infection: Experiments with Sendai virus were handled under CL-2 conditions. Cells were challenged with 100 HAU/ml of Sendai virus for 8 or 16 hours. Infected cultures were kept at 37°C until experimental analyses.

2.2.4.2 DENV-2, ZIKV and MAYV plaque assays

The day before infection, Vero cells (1.5×10^5 per well) were seeded into 24-well plates. Culture supernatants from DENV-2-, ZIKV-, or MAYV infected cells were 10-fold serially diluted in serum-free DMEM. To each well, 100 μ L of DMEM was added, after which 100 μ L of virus-containing dilution was added. Plates were placed in a 37°C with 5% CO₂ incubator for one hour, after which 1 mL of DMEM containing 0.5% methylcellulose (Table 2.1), and 100 units/mL penicillin and 100 μ g/mL streptomycin was added to each well. After 2, 4 and 6 days (for MAYV, ZIKV and DENV-2 respectively), cells were fixed with formaldehyde at a final concentration of 10% (v/v), and then stained with 1% (w/v) crystal violet in 20% (v/v) methanol (Table 2.1) for one hour. After rinsing wells with water, the plates were dried and the numbers of plaques in each well were counted.

2.2.4.3 Production and use of recombinant lentiviruses

Lentiviruses encoding myc-tagged PEX11B: To produce infectious lentiviral pseudoparticles, HEK293T cells (3×10^6) grown in 100 mm-diameter dishes were co-transfected with 5.6 μg of pTRIP-IRES-AcGFP- myc-PEX11B or pTRIP-IRES-AcGFP (Urbanowski and Hobman, 2013), 5.6 μg of pGag-Pol and 1.6 μg of pHCMV-VSV G using 48 μL of TransIT-LT1 transfection reagent. Transfection mixtures were added to cells with DMEM containing 3% (v/v) FBS, 4 $\mu\text{g}/\text{mL}$ polybrene (Table 2.1) and 20 mM HEPES (pH 7.4). and incubated for 48-hr. Lentivirus-containing media were collected and centrifuged at 1000xg to remove cell debris, passed through a 0.45 μm filter and then aliquoted into cryo-vials and stored at -80 °C until required.

To transduce U251 cells (4×10^5 per well), lentivirus stocks were diluted in DMEM containing 3% (v/v) FBS, polybrene (4 $\mu\text{g}/\text{mL}$ polybrene) and HEPES (20mM, pH 7.4) and then spinoculated for 1 hr at 37°C in an Eppendorf A-4-62 rotor. The lentivirus inoculum was replaced with DMEM containing 10% FBS. Transduced cells were analyzed 48 hr post-transduction.

2.2.5 Microscopy

2.2.5.1 Indirect Immunofluorescence

A549 (1×10^5 per well), HFA (2×10^5 per well) and U251 (1×10^5 per well) cells were cultured in 12-well plates with coverslips and then processed for indirect immunofluorescence microscopy after 24-, 48-, or 72-hr post-infection, post-transfection, post-transduction or post-treatment as indicated. Cells were washed with PBS three times and fixed with 4% (v/v) PFA for 10 min at room temperature. Fixed cells were washed three times with PBS before permeabilization with Blocking Buffer containing 3% (w/v) BSA and 0.2% (v/v) Triton X-100

(Table 2.1) for 1-hr at room temperature. Cover slips were incubated with primary antibodies (as indicated in Table 2.9) diluted in the same Blocking Buffer, followed by incubation at 4 °C overnight or 2-hr at room temperature. Following primary antibody incubation, coverslips were washed three times with PBS for 15 min each wash. Coverslips were then incubated with secondary antibodies (Table 2.10) and 1 µg/mL DAPI (Table 2.1) (as indicated in Table 2.9) diluted in the same Blocking Buffer at room temperature for 1-hr, which was followed by three PBS washes, for a total of 45-min. For experiments determining peroxisome density, coverslips were incubated with CellMask Deep Red (diluted in PBS according to manufacturer's recommendations) (Table 2.1) at room temperature for 30 min, which was followed by PBS wash for three times, 15 min each. Coverslips were mounted onto slides with Prolong Gold anti-fade reagent without DAPI (Table 2.1). Images were acquired on an Olympus I X 81 spinning-disk confocal microscope equipped with 60×/1.42 oil or 20×/0.85 -numerical-aperture oil PlanApo N objectives (Table 2.5). All images were acquired and processed using Volocity 6.2.1 software (PerkinElmer).

2.2.5.2 Quantification of peroxisomes and cell volume

Z-stack images acquired using a confocal microscope were exported from Volocity 6.2.1 as an OEM.tiff file. The exported images were then processed using Imaris 7.2.3 software (Bitplane, Concord, MA, USA). Peroxisomes within polygonal areas that excluded the nucleus were quantified (quality and voxel). Within the selected regions, the absolute intensity of the peroxisomes was determined and then entered into a Microsoft Excel spreadsheet. The data were then analyzed using the student's t-test. In each cell, peroxisomes were selected based on the absolute pixel intensity in the corresponding channel, and their numbers were then determined. Depending on the primary antibodies used, only those PEX14/PMP70/SKL-positive structures

with volumes between 0.001 and 0.05 μm^3 were included for measurement. Cell volume was determined by CellMask Deep Red staining and the values were then entered into a Microsoft Excel spreadsheet. Peroxisome density was calculated by dividing the number of peroxisomes by the cell volume.

2.2.6 Protein gel electrophoresis and detection

2.2.6.1 Preparation of protein samples

Cells were washed three times with cold PBS on ice, and then lysed in RIPA buffer (Table 2.6) containing a cocktail of protease inhibitors. Cell lysates were incubated on ice for 30 min and then centrifuged at 12,000 x g for 15 min at 4°C after which the supernatants were collected. The cells lysates were then mixed with a 5x Protein Sample Buffer (Table 2.6) containing 2-5% (v/v) β -mercaptoethanol and 0.2 μL /sample Benzoyl-DL-homoserine at a 1:5 ratio and then heated at 95 °C for 5 min. Proteins were resolved by SDS-PAGE, transferred to immobilon-polyvinylidene fluoride (PVDF) membranes (Table 2.5) and then detected by Western blotting as described below.

2.2.6.2 Sodium dodecyl-sulphate polyacrylamide gel electrophoresis (SDS-PAGE)

Proteins were separated by discontinuous gel electrophoresis (5% stacking gel and 10% resolving gels). Stacking gels were prepared by adding 5% acrylamide/bis-acrylamide to Stacking gel buffer (Table 2.6) with 0.1% (w/v) ammonium persulphate and 0.1% (v/v) TEMED. Resolving gels were prepared by combining appropriate amounts of acrylamide/bisacrylamide with Resolving gel buffer (Table 2.6), 0.1% (w/v) APS and 0.1% (v/v) TEMED. Protein samples were mixed with a 5x protein sample buffer (Table 2.6) and denatured at 95°C for 10 minutes. Electrophoresis was performed in a Bio-Rad Mini-Protean III system using SDS-PAGE running

buffer (Table 2.6) at 90 V. After electrophoresis, gels were processed for Western Blot analysis as described below.

2.2.6.3 Western Blot analysis

Following SDS-PAGE, proteins were transferred from gels to 0.45 μm PVDF membranes. PVDF membranes were incubated with methanol for at least 20 min at room temperature for activation and then incubated in Transfer Buffer (Table 2.6) for equilibration. Transfer was carried out using Western Blot Transfer Buffer (Table 2.6) and a Mini Trans-Blot Electrophoresis transfer cell apparatus (Bio-Rad) at a constant current of 320 mA for 2 hr in an ice-filled bucket. After the completion of the transfer, the PVDF membranes were incubated with a Blocking Buffer containing PBS-T or TBS-T (Table 2.6) with 5% (w/v) skim milk powder for at least 1 hr at room temperature on a rocking device.

Membranes were incubated with primary antibodies diluted in PBS-T or TBS-T containing 5% (w/v) skim milk powder for 3 hr at room temperature or at 4 °C overnight on a rocking device. After three washes (15 min each) with PBS-T or TBS-T at room temperature, membranes were incubated with fluorophore-conjugated secondary antibodies diluted in PBS-T or TBS-T containing 5% (w/v) skim milk powder for a minimum of 1 hr. Finally, membranes were washed three times with PBS-T or TBS-T (15 min each) and processed for protein detection as described below.

2.2.6.4 Detection of fluorophore-conjugated secondary antibodies

Membranes were washed with PBS (minimum of 5 min at room temperature) to remove any residual Tween-20. They were placed face-down on the scanner bed of an Odyssey Infrared Imaging system. The membranes were then scanned at 84- μm resolution on a quality setting of

“Medium” or “High”. Quantification of proteins was performed using Odyssey Image Studio Lite software Version 5.2.

2.2.7 Biochemical analysis of protein-protein interactions

2.2.7.1 Co-immunoprecipitation

Co-immunoprecipitation of PEX19 and ZIKV capsid protein: U251 cells (3×10^6) were seeded into p100 dishes one day before infection. The cells were infected with ZIKV (MOI=3) for 48 hr. Cells were washed once with ice-cold PBS and then lysed with NP-40 Lysis Buffer (Table 2.6) containing Complete protease inhibitors (Table 2.1) on ice for 30 min. The lysates were clarified by centrifuging at 14,000 rpm in a microfuge for 10 min at 4 °C. Small aliquots were kept for loading controls. The rest of the lysates were pre-cleared with protein G or protein A Sepharose beads (Table 2.1) for 10 min at 4 °C with rotation, after which the lysates were incubated with anti-PEX19 or anti-capsid antibodies for 3 hours at 4 °C with rotation. Twenty-microliters of protein A-Sepharose or protein G-Sepharose beads (50% suspension) were added to samples. Together, they were incubated for 2 hr at 4 °C with rotation. After centrifuging at 500xg for 15 seconds, the immunoprecipitants were washed three times with NP40 Lysis buffer, and the bound proteins were eluted by heating at 95 °C for 10 min in Protein Sample Buffer. Proteins were separated by SDS-PAGE and transferred to PVDF membranes for Western Blotting analysis.

2.2.8 RNA techniques

2.2.8.1 RNA isolation

Total RNA from cell lysates was isolated using RNeasy mini-Kits (QIAGEN) or Nucleospin RNA isolation kit (Macherey-Nagel) (Table 2.4) and then stored at -80 °C until required for use.

2.2.8.2 cDNA synthesis

The Improm-II Reverse Transcriptase system (Promega) (Table 2.4) was used to reverse transcribe isolated RNA into cDNAs. In a typical reaction (20 µL), 4 µL of RNA and 2 µL of random primers (200 ng/ µL) were added. cDNA synthesis reactions were carried out at 42 °C for 2 hr in a Bio-Rad T100 Thermal cycler. Reactions were terminated by incubation at 75 °C for 10 min after which the cDNAs were diluted (1:3) in nuclease-free water and then stored at -20 °C until use.

2.2.8.3 Quantitative reverse-transcription PCR (qRT-PCR)

QRT-PCR reactions were conducted using the Perfecta SYBR Green Supermix low Rox real-time PCR kit (Quanta Biosciences) (Table 2.4) in a BIO-RAD C1000 Touch™ thermocycler (Table 2.5). Reactions (15 µL) were performed in duplicate and contained 3 µL of cDNA and 100 nM of gene-specific primer sets (forward and reverse). The amplification program consisted of an initial denaturing step at 94 °C for 2 min, followed by 40 cycles of 20 sec at 94 °C, 20 sec at 55 °C, and 20 sec at 68 °C. Fluorescence was read after the 55 °C annealing step in each cycle. To obtain melting curves for analysis of gene product specificity, fluorescence was read after the amplification step at 68 °C in the final cycle. The comparative CT ($\Delta\Delta CT$) method (Livak and Schmittgen, 2001) was used to quantify the relative levels of each RNA transcript. The ΔCT

values were calculated using β -actin mRNA or GAPDH (CT value) as the internal control. The $\Delta\Delta$ CT values were determined using the appropriate control samples as the reference values. Relative levels of mRNAs of the gene of interest were calculated using the formula $2^{(-\Delta\Delta$ CT)

2.2.9 EC50 and CC50 determination

EC50 determination: The 50% effective concentrations of Wnt inhibitors (IWP-O1, KYA1797K and Pyrvinium) against SARS-CoV-2 (EC50; the compound concentration that reduces viral titers by 50%) were determined by using plaque assay. 5×10^4 Calu-3 cells were seeded and were grown in a 96-well plate and were pre-treated with 10-fold serial dilutions of compounds (0.01 nM to 1000 nM) or DMSO alone. After 24 hours, cells were infected with SARS-CoV-2/CANADA/VIDO 01/2020 strain (MOI=0.5) and virus-containing media were collected 24-hr later and then subjected to plaque assay. The number of plaques from each concentration of the compound treatment was counted and the viral titers were calculated.

CC50 determination: To determine CC50 values (the compound concentration that reduces the cell viability by 50%), Calu-3 cells were treated with the same concentration range of Wnt/ β -catenin as described above except that they were not infected. Seventy-two hours after drug addition, cell viabilities were measured using a CellTiter-Glo® Luminescent Cell Viability Assay kit (Promega; Madison, WI, USA). Briefly, cells grown in opaque-walled 96-well plates were treated with DMSO or Wnt/ β -catenin inhibitors for 72 hours. After removing culture media, 100 μ l of CellTiter-Glo® Reagent and 100 μ l of PBS were added to each well after which the plate was placed on an orbital shaker for 2 minutes to induce cell lysis. The plate was incubated at room temperature for an additional 10 minutes after which luminescence was recorded at an integration time of 1 second per well using Synergy HTX plate reader (Biotek; Winooski, VT, USA). EC50 and CC50 values were determined using logarithmic interpolation and data were then analyzed

and graphed using GraphPad Prism software version 7.0 (GRAPH PAD software Inc, California, USA). Selectivity Indexes were calculated by dividing CC50 by EC50.

Chapter 3

Interplay between Zika Virus and Peroxisomes during Infection

A version of this chapter has been published in:

“Wong CP, Xu Z, Hou S, et al. Interplay between Zika Virus and Peroxisomes during Infection. Cells. 2019;8(7):725. Published 2019 Jul 15. doi:10.3390/cells8070725”

3.1 Rationale

Zika virus (ZIKV) infection most often causes a mild self-limiting illness in humans. It started to raise public concerns over its association with neurological disorders after the outbreak in French Polynesia between 2013 and 2014 (Cao-Lormeau *et al.*, 2016). Since then, ZIKV has been considered an important human pathogen that can cause congenital defects in the fetus including microcephaly and neurological conditions in adults (e.g. Guillain-Barré syndrome). Molecular and immunologic studies have demonstrated the presence of ZIKV RNA or viral particles in the brains of fetuses diagnosed with microcephaly (Brasil *et al.*, 2016; Calvet *et al.*, 2016; de Araújo *et al.*, 2016; Driggers *et al.*, 2016; Oliveira Melo *et al.*, 2016) suggesting that the virus is to establish persistent infection in the fetal brain. Unfortunately, there are no specific therapeutic antivirals available for ZIKV. Mouse models have provided important information about ZIKV pathogenesis. For example, ZIKV infection of mice that are unable to mount an interferon (IFN) response resulted in higher viral loads and more severe clinical disease (Aliota *et al.*, 2016; Lazear *et al.*, 2016; Yockey *et al.*, 2016). These observations highlight the critical role of IFN in restricting replication of ZIKV.

In addition to localizing to mitochondria, a pool of the antiviral adaptor molecule MAVS is present on peroxisomes which allows them to function as antiviral signaling hubs that elicit type-I and type-III IFN signaling in response to viral infection (Dixit *et al.*, 2010; Odendall *et al.*, 2014). To counteract the antiviral response initiated by peroxisomes, viruses have evolved strategies to impair peroxisome biogenesis during infection, examples of which include depleting important peroxisomal proteins and interfering with transcription of the genes encoding peroxisomal proteins (reviewed in (Wong *et al.*, 2018)). Our laboratory is one of the pioneers in exploring the virus-peroxisome interactions. One study from the Hobman lab revealed that WNV

and DENV infection impairs peroxisome biogenesis to abrogate the innate immune response (You *et al.*, 2015). The study analyzed the functional consequences of the interaction between WNV and DENV capsid proteins and PEX19, a peroxisomal protein which is crucial for *de novo* biosynthesis of peroxisomes. It demonstrated that WNV and DENV infection induces loss of PEX19 and reduction in peroxisome numbers. The role of peroxisomes as antiviral signaling hubs was further validated in this study which showed that WNV and DENV suppressed induction of type-III IFN, likely as a result of reducing PEX19 levels and consequently the peroxisome pool.

Growing evidence indicates that other viruses impair antiviral signaling by downregulating peroxisome biogenesis or inhibiting functions of this organelle. HCV NS3 protease cleaves MAVS localized on peroxisomes to dampen the IFN induction (Bender *et al.*, 2015; Ferreira *et al.*, 2016). The alphacoronavirus porcine diarrhea epidemic virus NSP1 causes reduction of peroxisome numbers and inhibits the induction of type III IFN expression (Zhang *et al.*, 2018). HIV infection reduces peroxisome number by upregulating miRNAs that target peroxisome biogenesis factors (Xu *et al.*, 2017).

Given that multiple flaviviruses impairing peroxisome biogenesis during infection, I hypothesized that the recently emerged flavivirus ZIKV employs a similar strategy during infection of fetal brain tissue. I investigated the interplay between ZIKV and peroxisomes during infection of primary human fetal astrocytes (HFAs) and human astrocytoma U251 cells. ZIKV infection resulted in significant downregulation of peroxisomes in these cell types, an effect that appears to be mediated through the viral capsid protein, which binds PEX19. Conversely, we observed that inducing peroxisome proliferation by over-expression of PEX11B resulted in enhanced IFN production and reduced ZIKV replication.

3.2 Results

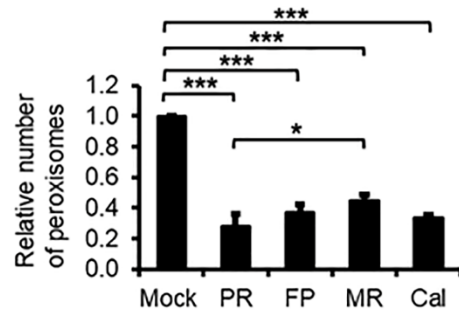
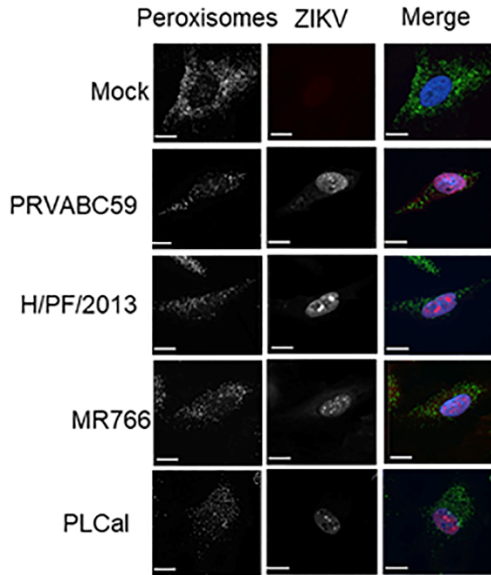
3.2.1 ZIKV infection reduces number of peroxisomes in primary human fetal astrocytes (HFAs) and U251 cells

Besides mediating innate immune responses, peroxisomes play critical roles in metabolism of lipids that affect the central nervous system. We therefore investigated the consequences of ZIKV infection on these organelles in astrocytes, which are the most abundant cell type in the brain. Primary HFAs were infected with four different ZIKV strains including two pandemic strains of Asian lineage; one isolated during the 2015/2016 outbreak in South America (PRVABC59) and one isolated from an outbreak in French Polynesia in 2013 (H/PF/2013). The other two strains included a third contemporary Asian strain (PLCa1) isolated from a returning Canadian traveler (Shepard et al., 2014) and the prototype African strain MR766. To investigate the number of peroxisomes in ZIKV infected primary HFAs, cells were infected with ZIKV and then processed for immunofluorescence and confocal microscopy analysis using antibodies to pmp70 and ZIKV NS5. Data in **Figure 3.1A** show that infection of the cells with different strains of ZIKV reduced the numbers of peroxisomes by more than 60%. To confirm the apparent loss of peroxisomes was not simply depletion of pmp70 alone, we used Western blotting to examine the abundance of multiple critical peroxisome biogenesis factors including PEX3, PEX7, PEX11B, PEX13 and PEX19.

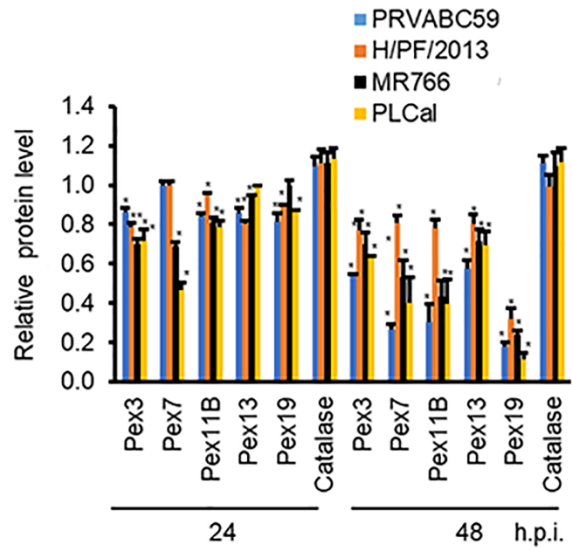
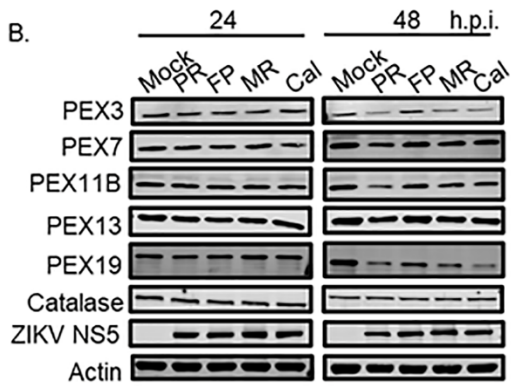
Consistent loss of peroxisomal proteins was observed in HFAs infected with ZIKV between 24- and 48-hr. At the latter timepoint, there was a dramatic drop in the levels of PEX3, PEX7, PEX11B, PEX13 and PEX19 (**Figure 3.1B**). Among these peroxisome biogenesis factors, PEX19 was the most affected with levels being reduced by more than 80% in ZIKV-infected cells. In contrast, levels of the peroxisomal matrix protein catalase were not affected by ZIKV infection

(Figure 3.1B). This indicates that the effects of ZIKV infection on peroxisome-associated proteins are highly specific. The greatest loss of peroxisomal protein levels was observed in HFAs infected with PRVABC59 and PLCal strains, a phenomenon that correlates with their increased replication in HFAs. In fact, the titers of PRVABC59 and PLCal strains were consistently lower than the other two strains of ZIKV **(Figure 3.1C).**

A.



B.



C.

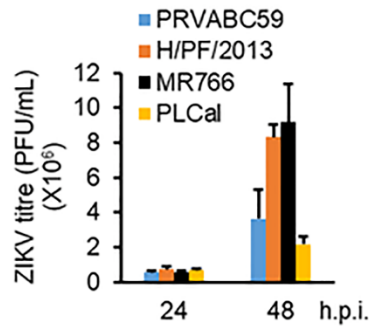
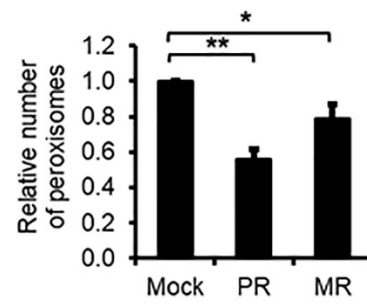
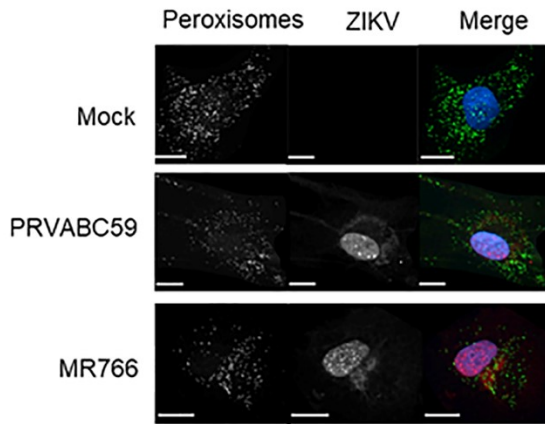


Figure 3.1. Zika virus (ZIKV) infection reduces number of peroxisomes in primary human fetal astrocytes (HFAs). (A) HFAs were infected with ZIKV (PRVABC59 (PR), H/PF/2013 (FP), MR766 (MR) or PLCal (Cal) strains) (MOI = 3) for 48 h and then processed for confocal microscopy. Peroxisomes were detected using a mouse monoclonal to PMP70 and infected cells were detected using a goat polyclonal antibody to ZIKV NS5. Primary antibodies were detected by donkey anti-mouse IgG conjugated to Alexa Fluor 488 and chicken anti-goat IgG conjugated to Alexa Fluor 647. Nuclei were stained with DAPI. Images were acquired using a spinning disc confocal microscope. Quantification of peroxisome numbers in 90 cells from three independent experiments were performed using Volocity image analysis software and the average number of peroxisomes were plotted. The average number of peroxisomes in mock-treated cells was normalized to 1.0. Bars represent standard error of the mean. *** $p < 0.001$, * $p < 0.05$. (B) HFAs infected with ZIKV strains (MOI = 5) were harvested at 24 h and 48 h.p.i. after which levels of catalase, PEX3, PEX7, PEX11B, PEX13, PEX19, ZIKV NS5 and actin were examined by Western blotting using the appropriate antibodies. Levels of actin and ZIKV NS5 protein are shown as loading and infection controls respectively. The relative levels of peroxisomal proteins (compared to actin) from three independent experiments were averaged and plotted. The average levels of peroxisomal proteins in mock-infected cells were normalized to 1.0. Error bars represent standard error of the mean. * $p < 0.05$. (C) HFAs infected with ZIKV (MOI = 1) were harvested at 24 h and 48 h.p.i after which cell supernatants were collected and viral titres were determined by plaque assay. The data are averaged from the results of three independent experiments. Bars represent standard error of the mean.

Given that primary HFAs have a finite lifespan and limited expansion capacity, we assessed whether the human astrocytoma U251 cell line could be used to further examine the interplay between ZIKV infection and peroxisome biogenesis. Similar to HFAs, infection of PRVABC59 and MR766 caused impaired peroxisome biogenesis in U251 cells. In comparison to MR766, infection of PRVABC59 caused greater reduction of peroxisome numbers and depletion of peroxisomal protein levels in U251 cells (**Figure 3.2A and Figure 3.2B**).

A.



B.

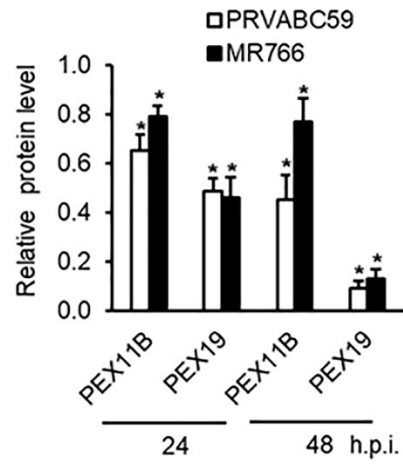
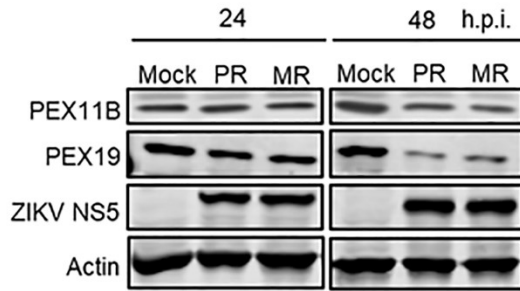


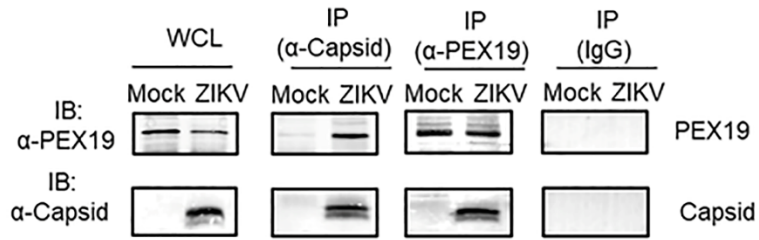
Figure 3.2. ZIKV infection reduces number of peroxisomes in U251 cells. (A) U251 cells were infected with ZIKV PRVABC59 (PR) or MR766 (MR) at MOI = 3 for 48 h and then processed for confocal microscopy. Peroxisomes were detected using a mouse monoclonal to PMP70 and infected cells were detected using a goat polyclonal antibody to ZIKV NS5. Primary antibodies were detected by donkey anti-mouse IgG conjugated to Alexa Fluor 488 and chicken anti-goat IgG conjugated to Alexa Fluor 647. Nuclei were stained with DAPI. Images were acquired using a spinning disc confocal microscope. Quantification of peroxisome numbers in 90 cells from three independent experiments were performed using Volocity image analysis software and the average number of peroxisomes were plotted. The average number of peroxisomes in mock-treated cells was normalized to 1.0. Bars represent standard error of the mean. ** $p < 0.01$, * $p < 0.05$. **(B)** U251 cells infected with ZIKV PRVABC59 or MR766 (MOI = 5) were harvested at 24 hr or 48 h.p.i. after which levels PEX11B, PEX19, ZIKV NS5 and actin were examined by Western blotting using the appropriate antibodies. Levels of actin and ZIKV NS5 protein are shown as loading and infection controls respectively. The relative levels of PEX11B and PEX19 proteins (compared to actin) from three independent experiments were averaged and plotted. The average levels of peroxisomal proteins in mock-infected cells were normalized to 1.0. Error bars represent standard error of the mean. * $p < 0.05$.

3.2.2 ZIKV capsid protein forms a stable complex with PEX19 and causes loss of peroxisomes

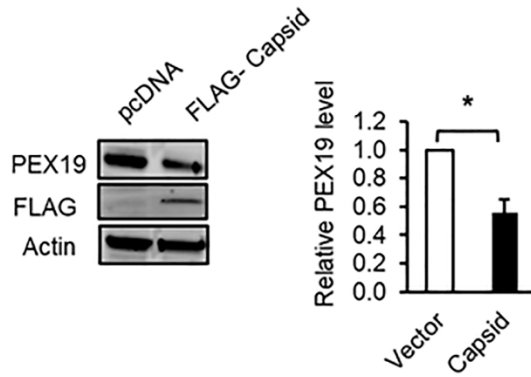
The fact that the capsid proteins of the flaviviruses WNV and DENV bind to PEX19 during infection, provided strong rationale to further investigate if the ZIKV capsid protein behaves similarly in interacting with PEX19 during infection. To investigate this, U251 cells were infected with ZIKV and then subjected to immunoprecipitation (IP) using antibodies to PEX19 and ZIKV capsid protein. Data from co-IP in **Figure 3.3A** reveals that PEX19 forms a stable complex with the capsid protein in ZIKV infected cells.

To analyze the functional consequences of the interaction between PEX19 and ZIKV capsid protein, Western blotting was used to assess PEX19 protein level in cells transfected with ZIKV capsid protein plasmid. In parallel, the numbers of peroxisomes were assessed in capsid-expressing cells by indirect immunofluorescence microscopy using antibodies to FLAG and the tripeptide Ser-Lys-Leu (SKL), a targeting motif found at the carboxyl termini of many peroxisomal matrix proteins (Gould *et al.*, 1989). Western blotting results in **Figure 3.3B** show that capsid expression reduced PEX19 protein levels by more than 50%. In **Figure 3.3C**, it can be seen that the peroxisome pools are reduced by 30% in capsid-expressing cells. Together, expression of ZIKV capsid protein in the absence of other viral proteins causes reduction of PEX19 protein levels and consequent loss of peroxisomes. This suggests that the capsid protein plays a pivotal role in disrupting peroxisome biogenesis during ZIKV infection. However, as the effect of capsid expression in reducing peroxisome numbers is less than what is observed during ZIKV infection, it is worth investigating if other viral proteins are involved in the downregulation of peroxisome biogenesis.

A.



B.



C.

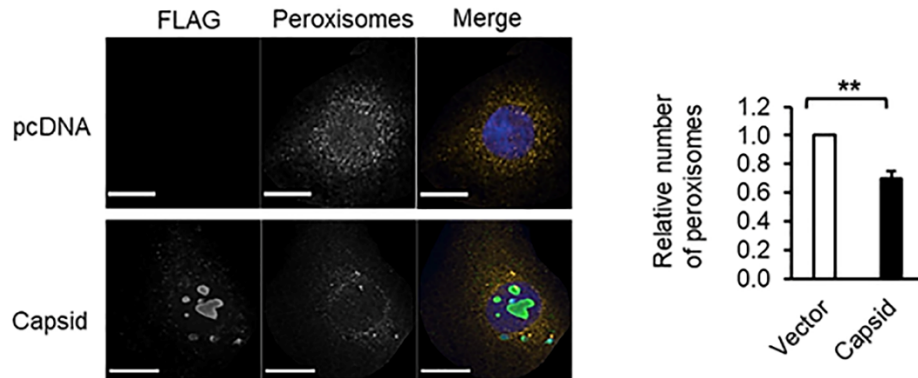


Figure 3.3. Expression of ZIKV capsid protein causes loss of peroxisomes. (A) U251 cells infected with ZIKV PRVABC59 (MOI = 1) were harvested at 48 h.p.i., after which the cell lysates were subjected to immunoprecipitation (IP) with rabbit anti-ZIKV capsid, rabbit anti-PEX19, or rabbit IgG followed by SDS-PAGE and Western blotting (IB) with antibodies to PEX19 or ZIKV-capsid. WCL, whole-cell lysate. Rabbit IgG was used as a control to evaluate non-specific binding. (B) HEK293T cells transfected with a plasmid encoding FLAG-tagged ZIKV capsid or empty vector (pcDNA3.1) were harvested at 48 h post transfection after which levels of PEX19, ZIKV-capsid and actin were examined by Western blotting using the appropriate antibodies. Levels of actin are shown as a loading control. The relative levels of PEX19 (compared to actin) from three independent experiments were averaged and plotted. The average level of PEX19 protein in cells transfected with the empty vector were normalized to 1.0. Error bars represent standard error of the mean. * $p < 0.05$. (C) U251 cells transfected with a plasmid encoding FLAG-tagged ZIKV capsid or empty vector (pcDNA3.1) were processed for confocal microscopy at 48 h post transfection. Peroxisomes were detected using a rabbit polyclonal antibody to the tri-peptide SKL, and transfected cells expressing capsid were detected with a mouse anti-FLAG epitope antibody. Primary antibodies were detected by donkey anti-rabbit IgG conjugated to Alexa Fluor 546 and donkey anti-mouse IgG conjugated to Alexa Fluor 488. Nuclei were stained with DAPI. Images were acquired using a spinning disc confocal microscope. Quantification of peroxisome numbers (SKL-positive structures) in 90 cells from three independent experiments were performed using Volocity image analysis software and the average number of peroxisomes were plotted. The average number of peroxisomes in mock-treated cells was normalized to 1.0. Bars represent standard error of the mean. ** $p < 0.01$.

3.2.3 Over-expression of PEX11B suppresses ZIKV replication

Given that multiple flaviviruses appear to weaken host innate immunity by depleting peroxisomes, I next tested whether increasing the peroxisome pool would boost the innate immune response and inhibit ZIKV replication. PEX11B is a peroxisomal membrane protein that increases peroxisome numbers by membrane remodeling, peroxisome elongation and division (Abe and Fujiki, 1998; Tanaka *et al.*, 2003). Lentiviruses encoding the reporter protein AcGFP alone as a control or AcGFP plus myc-tagged PEX11B were used to transduce U251 and Vero cells. Transduced cells were processed for indirect immunofluorescence using an antibody to the tripeptide SKL to detect peroxisomes. Transduced cells were identified by detecting AcGFP expression. Results of confocal microscopy and image analysis showed that 48-hr post-transduction, over-expression of PEX11B resulted in a 20% increase in the number of peroxisomes in both U251 cells and Vero cells (**Figure 3.4A**). Next, I quantified the effect of PEX11B over-expression on ZIKV replication. U251, A549 or Vero transduced with lentiviruses encoding the AcGFP alone or AcGFP plus myc-tagged PEX11B were infected with ZIKV after which plaque assays and qRT-PCR were used to assess the viral titers and relative levels of viral RNA. Results in **Figure 3.4B and C** show that over-expression of PEX11B significantly reduces viral replication and production of infectious virions in U251 and A549 cells. Specifically, viral titers were reduced by more than 80% and 60% respectively in U251 and A549 cells over-expressing PEX11B. Similarly, viral RNA levels were reduced 60-70% in these cells. In contrast, while over-expression of PEX11B increased the numbers of peroxisomes in Vero cells (**Figure 3.4A**), it had no effect on ZIKV replication or viral titers (**Figure 3.4B and C**). The inhibition of ZIKV replication in U251 or A549 cells was not due to cytotoxicity from over-expression of PEX11B (**Figure 3.4D**).

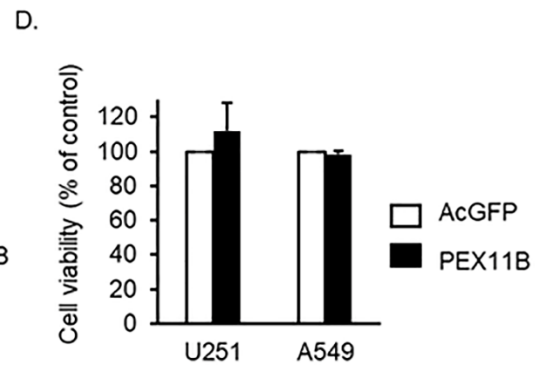
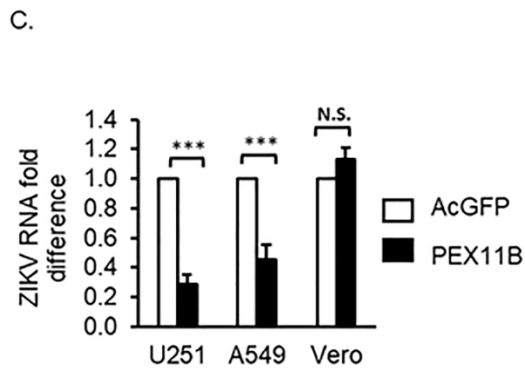
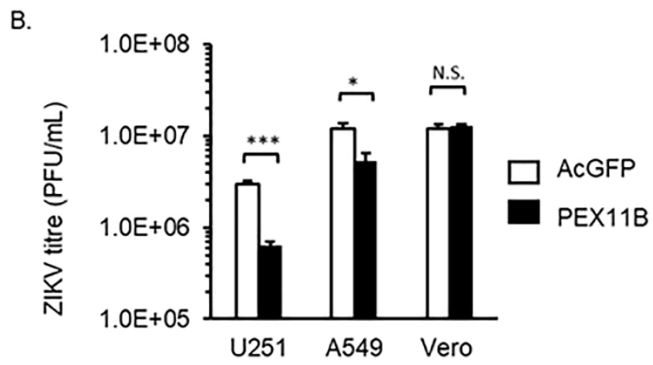
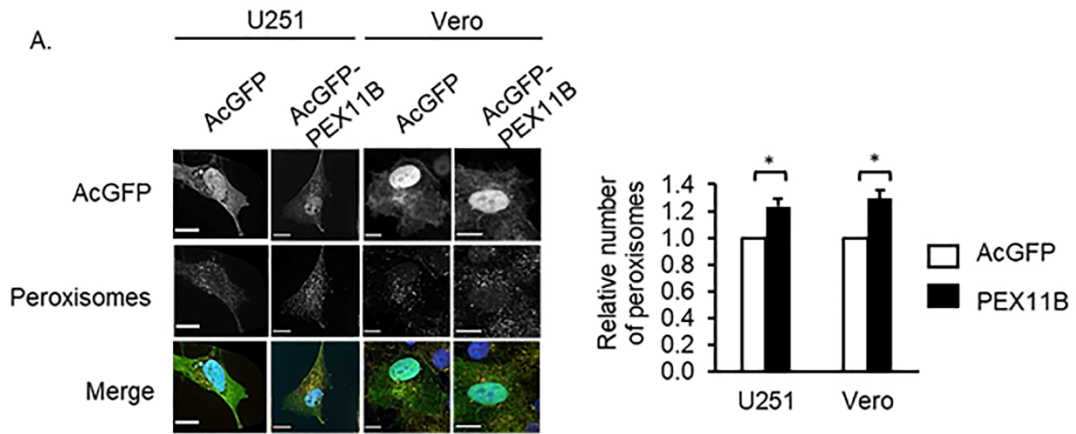


Figure 3.4. Over-expression of PEX11B suppresses ZIKV replication. (A) U251 or Vero cells transduced with lentiviruses encoding AcGFP alone or AcGFP plus myc-tagged PEX11B were processed for confocal microscopy at 48 h post transduction. Peroxisomes were detected using a rabbit polyclonal antibody to the tripeptide SKL. Primary antibody was detected by donkey anti-rabbit IgG conjugated to Alexa Fluor 546. Nuclei were stained using DAPI. Images were obtained using spinning disc confocal microscopy. Quantification of peroxisome numbers (SKL-positive structures) in 90 cells from three independent experiments were performed using Volocity image analysis software and the average number of peroxisomes were plotted. The average number of peroxisomes in mock-treated cells was normalized to 1.0. Bars represent standard error of the mean. * $p < 0.05$. (B) U251, A549 or Vero cells transduced with lentiviruses encoding the reporter protein AcGFP alone as a control or AcGFP plus myc-tagged PEX11B proteins for 48 h were infected with ZIKV PRVABC59 (MOI = 1) for another 48 h. Cell supernatants were collected and viral titers were determined by plaque assay. Cell lysates were also processed for RNA extraction and subsequent qRT-PCR to determine viral RNA level. The viral RNA level was normalized to ACT-B mRNA levels (C). U251 and Vero cell lysates were processed to determine cell viability. (D). The data are averaged from the results of three independent experiments. Bars represent standard error of the mean. *** $p < 0.001$, * $p < 0.05$. N.S. = not significant.

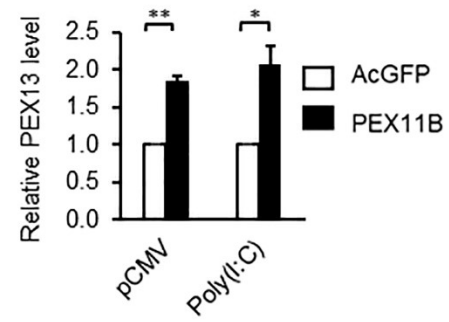
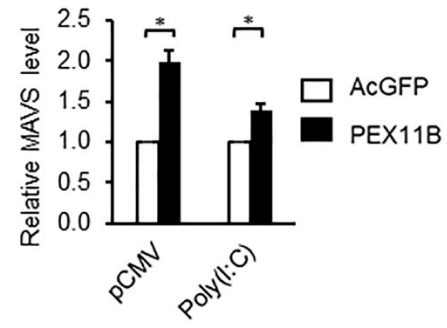
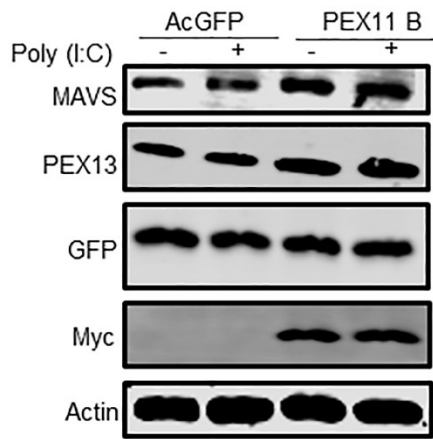
3.2.4 Over-expression of PEX11B up-regulates the innate immune response

A possible reason for the impaired ZIKV replication in U251 and A549 cells over-expressing PEX11B is an enhanced IFN response. IFN induction occurs following detection of viral RNA by the pattern recognition receptors (PRRs) including RIG-I-like receptors (RLRs) such as RIG-I and MDA5 (Goubau *et al.*, 2013; Hartmann, 2017). Activated RLRs interact with the critical adapter molecule mitochondrial antiviral signaling (MAVS) to eventually induce IFN expression (Hou *et al.*, 2011; Liu *et al.*, 2015; Seth *et al.*, 2005). As such, MAVS is targeted for cleavage by multiple viruses including HCV and SARS-CoV-2 (Bender *et al.*, 2015; Ferreira *et al.*, 2016; Fu *et al.*, 2021). Given the essential role of MAVS in eliciting the IFN response, we questioned if expansion of the peroxisome pool was accompanied by increased expression of MAVS. U251 cells were transduced with lentiviruses encoding the reporter protein AcGFP alone or AcGFP plus myc-tagged PEX11B. Data in **Figure 3.5A** show that levels of MAVS protein were ~2-fold higher in cells over-expressing PEX11B. As expected, levels of the peroxisome integral membrane protein PEX13 were also significantly increased in these cells as would be expected with an expanded pool of peroxisomes. In addition, over-expression of PEX11B potentiated the expression of IFN β and IFN λ 2 as well as multiple ISGs (Viperin, Mx2, IFIT1, RIG-I and MDA5) in response to the dsRNA mimic poly(I:C) (**Figure 3.5B**). These results indicate that over-expression of PEX11B enhances the innate immune response.

While the over-expression of PEX11B increased the number of peroxisomes in Vero cells by an average of 35% (**Figure 3.4A**), unlike in U251 or A549 cells, this peroxisome biogenesis factor did not reduce ZIKV replication or viral titers (**Figure 3.4B and C**). The observation that over-expression of PEX11B in IFN-deficient Vero cells did not inhibit ZIKV replication, indicates

that the enhanced antiviral response caused by peroxisome proliferation requires expression of IFNs (Desmyter *et al.*, 1968).

A.



B.

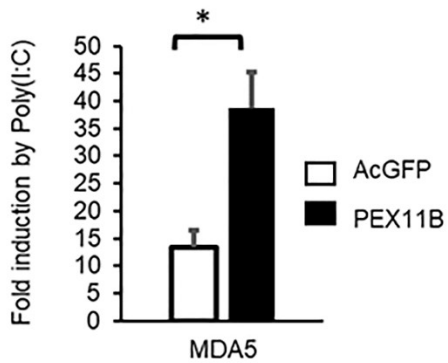
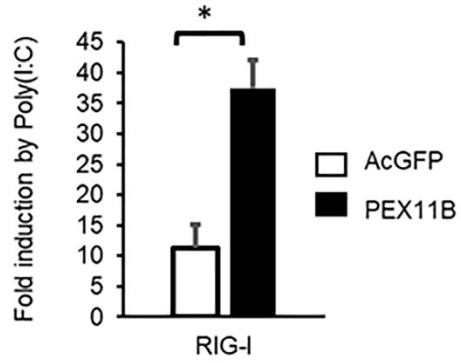
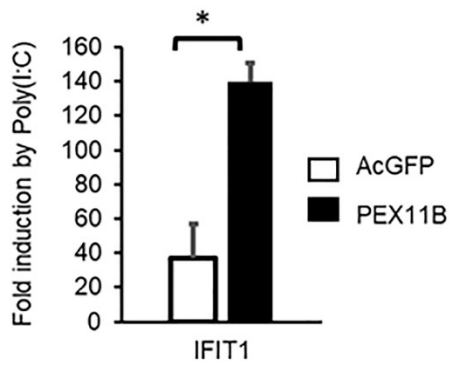
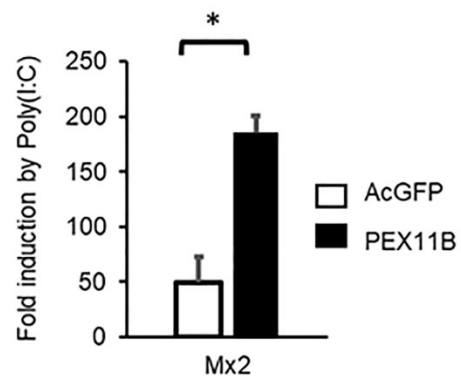
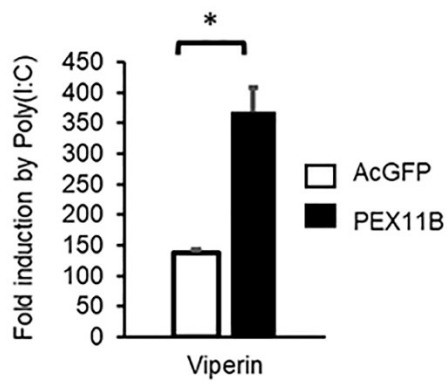
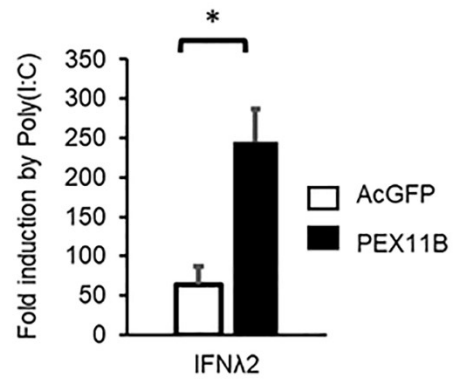
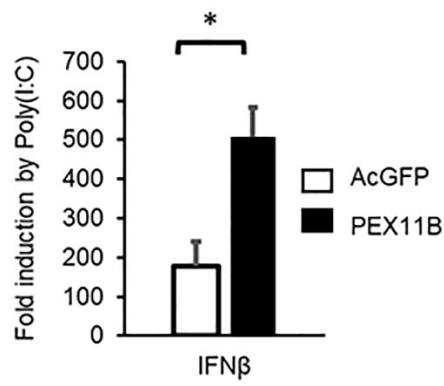


Figure 3.5. Over-expression of PEX11B up-regulates the innate immune response. (A) U251 cells transduced with lentiviruses encoding AcGFP alone or AcGFP plus myc-tagged PEX11B for 48 h were transfected with poly(I:C) (+) or an empty plasmid vector (-) for another 12 h, after which levels of MAVS, PEX13, GFP, myc, and actin were examined by Western blotting using the appropriate antibodies. Levels of actin are shown as a loading control. The relative levels of MAVS and PEX13 (compared to actin) from three independent experiments were averaged and plotted. The average levels of proteins in cells transduced with AcGFP alone were normalized to 1.0. Error bars represent standard error of the mean. ** $p < 0.01$, * $p < 0.05$. (B) U251 cells were transduced with lentiviruses encoding AcGFP alone or AcGFP plus myc-tagged PEX11B for 48 h and then transfected with poly(I:C) for 12 h. Cell lysates were processed for RNA extraction and subsequent qRT-PCR. Fold induction of selected ISG transcripts in response to poly(I:C) was determined. The mRNA levels of ISGs were normalized to ACT-B mRNA levels. The data represent the average from the results of three independent experiments. Bars represent standard error of the mean. * $p < 0.05$.

3.2.5 Summary

The results from experiments described in this chapter reveal that ZIKV infection results in major disruption to the cellular peroxisome pool; likely by disrupting biogenesis of this organelle. Conversely, increasing the peroxisome pool by over-expression of PEX11B, inhibits ZIKV replication, likely by enhancing the IFN response. Levels of the critical biogenesis factor PEX19 were reduced by as much as 90% in HFAs and astrocytoma cells infected with ZIKV. Because PEX19 is absolutely essential for peroxisome biogenesis, capsid-mediated sequestration and ultimately degradation of PEX19 would be expected to impair *de novo* synthesis of peroxisomes. As of yet, it is not clear how ZIKV capsid protein induces loss of PEX19 and peroxisomes.

The antiviral effect of PEX11B over-expression is likely the result of increased MAVS expression on an expanded peroxisome pool which enhances IFN and ISG induction following detection of viral RNA. This scenario is supported by the observation that while over-expression of PEX11B induced peroxisome proliferation in Vero cells, ZIKV replication was not affected in this cell line which cannot produce type I IFN (Desmyter *et al.*, 1968). Together, my findings indicate that PEX11B is a restriction factor for ZIKV replication and further establishes the role of peroxisomes as important IFN antiviral signaling hubs. It also supports the need to investigate whether drugs that increase peroxisome proliferation and or function have antiviral activity and indeed, this is the focus of Chapter 4 of this thesis. Also, studying the cellular pathways involved in modulating peroxisome biogenesis is fundamental in identifying novel antiviral compounds. Finally, it will be of interest to determine how flavivirus proteins, including capsid proteins and possibly other viral proteins, result in loss of PEX19 protein.

Chapter 4

Wnt/ β -catenin signaling pathway inhibitors potently block SARS-CoV-2 replication

4.1 Rationale

The outbreak of coronavirus disease (COVID-19) caused by Severe Acute Respiratory Syndrome Coronavirus 2 (SARS-CoV-2) has resulted in unprecedented disruptions on society and public health. As of April 13, 2022, the virus has infected over 500 million people resulting in more than 6.1 million deaths (WHO, 2022a). In response to the outbreaks, many countries granted Emergency Use Authorization to antivirals for patients hospitalized with COVID-19. Examples include direct-acting antiviral drugs that target the viral protease (e.g. PAXLOVID) or viral polymerase (e.g. Molnupiravir) (Owen *et al.*, 2021; Wahl *et al.*, 2021). While these drugs appear to be highly effective, it is possible and quite likely that variants will develop resistance to these antivirals. There is also significant interest in developing antivirals that target host factors rather than SARS-CoV-2 proteins. A purported advantage of host-directed antivirals is that the barrier of resistance to these drugs should be much higher.

IFNs are an important part of the innate immune response against viral infections. They have been shown to restrict the replication and pathogenesis of SARS-CoV-2 and other RNA viruses (Bayer *et al.*, 2016; Caine *et al.*, 2019; Gobillot *et al.*, 2020; Hoagland *et al.*, 2021; Humphries *et al.*, 2021; Lazear *et al.*, 2016; Mantlo *et al.*, 2020; Stanifer *et al.*, 2020). Clinical trials have evaluated the efficacies of IFNs in treating patients who were hospitalized with COVID-19 (Feld *et al.*, 2021; Hung *et al.*, 2020; Monk *et al.*, 2020). Results revealed that patients who were treated with IFN β or IFN λ experienced shorter hospital stays and lower viral loads. However, a major limitation of using IFN as an antiviral is that patients must be treated in a hospital setting because it is administered through injection or inhalation. Conversely, drugs that boost the IFN induction in response to viral infection may offer similar clinical benefits without the need for obtaining treatment in hospitals.

Both mitochondria and peroxisomes are antiviral signaling platforms that induce the IFN response (Bender *et al.*, 2015; Dixit *et al.*, 2010; Odendall *et al.*, 2014; Seth *et al.*, 2005). I previously showed that expansion of the peroxisome pool by over-expressing PEX11B restricted ZIKV replication by enhancing the IFN response (Wong *et al.*, 2019). We then wondered whether pharmacological compounds that induce peroxisome proliferation would have antiviral activity. Recently our laboratory reported that activation of the Wnt/ β -catenin signaling pathway impairs peroxisome biogenesis (Xu *et al.*, 2020). This study opened the door to another possible approach to modulate peroxisome biogenesis by inhibiting Wnt/ β -catenin signaling. I therefore hypothesize that Wnt/ β -catenin signaling inhibitors promote peroxisome proliferation and consequently enhance IFN induction.

In this chapter, I examined the antiviral effects of commercially available Wnt/ β -catenin inhibitors on SARS-CoV-2. Many of the Wnt/ β -catenin inhibitors reported in this chapter are already licensed for use in other indications or are at advanced clinical trials or pre-clinical development. After screening more than three dozen Wnt/ β -catenin inhibitors, I focused on 10 drugs that potently block replication of SARS-CoV-2, including the common variants of concern.

The 10 Wnt/ β -catenin inhibitors reported in this study modulate critical steps of the Wnt/ β -catenin pathway which include 1) the secretion of Wnt ligands processed by the acyltransferase porcupine, 2) translocation of the glycogen synthase kinase 3 (GSK3), casein kinase 1 α (CK1 α), adenomatous polyposis coli (APC) and Axin complex to plasma membrane, 3) β -catenin stabilization and nuclear translocation, and 4) β -catenin binding with Lymphoid enhancer factor/T-cell factor (LEF/TCF) family of transcription factors for transcriptional activation, a process that is induced by the phosphorylation of Traf2 and Nck-interacting kinase (TNIK) (reviewed in (Kimelman and Xu, 2006)). In addition, novel targets of Wnt pathway modulation

have recently been discovered. For example, CDC-like kinase inhibitors have been shown to reduce expression of Wnt signaling genes, possibly by inhibiting phosphorylation of serine and arginine rich splicing factor (SRSF) and disruption of the splicing of Wnt pathway genes such as *LEF1* and *TCF7* (Tam et al., 2020) . The actions of the 10 Wnt/ β -catenin inhibitors are summarized in **Table 4.1**.

Table 4.1 A summary of the action of the 10 Wnt/ β -catenin inhibitors reported in the study

Inhibitors	Action	Clinical Trials / FDA approved	Indications
IWP-O1	Inhibiting porcupine (Lee et al., 2013; Liu et al., 2013; Proffitt et al., 2013; You et al., 2016)	N.A.	
LGK974		Phase II completed (NCT02278133)	Metastatic colorectal cancer
Wnt-C59		N.A.	
NCB-0846	Inhibiting TNIK (Mahmoudi et al., 2009; Masuda et al., 2016)	N.A.	
KYA1797K	Activating axin to promote β -catenin degradation (Cha et al., 2016)	N.A.	
ETC-1922159	Inhibiting porcupine (Madan et al., 2016)	Phase I Recruitment (NCT0252184)	Advanced solid tumors
Pyrvinium	Activating CK1 α activity to reduce β -catenin level, and to promote degradation of pygopus, a nucleus factor which controls nuclear import or retention of β -catenin (Thorne et al., 2010; Townsley et al., 2004)	FDA-approved	Pinworm infection
iCRT-14	Blocking β -catenin and TCF4 interaction; and blocking TCF binding to DNA (Gonsalves et al., 2011)	N.A.	
SM04755	Blocking CDC-like kinase 2 (CLK2) and dual specificity tyrosine phosphorylation-regulated kinase 1A (DYRK1A). (Deshmukh et al., 2020)	Phase I completed (NCT02191761)	Advanced colorectal, gastric, hepatic, or pancreatic cancer
E7449	Inhibiting tankyrase to stabilize axin, thereby reducing β -catenin protein level (Huang et al., 2009; McGonigle et al., 2015)	Phase II completed (NCT01618136)	Solid tumors

4.2. Results

4.2.1. Wnt/ β -catenin signaling inhibitors reduce SARS-CoV-2 titer and replication

Peroxisomes function to induce IFN expression, thereby restricting viral infections (Bender *et al.*, 2015; Dixit *et al.*, 2010; Odendall *et al.*, 2014). Induction of peroxisome proliferation by over-expression of PEX11B resulted in a cellular antiviral state that blocks ZIKV replication (Wong *et al.*, 2019). In a recent study, our laboratory showed that activation of Wnt/ β -catenin signaling pathway during HIV infection impaired peroxisome biogenesis (Xu *et al.*, 2020). To this end, I hypothesized that pharmacological compounds inhibiting Wnt/ β -catenin signaling pathway would induce peroxisome proliferation and enhance the IFN response.

Commercially available Wnt/ β -catenin signaling pathway inhibitors were tested for antiviral activity in Calu-3 cells infected with SARS-CoV-2. Calu-3 is an ACE2 expressing human lung epithelial cell line that is susceptible to SARS-CoV-2 infection (Chu *et al.*, 2020). Cells were pre-treated with DMSO as a control or Wnt/ β -catenin inhibitors (dissolved in DMSO) for 24 hours prior to infection with SARS-CoV-2 (CANADA/ON-VIDO-01/2020 isolate). Cell media as well as RNA and proteins extracted from cells were collected 24 hours post-infection for analyses. Viral titers were determined by plaque assay and viral genomic RNA and viral spike protein levels were assessed by qRT-PCR and Western blotting respectively. In parallel, infected cells were fixed and processed for indirect immunofluorescence. Infection of SARS-CoV-2 was assessed by confocal microscopy using an antibody to viral spike protein.

Figure 4.1A and 4.1B show that Wnt/ β -catenin inhibitors block SARS-CoV-2 replication. SARS-CoV-2 titers and viral RNA level were reduced by more than 80% and 50% respectively as revealed by plaque assay and qRT-PCR analyses. Western blotting demonstrated that the inhibitors remarkably reduced the levels of viral spike protein in infected cells (**Figure 4.1C**). In

addition, immunofluorescence analysis revealed that the percentage of SARS-CoV-2 infected cells decreased in response to the treatment with Wnt/ β -catenin inhibitors (**Figure 4.1D**).

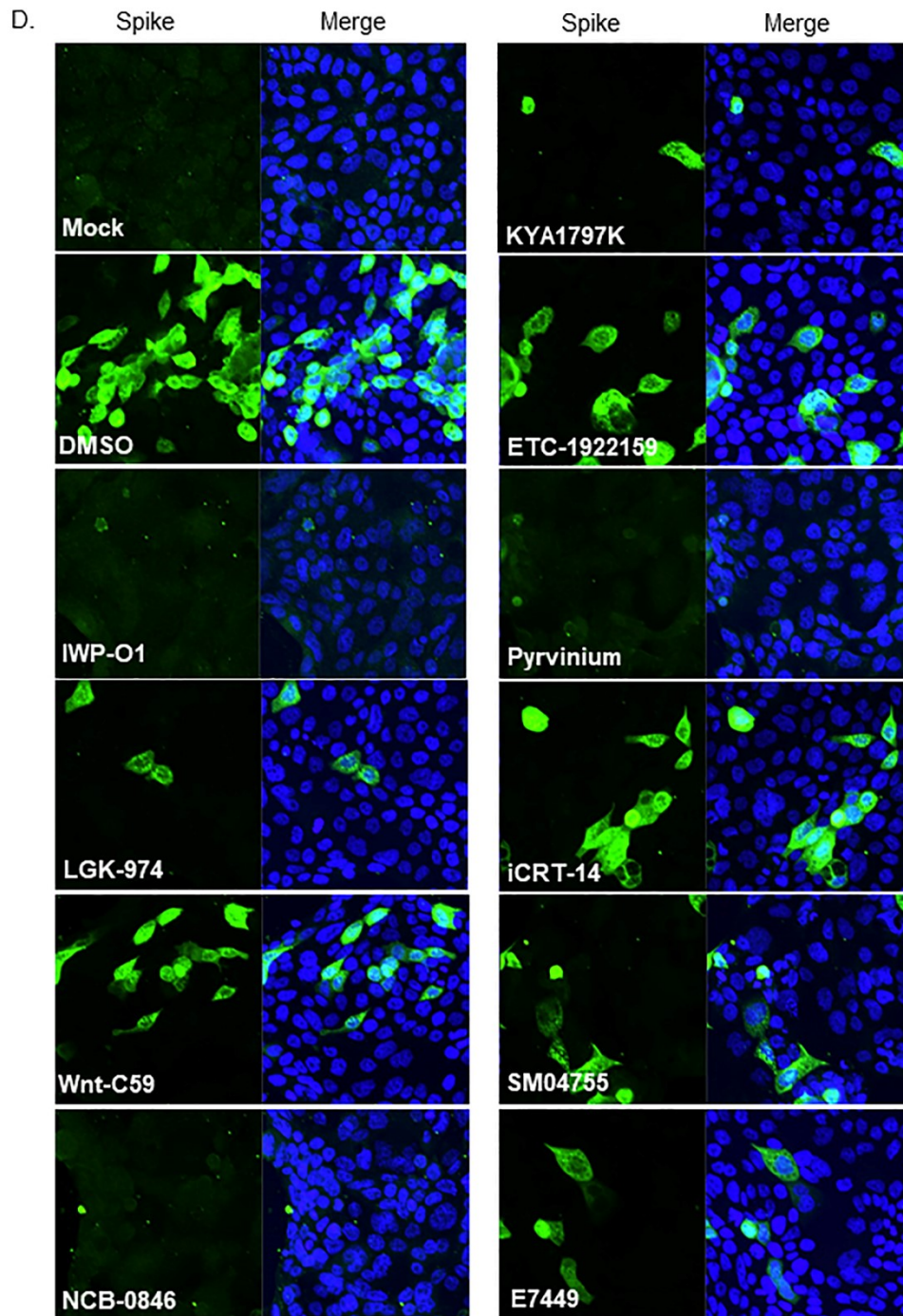


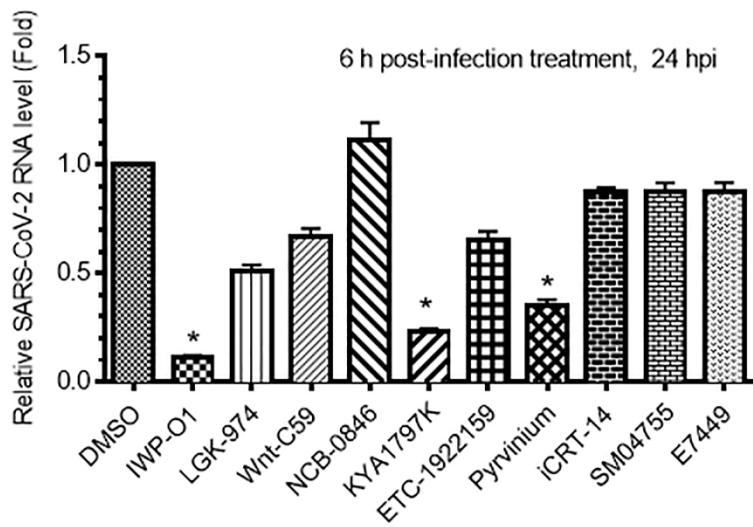
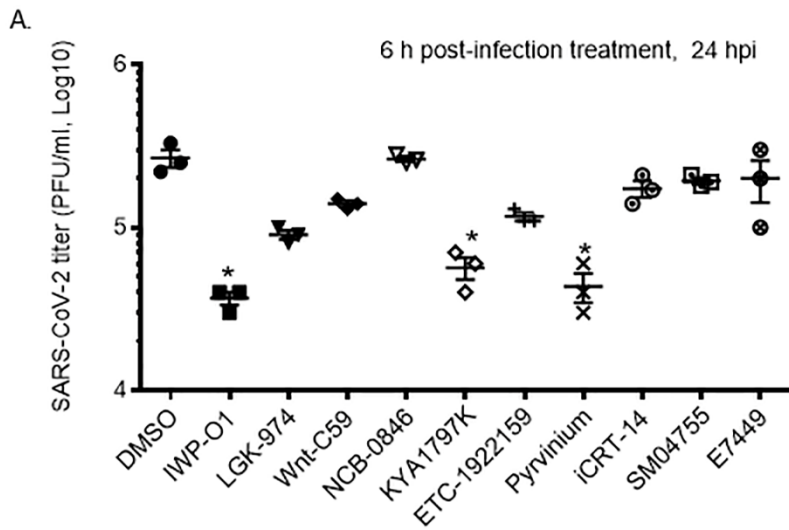
Figure 4.1. Wnt inhibitors significantly reduce SARS-CoV-2 infection in Calu3 cells. Calu3 cells were pre-treated with DMSO as a control or the indicated Wnt inhibitors (1 μ M) or Pyrvinium (100 nM) for 24 hours and then infected with SARS-CoV-2 (CANADA/VIDO01/2020 strain) at MOI of 0.5. Twenty-four hours later, media were collected and subjected to plaque assay to determine viral titers **(A)**. Data shown are averaged from 3 independent experiments. Error bars represent standard error of the mean, * $p < 0.05$. **(B)**. Total RNA extracted from infected cells at 24 hours post infection was subjected to qRT-PCR analysis. The average levels of SARS-CoV-2 viral RNA relative to actin mRNA from 3 independent experiments are shown. Error bars represent standard error of the mean, * $p < 0.05$. **(C)**. Cell lysates harvested at 24 hours post-infection were processed for Western blot analyses with antibodies to SARS-CoV-2 Spike protein and actin. Levels of actin are shown as a loading control **(D)**. Calu3 cells grown on coverslips were pre-treated with DMSO as a control or Wnt inhibitors (1 μ M) or Pyrvinium (100 nM) for 24-hours and then infected with SARS-CoV-2 (CANADA/VIDO01/2020 strain) at MOI of 0.5. Twenty-four hours, cells were processed for indirect immunofluorescence and confocal microscopy using a mouse monoclonal antibody to viral Spike protein and donkey anti-mouse IgG conjugated to Alexa Fluor 488. Nuclei were stained using DAPI.

Strong inhibitory effects on SARS-CoV-2 replication were observed in cells pre-treated with Wnt/ β -catenin inhibitors and we next investigated whether the drugs were effective when added post-infection. Cells were infected with SARS-CoV-2, after which Wnt/ β -catenin inhibitors were added at 6- and 12-hours post-infection. Cell media and total cellular RNA were collected at 24- and 48-hours after infection for plaque assay and qRT-PCR analyses respectively. Results show that IWP-O1, KYA1797K and Pyrvinium reduced viral titers by more than 70% and viral RNA levels by more than 60% when added post-infection (**Figures 4.2 and 4.3**).

To verify that Wnt/ β -catenin inhibitors also block SARS-CoV-2 replication in physiologically relevant primary human cells, normal human bronchial epithelial (NHBE) lung cells obtained from bronchoscopy patients were treated with DMSO or Wnt/ β -catenin inhibitors for 24 hours, after which the cells were infected with SARS-CoV-2 for another 24 hours. **Figure 4.4** shows that Wnt/ β -catenin inhibitors had even more potent antiviral effects on SARS-CoV-2 in these primary lung epithelial cells. Viral titers were reduced by 80% or more by these drugs as determined by plaque assay analyses. Remarkably, no infectious virus could be detected in the media of cells treated with KYA1797K or Pyrvinium. The reduction in the viral titer in the drug-treated cells was not due to the cytotoxicity of the Wnt/ β -catenin inhibitors as the viabilities of Calu-3 cells and NHBE cells were not adversely affected by concentrations of the inhibitors used for the plaque assays (**Figure 4.5**).

The experiments described above were performed with an early isolate of SARS-CoV-2 (CANADA/ON-VIDO-01/2020) that preceded the emergence of D614G strains and variants of concern. Next, we treated Calu-3 cells with Wnt/ β -catenin inhibitors for 24 hours and infected them with D614G, alpha, beta, gamma, delta or omicron variants of SARS-CoV-2 for another 24-hours, after which the samples were collected for plaque assay analyses. In this experiment, we focused on three Wnt/ β -catenin inhibitors (IWP-O1, KYA1797K and Pyrvinium) because they

showed the highest selectivity indexes (**Figure 4.6 A**). Data from plaque assays showed that IWP-O1 (1 μ M), KYA1797K (1 μ M) and Pyrvinium (100 nM) reduced titers of D614G, alpha, beta, gamma, delta, and omicron variants by more than 80%. Of note, no infectious virus was detected in the media of cells treated with KYA1797K (10 μ M) prior to infection with D614G, beta, gamma, delta, or omicron variants (**Figure 4.6 B-G**).



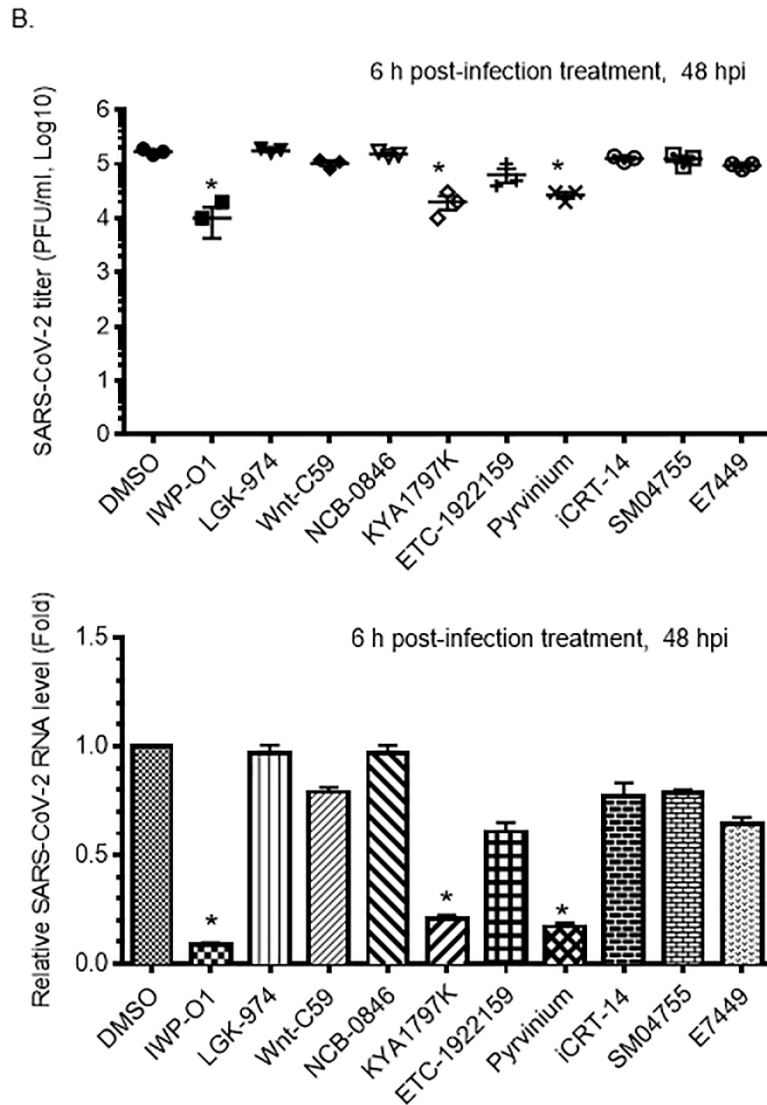
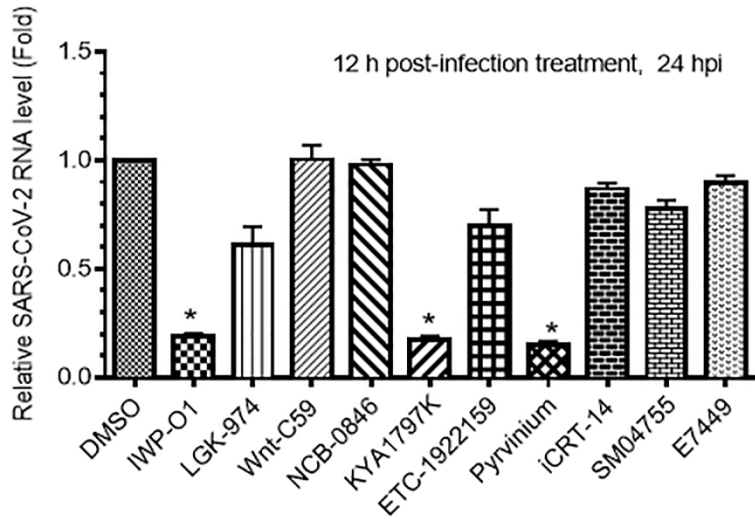
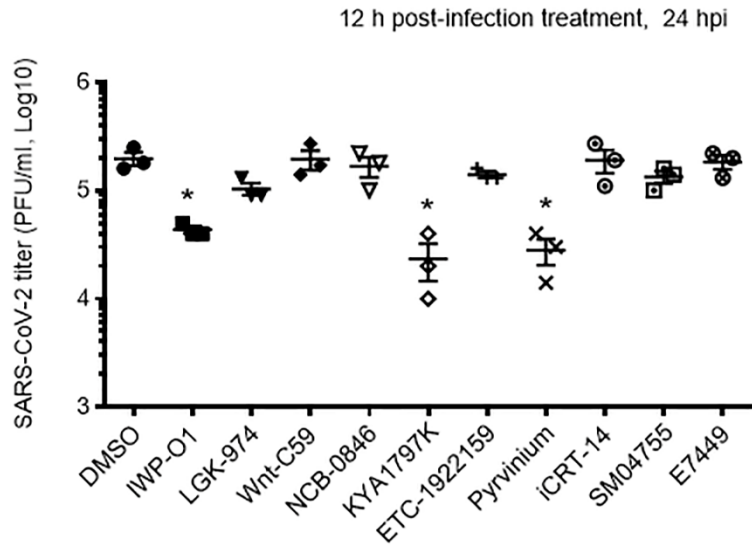


Figure 4.2. The Wnt/ β -catenin inhibitors IWP-O1, KYA1797K and Pyrvinium reduce SARS-CoV-2 replication when added 6-hours post-infection. Calu3 cells were infected with SARS-CoV-2 (CANADA/VIDO01/2020 strain, MOI of 0.5) for 6-hours after which IWP-O1 (1 μ M), KYA1797K (1 μ M) or Pyrvinium (100 nM) were added. Twenty-four (A) and forty-eight (B) hours later, virus-containing media were subjected to plaque assays (left panels) and total RNA extracted from cells was subjected to qRT-PCR to determine relative levels of viral RNA (right panels). Average viral titers and genomic RNA levels from drug-treated cells from 3 independent experiments are shown (A and B, left panels). Error bars represent standard error of the mean, * $p < 0.05$.

A.



B.

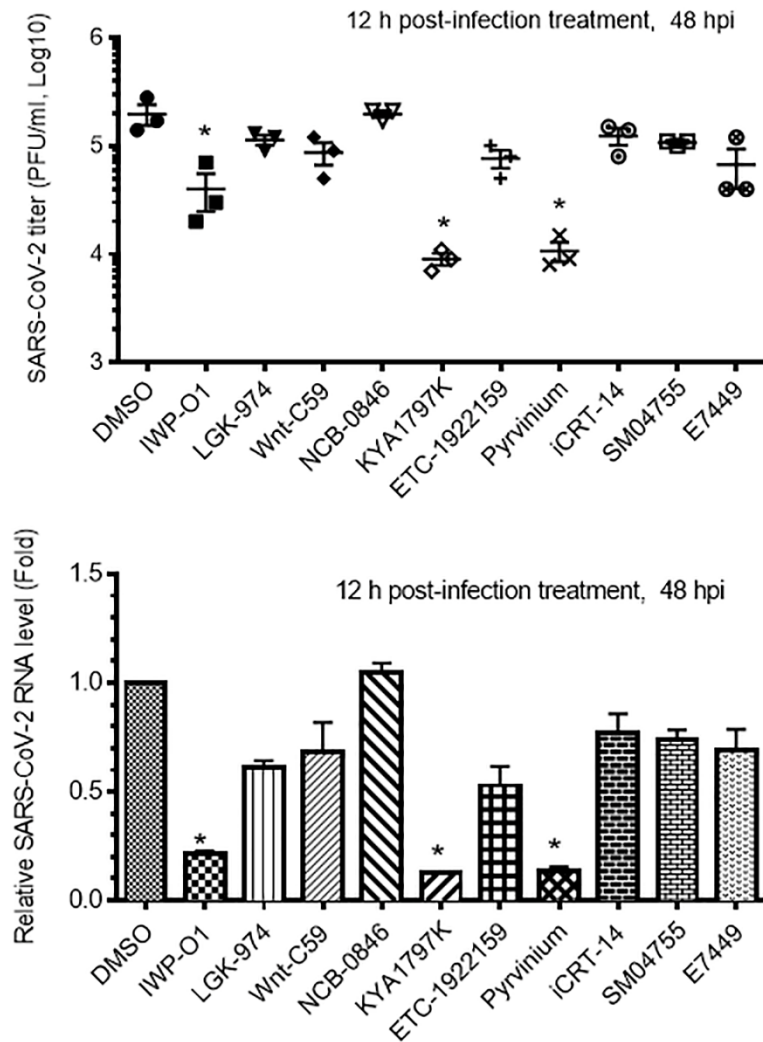


Figure 4.3. The Wnt/ β -catenin inhibitors IWP-O1, KYA1797K and Pyrrvinium reduce SARS-CoV-2 replication when added 12-hours post-infection. Calu3 cells were infected with SARS-CoV-2 (CANADA/VIDO01/2020 strain, MOI of 0.5) for 12-hours after which IWP-O1 (1 μ M), KYA1797K (1 μ M) or Pyrrvinium (100 nM) were added. Twenty-four (A) and forty-eight (B) hours later, virus-containing media were subjected to plaque assays (left panels) and total RNA extracted from cells was subjected to qRT-PCR to determine relative levels of viral RNA (right panels). Average viral titers and genomic RNA levels from drug-treated cells from 3 independent experiments are shown (A and B, left panels). Error bars represent standard error of the mean, * $p < 0.05$.

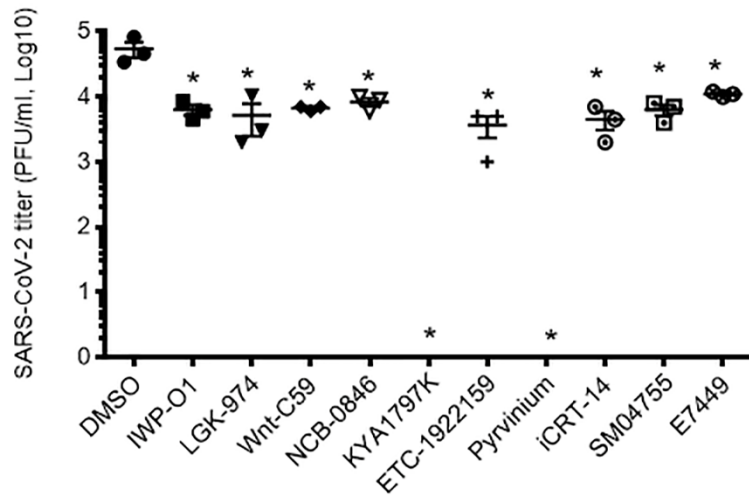


Figure 4.4. Wnt inhibitors significantly reduce SARS-CoV-2 virus titer in normal human bronchial epithelial (NHBE) lung cells. NHBE cells were pre-treated with Wnt inhibitors (1 μ M) or IWP-O1 (100 nM) or NCB-0846 (100 nM) or Pyrvinium (100 nM) or SM04755 (100 nM) for 24 hours and then infected with SARS-CoV-2 (CANADA/VIDO01/2020 strain) using MOI of 0.5 for 24-hours. Cell media were then subjected to plaque assay to determine viral titers. The average titers from 3 independent experiments are shown. Note, in cells treated with KYA17997K or Pyrvinium, no infectious virus was detected in the media. Error bars represent standard error of the mean, * $p < 0.05$.

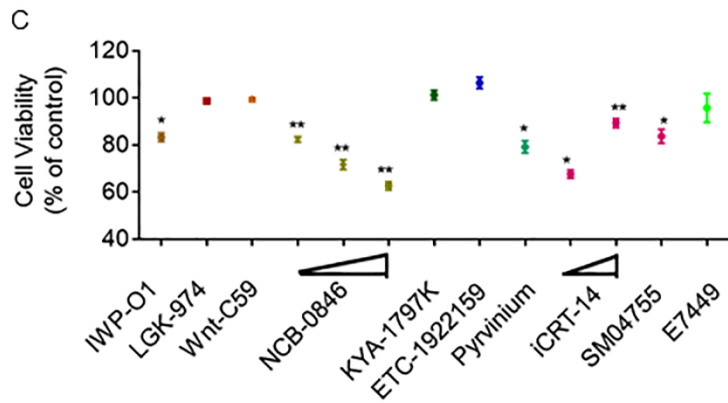
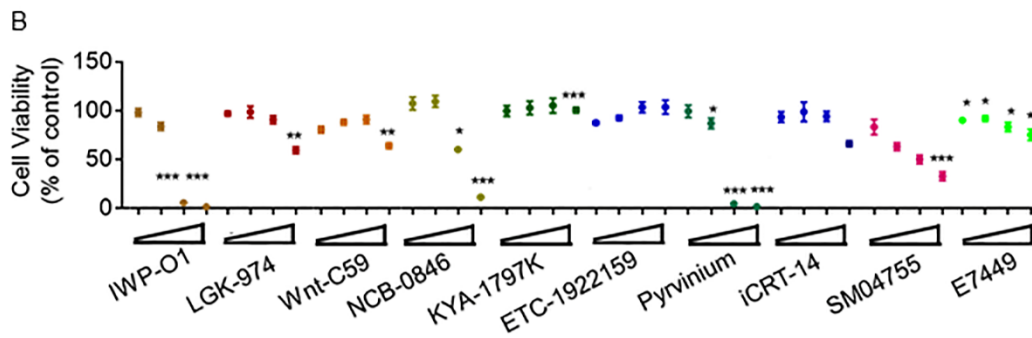
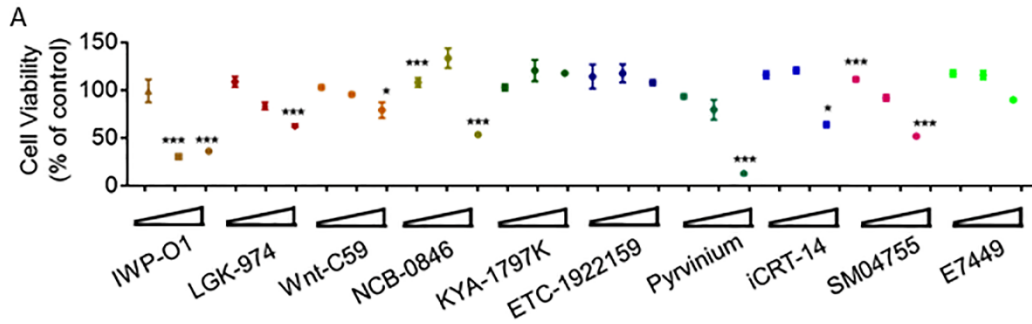
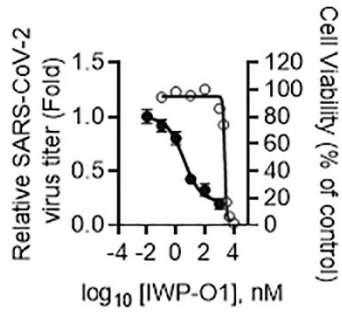
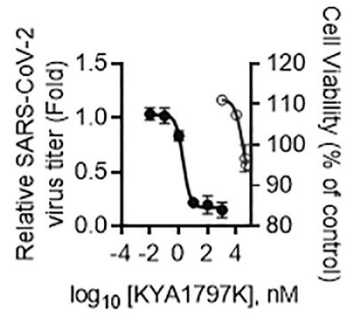


Figure 4.5. Effect of Wnt/ β -catenin inhibitors on cell viability. Calu-3 (A), NHBE (B) and A549 (C) cells were treated with DMSO alone or Wnt/ β -catenin inhibitors for 72-hours after which the relative cell viabilities were determined using a CellTiter-Glo® Luminescent Cell Viability Assay kit. Calu-3 cells were treated with the indicated Wnt/ β -catenin inhibitors at 3 different concentrations (1 μ M, 10 μ M and 40 μ M). NHBE cells were treated with the indicated Wnt/ β -catenin inhibitors at 4 different concentrations (10 nM, 100nM, 1 μ M and 10 μ M). A549 cells were treated with the indicated Wnt/ β -catenin inhibitors (10 μ M) or IWP-O1 (1 μ M) or LGK-974 (1 μ M) or NCB-0846 (500 nM, 1 μ M and 10 μ M) or iCRT-14 (1 μ M) or SM04755 (100 nM and 1 μ M) or E7449 (1 μ M). The relative average cell viabilities (normalized to DMSO) from 3 independent experiments are shown. Error bars represent standard errors of the means. *, P < 0.05; **, P < 0.01; ***, P < 0.001

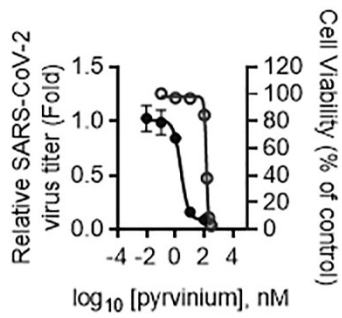
A.



EC50: 3.414 nM CC50: 2362 nM
Selectivity Index: 691.86

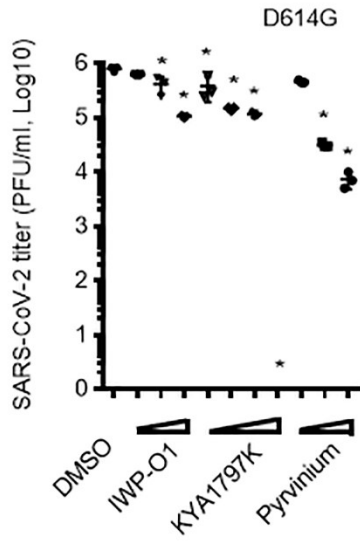


EC50: 2.008 nM CC50: 26756 nM
Selectivity Index: 13324

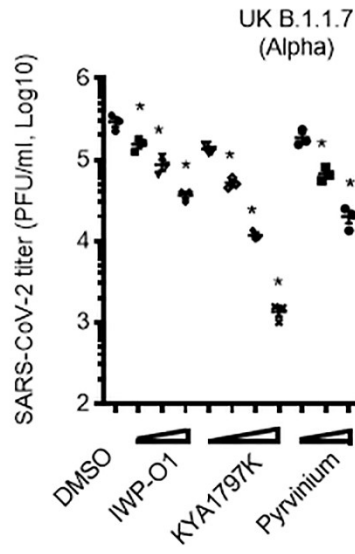


EC50: 2.397 nM CC50: 137.3 nM
Selectivity Index: 57.28

B.



C.



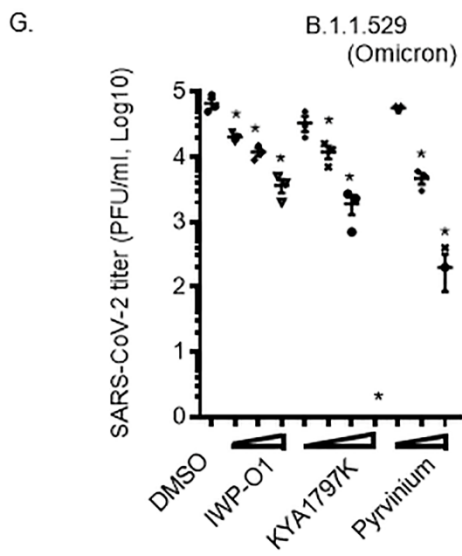
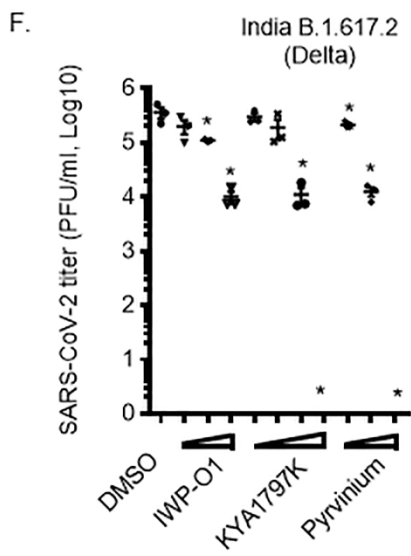
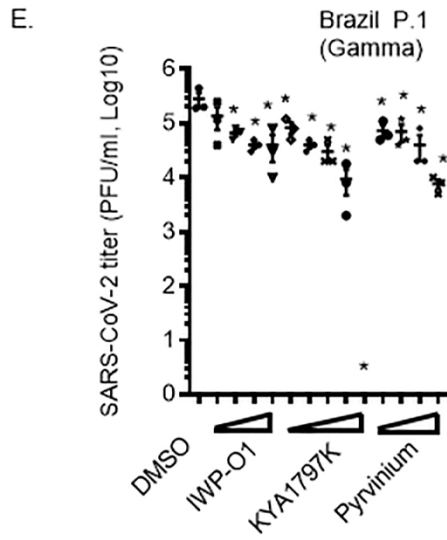
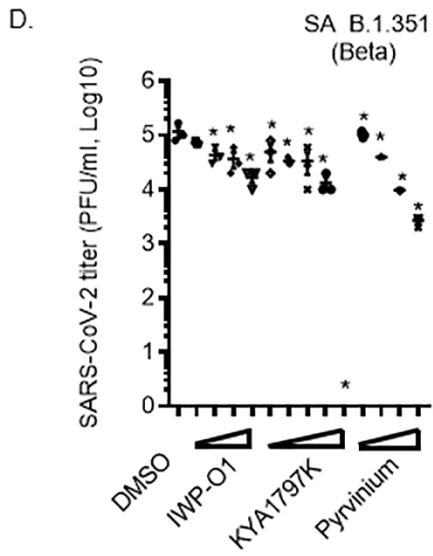
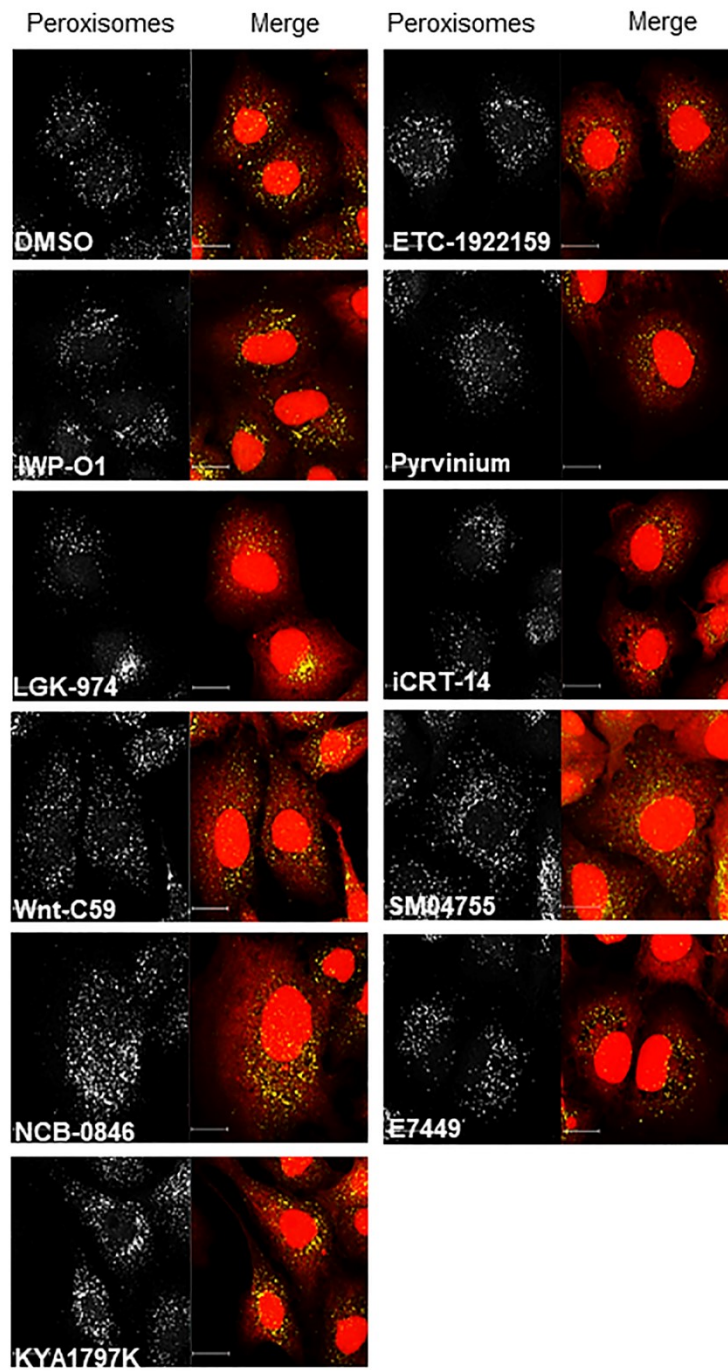


Figure 4.6. Wnt inhibitors inhibit replication of SARS-CoV-2 variants of concern. Calu-3 cells were pre-treated with the indicated concentrations of Wnt inhibitors IWP-O1, KYA1797K and Pyrvinium (0.01 nM to 1 mM) for 24 hours and then infected with SARS-CoV-2 (CANADA/VIDO01/2020 strain) using MOI of 0.5. Twenty-four hours later, cell media and lysates were collected and subjected to plaque and cytotoxicity assays to determine viral titers and cell viability respectively. A. Relative average viral titers obtained from 3 independent experiments are shown as are the relative cell viabilities of cells treated with Wnt inhibitor for 48 hours in the absence of infection. EC_{50} and CC_{50} values were determined and then used to calculate the selectivity indexes (CC_{50}/EC_{50}) for each drug. (B-E) Calu3 cells were pre-treated with IWP-O1, KYA1797K and Pyrvinium for 24 hours and then infected with SARS-CoV-2 variants ((B) D614G, (C) UK B.1.1.7 (Alpha), (D) SA B.1.351 (Beta), (E) Brazil P.1 (Gamma), (F) India B.1.617.2 (Delta) and (G) B.1.1.529 (Omicron)) using MOI of 0.5. In (B-C) and (F-G), cells were pretreated with IWP-O1 and Pyrvinium at 3 different concentrations (10 nM, 100 nM, and 1 μ M), and KYA1797K at 4 different concentrations (10 nM, 100nM, 1 μ M, and 10 μ M). In (D-E), cells were pretreated with IWP-O1 and Pyrvinium at 4 different concentrations (1 nM, 10 nM, 100 nM, and 1 μ M) and KYA1797K at 5 different concentrations (1 nM, 10 nM, 100nM, 1 μ M, and 10 μ M). Twenty-four hours later, cell media were subjected to plaque assay. Viral titers from 3 independent experiments were determined and averaged. Error bars represent standard error of the mean, * $p < 0.05$.

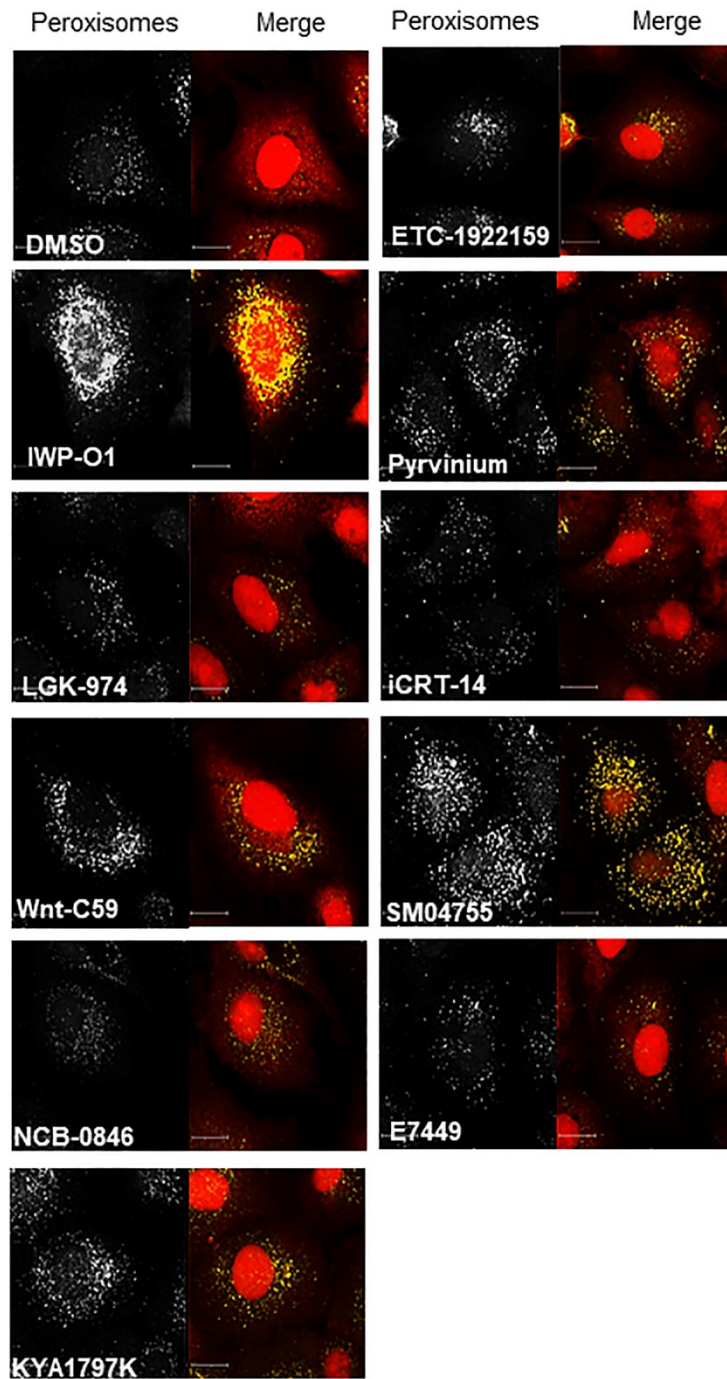
4.2.2. Wnt/ β -catenin inhibitors increase peroxisome density and potentiate the interferon response

I next investigated how Wnt/ β -catenin inhibitors functioned to restrict SARS-CoV-2 replication. The fundamental hypothesis is that Wnt/ β -catenin inhibitors promote peroxisome proliferation and consequently enhance the IFN response. First, I determined if Wnt/ β -catenin inhibitors actually promoted peroxisome proliferation. Cells were treated with Wnt/ β -catenin inhibitors for 24 or 48 hours, after which they were processed for indirect immunofluorescence and confocal microscopy. Peroxisomes were stained using an antibody to PEX14, a peroxisome membrane protein which forms docking complexes for matrix protein import. In order to estimate cell volume, prior to mounting, samples were also incubated with a fluorescent dye (CellMask) that stains the entire cell. Peroxisome density was calculated by dividing the number of peroxisomes by the cell volume. **Figure 4.7** shows that peroxisome density was significantly increased by drug treatment after 24 and 48 hours. Half of the inhibitors investigated (IWP-01, NCB-0846, KYA1979K, iCRT-14, and SM04755) increased the peroxisome density by more than 50%.

A.



B.



C.

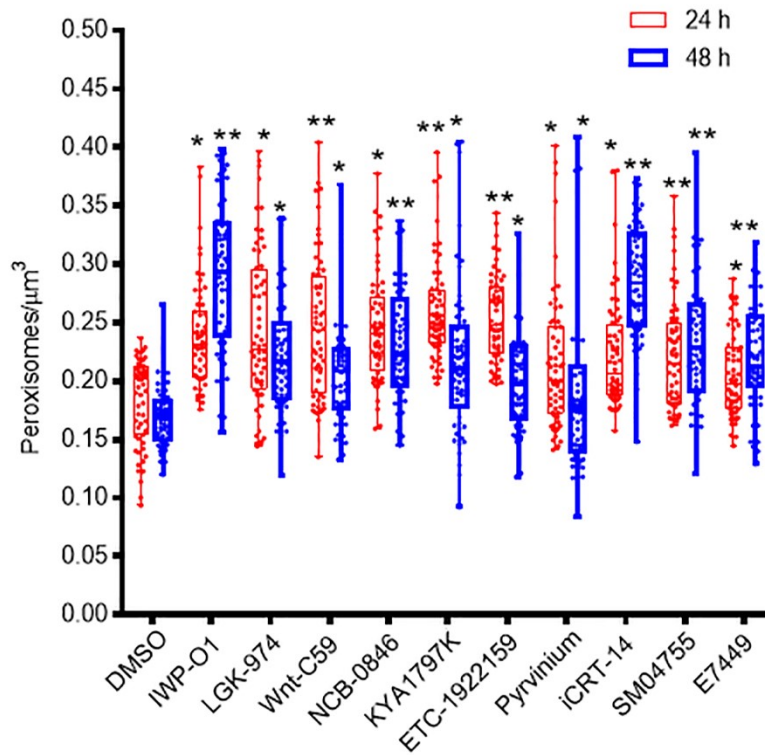


Figure 4.7. Inhibitors of the Wnt/ β -catenin pathway increase peroxisome density in human cells. A549 cells were treated with DMSO alone or 10 different commercially available drugs (1 μ M) or NCB-0846 (500 nM) or SM04755 (100 nM) that block Wnt/ β -catenin signaling for (A) 24 or (B) 48 hours before fixing and processing for indirect immunofluorescence. Peroxisomes were detected with a rabbit polyclonal antibody to PEX14 and donkey anti-rabbit IgG conjugated to Alexa Fluor 546. Prior to mounting, samples were incubated with CellMask Deep Red to label the entire cell. Images were obtained using a spinning-disc confocal microscope. (C) Box-and-whisker plot of the peroxisomal density is shown. Peroxisomal density ($\#/\mu\text{m}^3$) was calculated by quantifying the number of PEX14 puncta structures from Z-stack confocal images of the entire cell and dividing by the cell volume. Boxes show the 25th, 50th, and 75th percentiles. Points represent a minimum of 60 cells which were analyzed in three independent experiments. *, $P < 0.05$; **, $P < 0.01$.

Next, I investigated whether Wnt/ β -catenin inhibitors enhanced the IFN response in response to viral infection. Cells were treated with DMSO as a control or Wnt/ β -catenin inhibitors for 24-hours, after which the cells were mock infected or infected with Sendai virus, an RNA virus that induces a robust IFN response (Cantell et al., 1981). At 8- and 16-hours post-infection, total cellular RNA was collected and relative levels of IFN transcripts were determined by qRT-PCR. Data in **Figure 4.8** show that Sendai virus infected cells treated with Wnt/ β -catenin inhibitors exhibited higher IFN expression in comparison to Sendai virus infected DMSO-treated cells. At 8 hours post infection of Sendai virus, induction of *IFN β* was significantly enhanced in cells treated with IWP-O1, LGK-974, Wnt-C59, NCB-0846, KYA1979K, and ETC1922159. At 16 hours post infection of Sendai virus, induction of *IFN β* was significantly enhanced in cells treated with LGK-974, NCB-0846, KYA1979K, Pyrvinium, and SM04755. Nine out of the ten inhibitors upregulated expression of *IFN λ* at 8 hours post infection with Sendai virus. Induction of *IFN λ* was highest in cells treated with NCB-0846, Pyrvinium, iCRT-14 and SM04755 at 16 hours post infection with Sendai virus. Of note, Wnt/ β -catenin inhibitors did not up-regulate IFN response in the absence of viral infection (**Figure 4.9**).

To determine how Wnt/ β -catenin inhibitors boost IFN induction in response to viral infection, I initially assessed whether these drugs affect MAVS protein levels. This antiviral signaling protein is localized on both peroxisomes and mitochondria where it functions in IFN induction (Bender et al., 2015; Dixit et al., 2010; Odendall et al., 2014). I previously showed that PEX11B-dependent induction of concomitantly increased MAVS protein levels (Wong et al., 2019). Calu-3 cells were treated with DMSO as a control or Wnt/ β -catenin inhibitors for 48-hours, after which relative levels of MAVS protein were determined by Western blotting. **Figure 4.10**

shows that MAVS protein levels did not increase in response to treatment with Wnt/ β -catenin inhibitors.

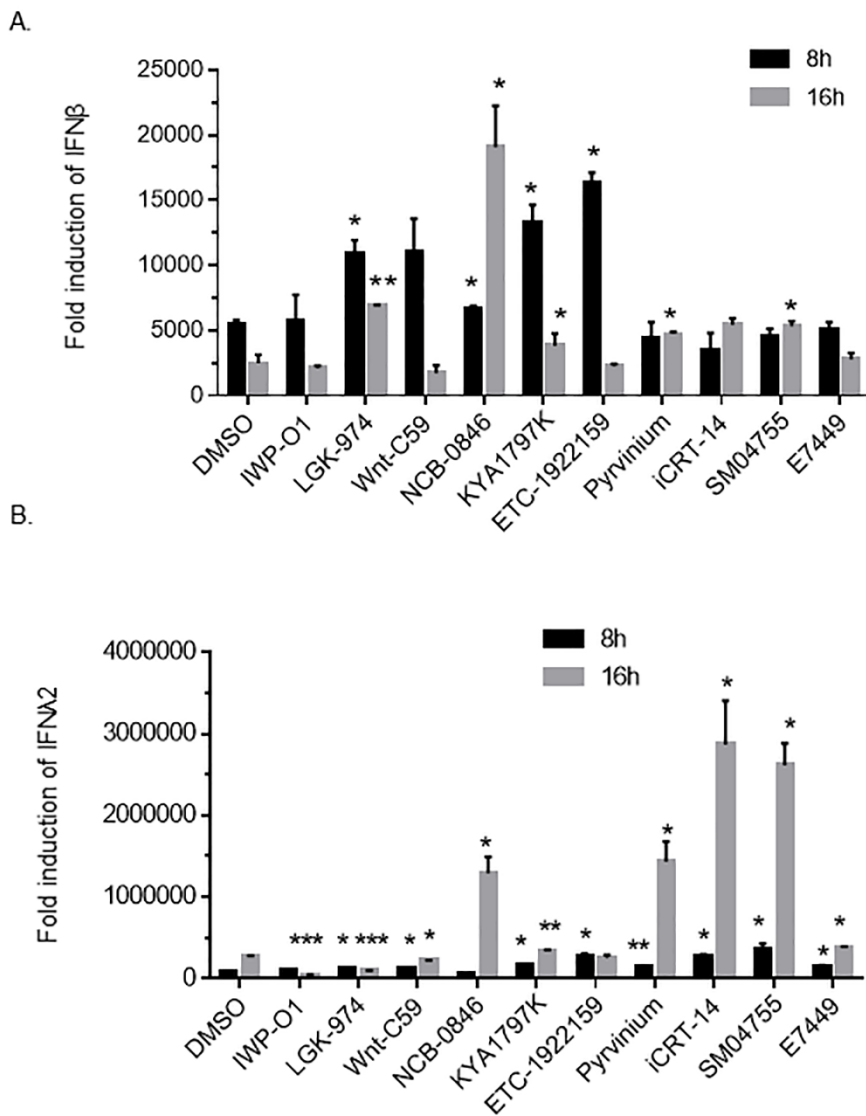


Figure 4.8. Wnt/b-catenin pathway inhibitors enhance production of type I and III interferons in response to viral infection. A549 cells were treated with DMSO alone or 10 different commercially available drugs (1 μ M) or NCB-0846 (500 nM) or SM04755 (100 nM) that block Wnt/ β -catenin signaling. Twenty-four hours later, cells were challenged with 100 HAU/ml of Sendai virus for 8- or 16-hours after which total cellular RNA was harvested and subjected to qRT-PCR to determine relative levels mRNA encoding type I (IFN β) and type III (IFN λ 2) interferons. Values averaged from three independent experiments are shown. Error bars represent standard errors of the mean. *, P < 0.05; **, P < 0.01; ***, P < 0.001; N.S. (not significant)

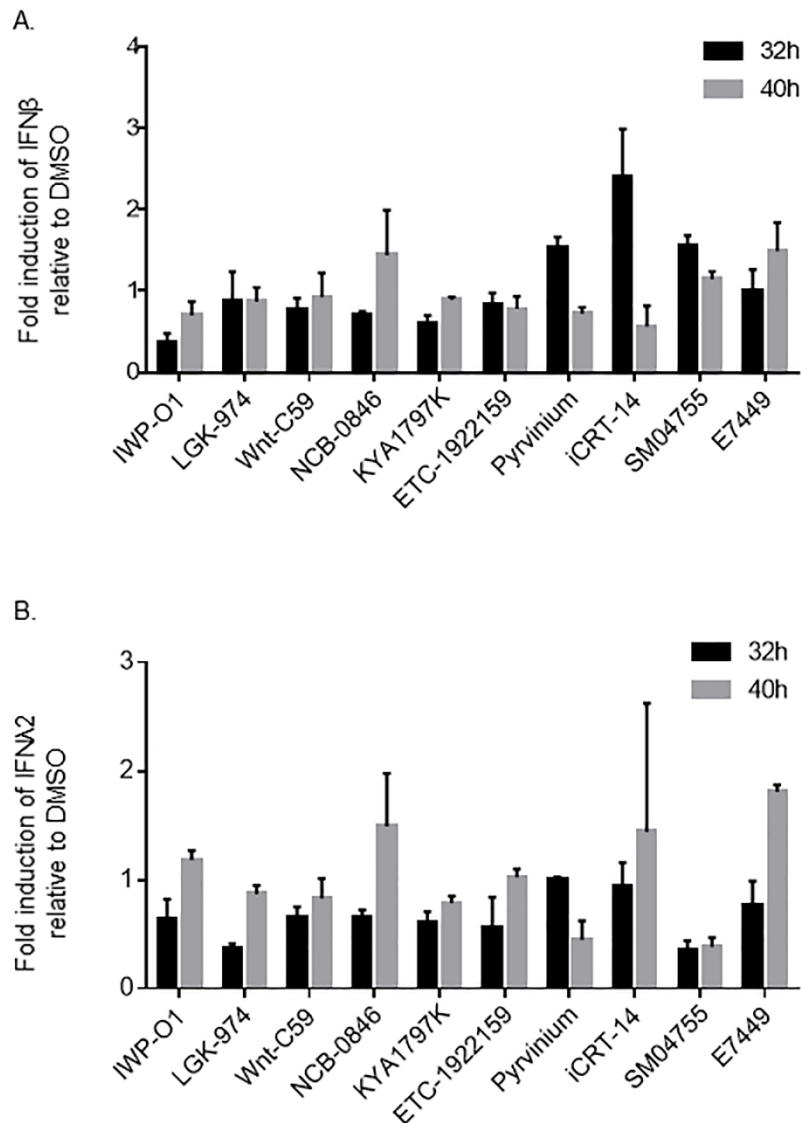


Figure 4.9. Wnt/ β -catenin pathway inhibitors do not induce expression of interferon in the absence of viral infection. A549 cells were treated Wnt/ β -catenin inhibitors (1 μ M) or NCB-0846 (500 nM) or SM04755 (100 nM) or DMSO alone for 32- or 40-hours after which total RNA was extracted from cells. Relative levels of IFN β and IFN λ 2 were determined by RT-qPCR. The average levels of expression IFN β and IFN λ 2 transcripts (normalized to actin mRNA) from 3 independent experiments are shown. Error bars represent standard errors of the means. N.S. (not significant)

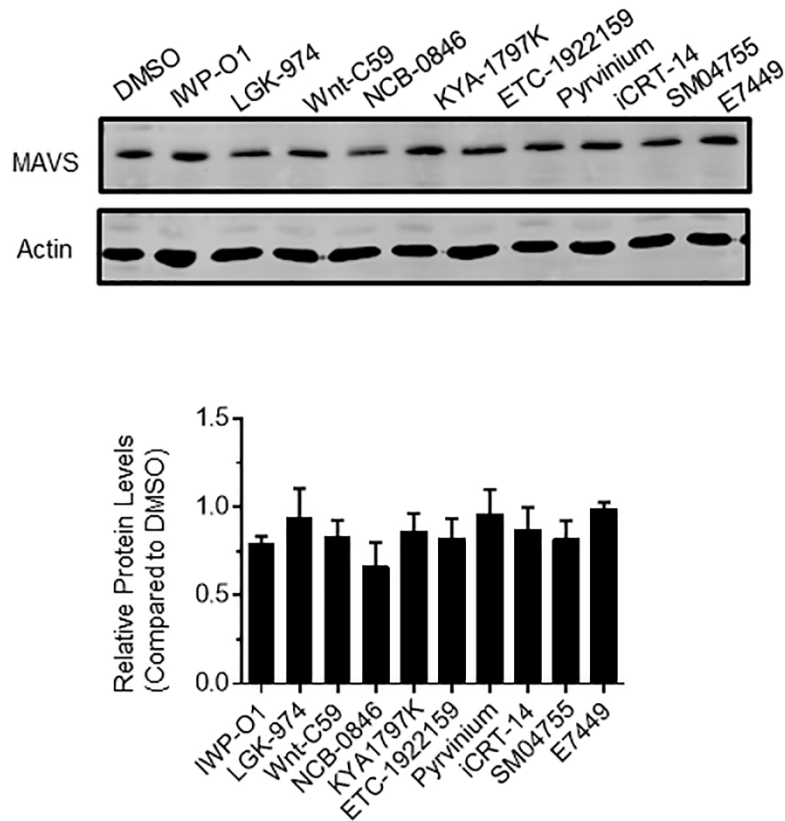
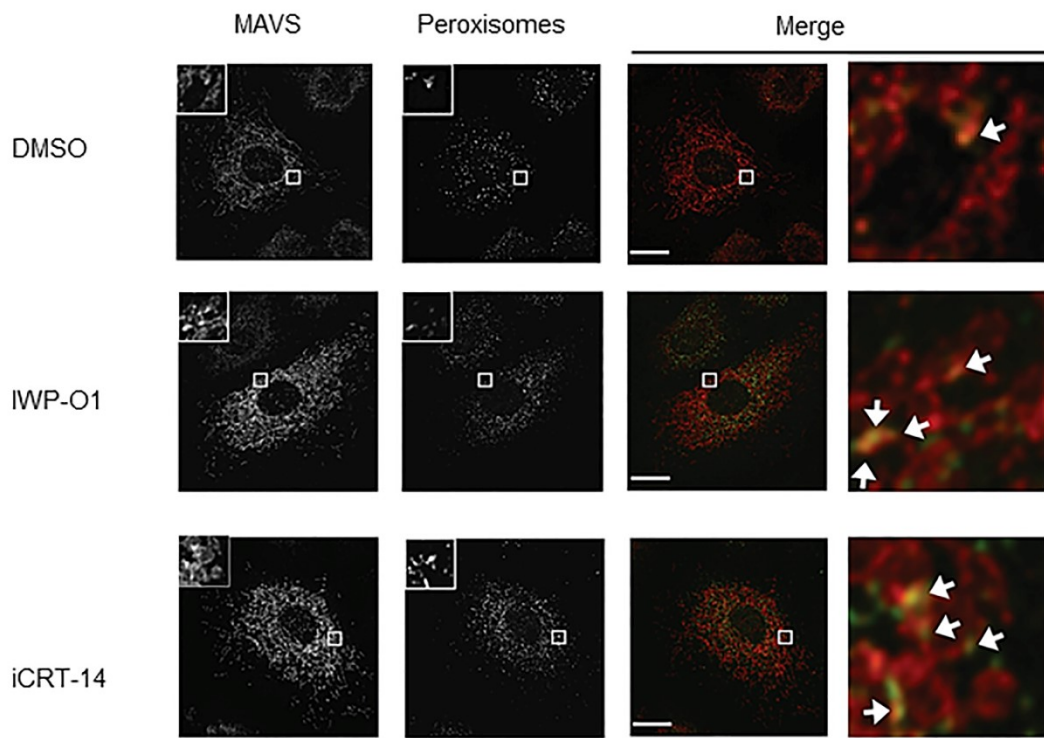


Figure 4.10. Wnt inhibitors do not increase MAVS protein levels. Calu3 cells were treated with DMSO as a control or the indicated Wnt inhibitors (1 μ M) or Pyrvinium (100 nM) for 48 hours after which levels of MAVS and actin were examined by Western blotting using the appropriate antibodies. Levels of actin are shown as a loading control. The relative levels of MAVS protein (compared to actin) from three independent experiments were averaged and plotted. The average levels of proteins in cells treated with DMSO were normalized to 1.0. Error bars represent standard error of the mean. N.S. (not significant)

Next, I investigated whether the intracellular distribution of MAVS changed in response to treatment with Wnt/ β -catenin inhibitors. Since these drugs did not increase levels of MAVS proteins, I hypothesized that increased localization of MAVS to peroxisomes could account for the enhanced IFN response. To test this theory, A549 cells were treated with DMSO alone or IWP-O1 or iCRT-14 for 48 hours and then processed for indirect immunofluorescence and confocal microscopy analyses. IWP-O1 or iCRT-14 were used for these experiments because they increased peroxisome density more than the other 10 Wnt/ β -catenin inhibitors tested (**Figure 4.7C**). Peroxisomes were stained using anti-PMP70 and association of MAVS with peroxisomes was determined using Mander's coefficient. Data in **Figure 4.11** show that in drug-treated cells, the proportion of MAVS associated with peroxisomes was increased by 30%.

The underlying hypothesis for investigations described in this chapter are that Wnt/ β -catenin inhibitors reduce replication of SARS-CoV-2 by enhancing IFN expression. If this is true, these drugs will not exhibit antiviral activity in cells that cannot produce IFN, regardless of whether peroxisome density increases or not. To test this, SARS-CoV-2 replication in the presence and absence of Wnt/ β -catenin inhibitors was assessed in Vero E6 cells which do not produce type I IFN. First, I investigated whether Wnt/ β -catenin inhibitors induced peroxisome proliferation in Vero E6 cells. Data in **Figure 4.12** show that peroxisome density increased by at least 25% in drug-treated Vero E6 cells relative to those treated with DMSO alone.

A



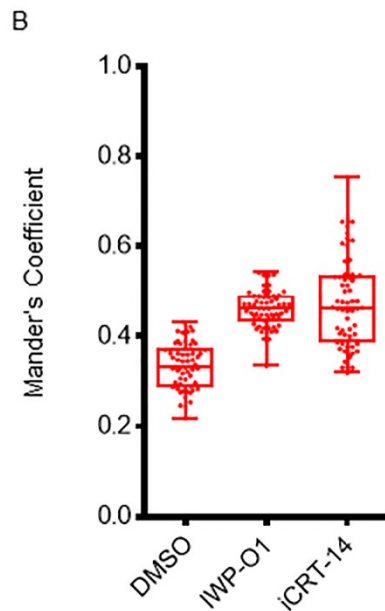


Figure 4.11. Wnt inhibitors increase the colocalization between MAVS and peroxisomes. A549 cells were treated with DMSO alone or 1mM IWP-O1 or iCRT-142 for 48 hours before fixing and processing for indirect immunofluorescence. MAVS was detected by a rabbit polyclonal antibody to MAVS and donkey anti-rabbit IgG conjugated to Alexa Fluor 546. Peroxisomes were detected with a mouse monoclonal antibody to PMP70 and donkey anti-mouse IgG conjugated to Alexa Fluor 488. Images were obtained using a spinning-disc confocal microscope. **(A)** Subcellular localization of MAVS in A549 cells was determined by indirect immunofluorescence. White arrows indicate co-localization of MAVS (red) with the peroxisomal marker PMP70 (green) in the enlarged merged images. **(B)** Box-and-whisker plot of the quantification of subcellular localization of MAVS on peroxisomes as determined with the Mander's coefficient. Boxes show the 25th, 50th, and 75th percentiles. Points represent a minimum of 60 cells which were analyzed in three independent experiments. *, $P < 0.05$.

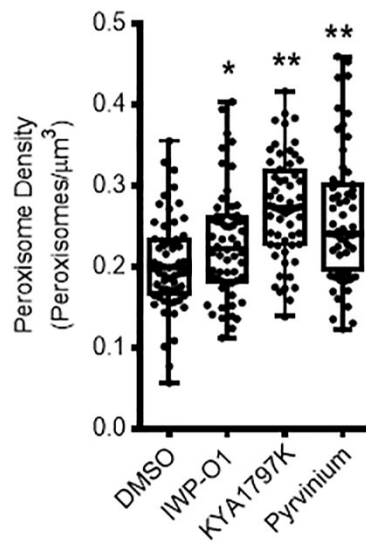
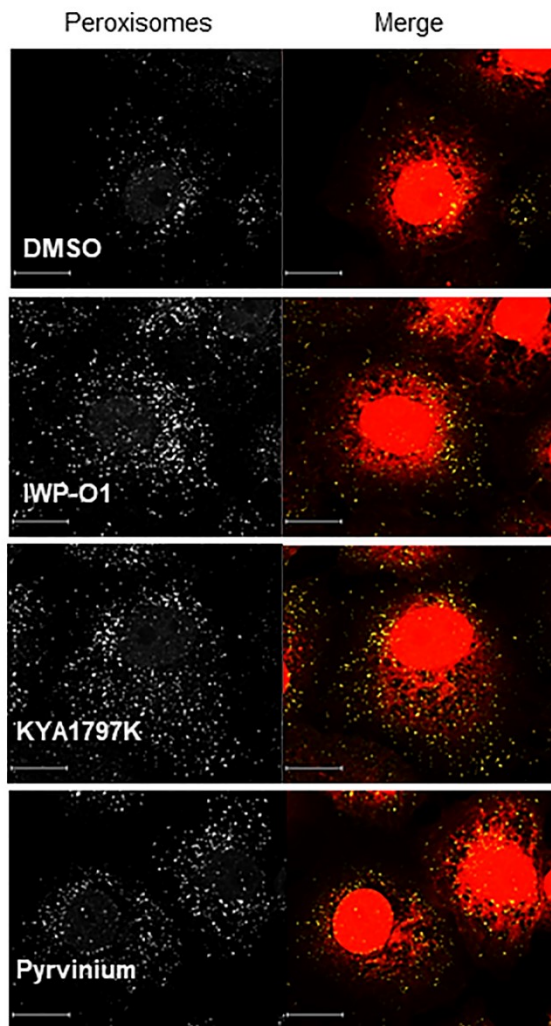


Figure 4.12. Inhibition of the Wnt/ β -catenin pathway increases peroxisome density in Vero cells. Vero E6 cells were treated with 1 μ M IWP-O1, KYA17978K, Pyrvinium (100 nM) or DMSO alone for 48 hours before processing for confocal microscopy. Peroxisomes were detected with a rabbit polyclonal antibody to PEX14 and donkey anti-rabbit IgG conjugated to Alexa Fluor 546. Prior to mounting, samples were incubated with CellMask Deep Red. Images were obtained using a spinning-disc confocal microscope. Box-and-whisker plot of the peroxisomal density in Vero cells are shown on the right. Peroxisomal density was calculated by quantifying the number of PEX14 puncta structures from Z-stack confocal images of the entire cell and dividing by the cell volume. Boxes show the 25th, 50th, and 75th percentiles. Points represent a minimum of 60 cells which were analyzed in three independent experiments. *, $P < 0.05$; **, $P < 0.01$.

Next, Vero E6 cells were treated with DMSO or Wnt/ β -catenin inhibitors for 24-hours and then infected with SARS-CoV-2. Total cellular RNA and media were collected 24-hours post-infection for qRT-PCR analyses and plaque assay respectively. Data in **Figure 4.13** show that SARS-CoV-2 genomic RNA levels and titers were comparable between Vero cells treated with DMSO and Wnt/ β -catenin inhibitors. These results are consistent with our hypothesis that the antiviral effects of Wnt/ β -catenin inhibitors require expression of IFNs.

4.2.3. Reducing β -catenin levels induces peroxisome proliferation and reduces SARS-CoV-2 infection

Activation of the Wnt/ β -catenin pathway results in stabilization of β -catenin in the cytoplasm followed by its translocation into the nucleus where it interacts with other transcriptional factors to induce expression of Wnt target genes (reviewed in (MacDonald et al., 2009)). To determine if reduction of β -catenin protein levels in cells would affect replication of SARS-CoV-2 similar to Wnt/ β -catenin inhibitors, Calu-3 cells were transfected with non-targeting siRNA or β -catenin-specific siRNA for 48-hours. Western blotting confirmed that levels of β -catenin protein were greatly reduced by β -catenin-specific siRNA (**Figure 4.14A**). Next, cells were transfected with non-targeting siRNA or β -catenin-specific siRNA for 24-hours and then infected with SARS-CoV-2 for another 24-hours after which total cellular RNA and media were subjected to qRT-PCR and plaque assays respectively. Results from these experiments showed that siRNA-mediated knockdown of β -catenin reduced SARS-CoV-2 genomic RNA levels and titers by 60% and 75% respectively (**Figures 4.14B and C**).

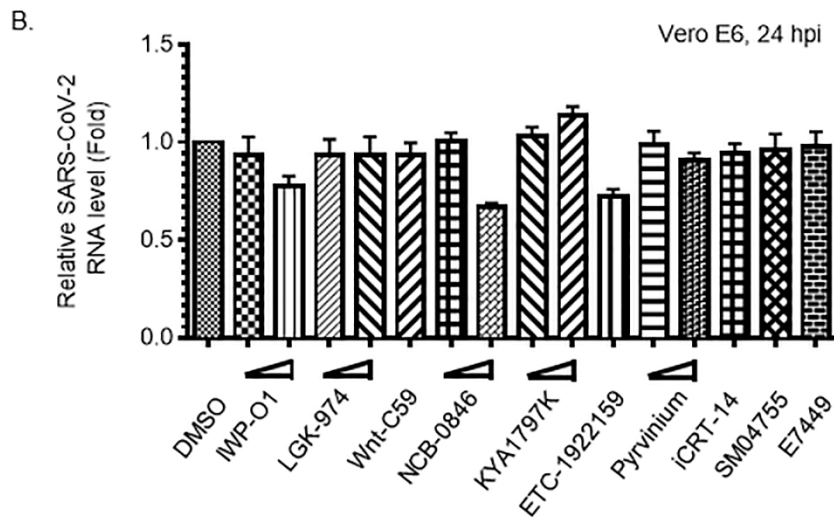
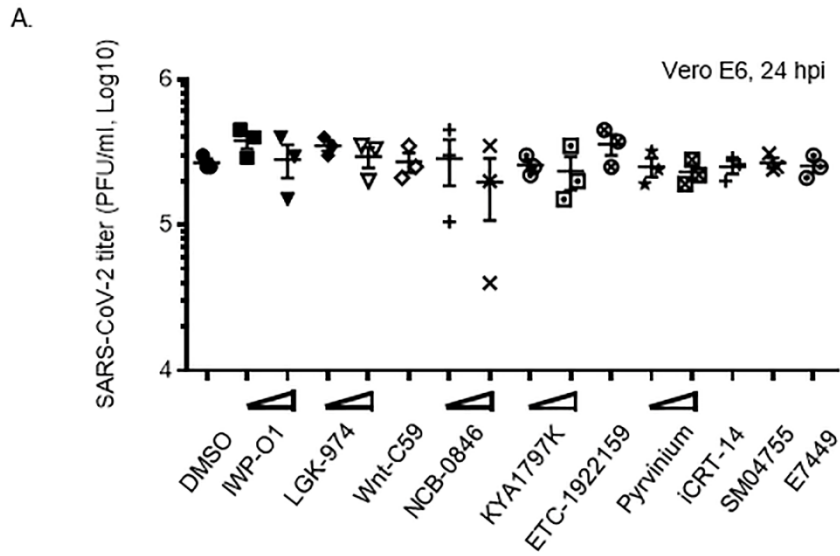
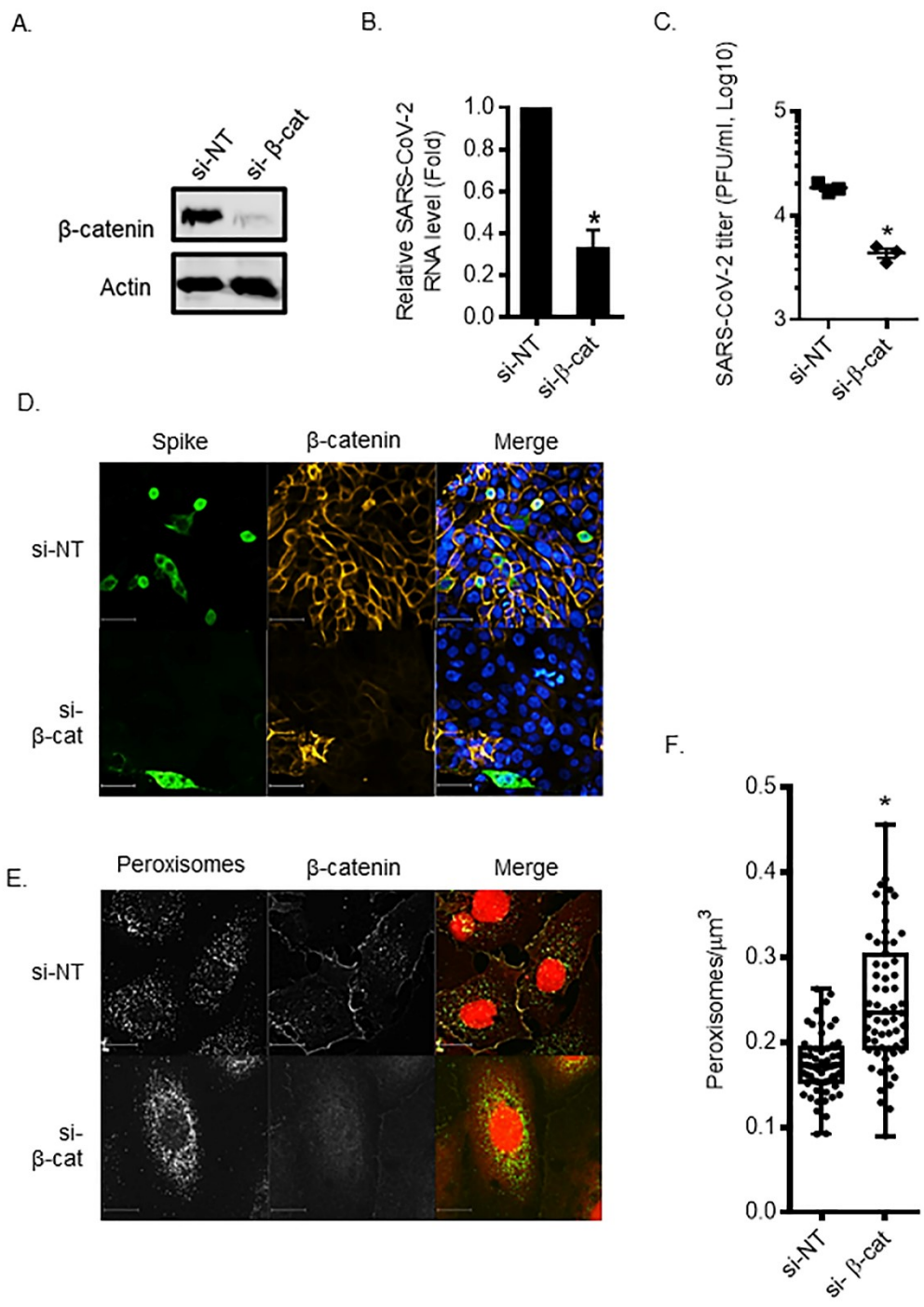


Figure 4.13. Wnt/ β -catenin inhibitors do not reduce SARS-CoV-2 replication in Vero cells. Vero E6 cells were pre-treated with DMSO alone or Wnt inhibitors at specific concentrations (IWP-O1 (1 μ M and 10 μ M), LGK-974 (1 μ M and 10 μ M), Wnt-C59 (10 μ M), NCB-0846 (1 μ M and 10 μ M), KYA1797K (1 μ M and 10 μ M), ETC-1922159 (10 μ M), Pyrvinium (10 nM and 100 nM), iCRT-14 (1 μ M), SM04755 (1 μ M), and E7449 (1 μ M)) for 24 hours and then infected with SARS-CoV-2 (CANADA/VIDO01/2020 strain, MOI of 0.5). Twenty-four hours later, virus-containing media were subjected to plaque assays and total RNA extracted from cells was subjected to qRT-PCR to determine relative levels of viral RNA. Average viral titers (A) and genomic RNA levels (B) from drug-treated cells from 3 independent experiments are shown. Error bars represent standard error of the mean.



G.

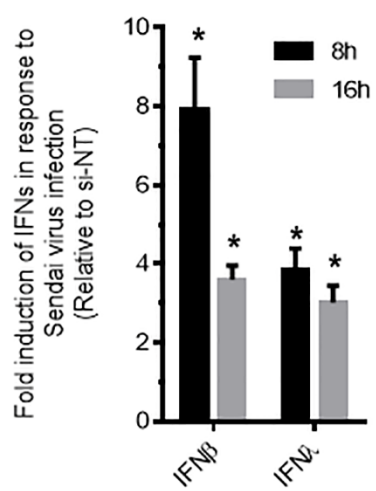


Figure 4.14. Reducing β -catenin expression increases peroxisome density and inhibits replication of SARS-CoV-2. Calu-3 cells were transfected with siRNA against β -catenin or a control non-targeting siRNA for 48 hours after which cell lysates were processed for Western blot analyses with antibodies to β -catenin and actin (**A**) or qRT-PCR to determine levels of viral genomic RNA relative to actin mRNA (**B**). Cell media were subjected to plaque assay to determine viral titers (**C**). The average levels of expression (normalized to actin) from 3 independent experiments were determined. Error bars represent standard errors of the means. **D.** A549 cells were transfected siRNA against β -catenin or a control non-targeting siRNA for 24 hours and then infected with SARS-CoV-2 (CANADA/VIDO01/2020 strain) at MOI of 0.5. At twenty-four hours post infection, cells were fixed and processed for indirect immunofluorescence and confocal microscopy using a mouse monoclonal antibody to Spike protein and donkey anti-mouse IgG conjugated to Alexa Fluor 488. β -catenin was detected by a rabbit polyclonal antibody to β -catenin and donkey anti-rabbit IgG conjugated to Alexa Fluor 546. Nuclei were stained using DAPI. Images were obtained using a spinning-disc confocal microscope. **E.** A549 cells were transfected siRNA against β -catenin or a control non-targeting siRNA for 48 hours. Cells were then fixed and processed for indirect immunofluorescence and confocal microscopy. Peroxisomes were detected with a mouse monoclonal antibody to PMP70 and donkey anti-mouse IgG conjugated to Alexa Fluor 488. β -catenin was detected by a rabbit polyclonal antibody to β -catenin and donkey anti-rabbit IgG conjugated to Alexa Fluor 546. Prior to mounting, samples were incubated with CellMask Deep Red. Images were obtained using a spinning-disc confocal microscope. **F.** Box-and-whisker plot of the peroxisomal density of cells. The peroxisomal densities were calculated by quantifying the number of PEX14 puncta structures from Z-stack confocal images of the entire cell and dividing by the cell volume. Boxes show the 25th, 50th, and 75th percentiles. Points represent a minimum of 60 cells which were analyzed in three independent experiments. *, $P < 0.05$. **G.** A549 cells were transfected with non-targeting siRNAs as a control or si-RNA targeting β -catenin. Forty-eight hours later, cells were challenged with 100 HAU/ml of Sendai virus for 8- or 16-hours after which total cellular RNA was harvested and subjected to qRT-PCR to determine relative levels mRNA encoding type I (IFN β) and type III (IFN λ 2) IFNs. Values from three independent experiments are shown. Error bars represent standard errors of the mean. *, $P < 0.05$

In addition to reducing virus replication and titers, si-RNA mediated knockdown of β -catenin reduced the susceptibility of Calu-3 cells to SARS-CoV-2 infection (**Figure 4.14D**).

To determine if silencing β -catenin expression induced peroxisome proliferation and enhanced IFN induction in response to Sendai virus infection, A549 cells were transfected with non-targeting siRNA as a control or siRNA targeting β -catenin for 48-hours and then processed for indirect immunofluorescence and confocal microscopy or qRT-PCR to assess IFN induction. Data shown in **Figures 4.14E and F** revealed that peroxisome density increased by 43% in cells transfected with siRNA targeting β -catenin compared to those transfected with non-targeting siRNA. In addition, expression of IFN β and IFN λ in response to Sendai virus infection was significantly increased in cells transfected with siRNA targeting β -catenin (**Figure 4.14G**). Together, these results suggest that β -catenin possibly exerts its pro-viral effects by downregulating peroxisome biogenesis and IFN expression.

4.2.4. Wnt/ β -catenin inhibitors have broad-spectrum antiviral activity

IFNs have been shown to restrict the replication of other human pathogenic viruses including Zika virus (ZIKV) and Mayaro virus (MAYV) (Bayer *et al.*, 2016; Caine *et al.*, 2019; Corry *et al.*, 2017; Figueiredo *et al.*, 2019; Gobillot *et al.*, 2020). Therefore, I next investigated if/how Wnt/ β -catenin inhibitors affected replication of ZIKV and MAYV. In this experiment, I focused on IWP-O1, KYA1797K and Pyrvinium because they showed the highest selectivity indexes against SARS-CoV-2 in Calu-3 cells (**Figure 4.6 A**). A549 cells were treated with DMSO as a control or Wnt/ β -catenin inhibitors for 24-hours, after which the cells were infected with ZIKV or MAYV for another 48- or 24-hours respectively after which cell media and total cellular RNA were collected. Results from plaque assays and qRT-PCR analyses showed that Wnt/ β -catenin inhibitors reduced the titers of ZIKV and MAYV by at least 50% and 70% respectively

(Figure 4.15). Specifically, KYA1797K potently reduced the titers of ZIKV and MAYV by more than 85% and 95% respectively. However, the antiviral effects of the inhibitors on the replication of ZIKV and MAYV are less potent in comparison to SARS-CoV-2.

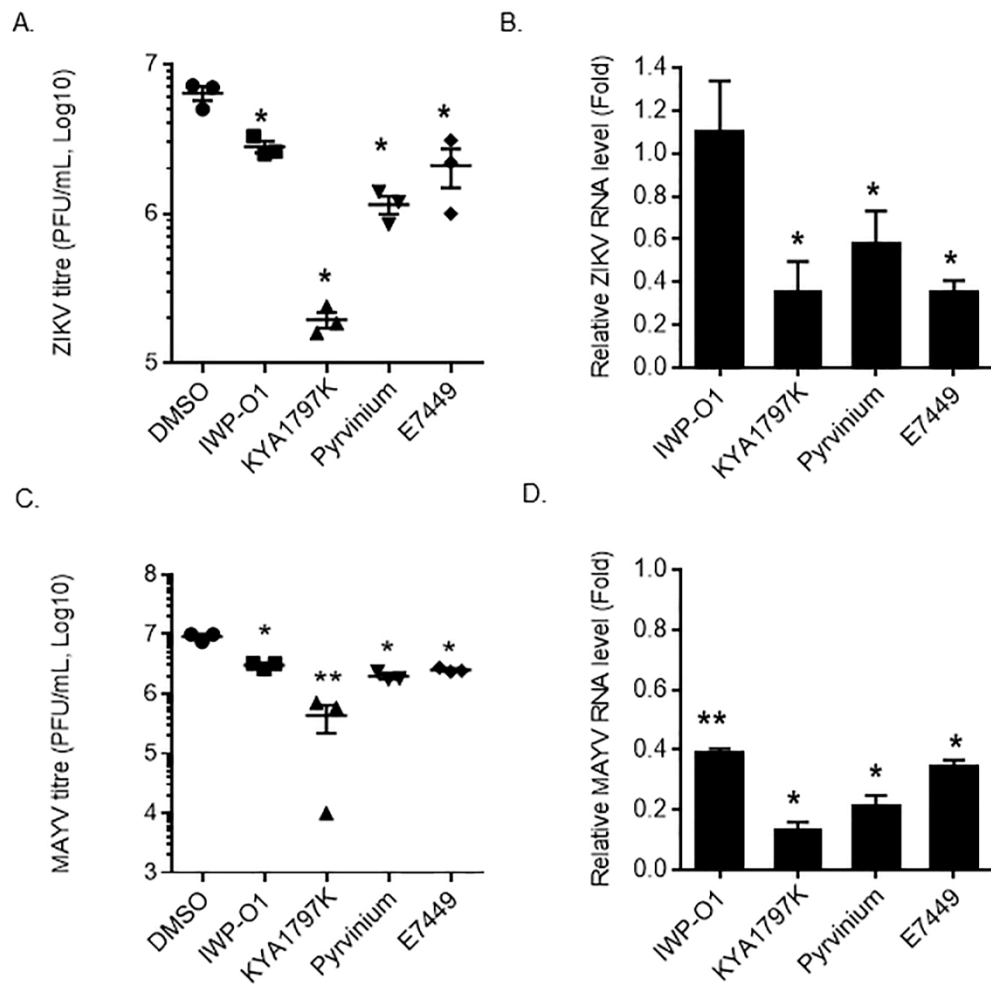


Figure 4.15. Wnt/ β -catenin inhibitors reduce replication of other RNA viruses. A549 cells were treated with Wnt/ β -catenin inhibitors (IWP-O1 (1 μ M), KYA1797K (1 μ M), Pyrvinium (100 nM), E7449 (1 μ M)) or DMSO alone for 24 hours, after which the cells were infected with 0.1 MOI of Zika virus (ZIKV) for another 48 hours or Mayaro virus (MAYV) for another 24 hours. Cell media were subjected to plaque assays and total RNA extracted from cells was subjected to qRT-PCR to determine relative levels of viral RNA. Average viral titers (A, C) and genomic RNA levels (B, D) from drug-treated cells from 3 independent experiments are shown. Error bars represent standard error of the mean. *, $P < 0.05$; **, $P < 0.01$; N.S. (not significant).

4.2.6. Summary

In this chapter, I investigated the antiviral effects of Wnt/ β -catenin inhibitors on SARS-CoV-2 as well as ZIKV and MAYV. My data show Wnt/ β -catenin inhibitors that act at different points in the signaling pathway (Table 4.1) potentially inhibit replication of SARS-CoV-2 in Calu-3 cells and primary NHBE cells. Among the 10 Wnt/ β -catenin inhibitors tested, IWP-O1, KYA1797K and Pyrvinium also showed strong antiviral effects on the viral replication when they were added post-infection. These three inhibitors, which have high selectivity indexes, also inhibited the replication of SARS-CoV-2 variants of concern.

Activation of Wnt/ β -catenin signaling pathway was previously shown to impair peroxisome biogenesis during viral infection (Xu *et al.*, 2020). Here, I demonstrated that Wnt/ β -catenin inhibitors increase peroxisome density in multiple cell types. Furthermore, the inhibitors also enhanced IFN expression in response to Sendai virus infection, possibly by promoting the localization of MAVS to peroxisomes. The strong inhibitory effects on SARS-CoV-2 replication are likely the result of the increased peroxisome biogenesis which enhances IFN expression. This is supported by the finding that Wnt/ β -catenin inhibitors did not affect the replication of SARS-CoV-2 in Vero cells which do not produce IFNs (Desmyter *et al.*, 1968). In addition to SARS-CoV-2, Wnt/ β -catenin inhibitors also reduced replication of ZIKV and MAYV. As such, the host-directed immune response activated by Wnt/ β -catenin inhibitors may have broad treatment applications to other human pathogenic RNA viruses. Reducing β -catenin levels using siRNA also had a potent antiviral effect on SARS-CoV-2 replication indicating that β -catenin is a host-dependency factor for this virus. The knockdown of β -catenin also increased peroxisome density and enhanced IFN induction in response to Sendai virus infection.

Collectively, the findings in Chapter 4 highlight the potential use of Wnt/ β -catenin inhibitors as prophylactics and/or therapeutics for treating COVID-19 and potentially other viral infection. Further investigation will focus on whether Wnt/ β -catenin inhibitors can block SARS-CoV-2 infection *in vivo*. In addition, it is also fundamental in elucidating how the inhibition of Wnt/ β -catenin signaling pathway induces peroxisome proliferation. Possible mechanisms will be discussed in Chapter 5.

Chapter 5

Discussion

5.1 Synopsis

My thesis work focused on using two different approaches to induce peroxisome proliferation and consequently enhance IFN response. In Chapter 3, I showed that peroxisomes are depleted during ZIKV infection, and demonstrated that over-expression of PEX11B inhibits ZIKV replication, likely by boosting IFN response which results from the increased peroxisome proliferation. As such, I will begin this chapter by discussing the antiviral roles of peroxisomes and how ZIKV causes depletion of these organelles during infection.

In Chapter 4, I showed that Wnt/ β -catenin signaling pathway inhibitors potently block SARS-CoV-2 replication. I further proposed plausible antiviral effects of the inhibitors by presenting evidence that Wnt/ β -catenin inhibitors potentiated the IFN response by inducing peroxisome proliferation. As such, I will discuss the potential roles for IFNs and IFN agonists in treating COVID-19. Moreover, I will discuss the various mechanisms that have been proposed for inducing peroxisome proliferation. Finally, I will finish this section by discussing possible IFN-independent antiviral effects of Wnt/ β -catenin signaling pathway.

5.2 Peroxisomes are antiviral organelles

For more than a decade now, peroxisomes have been recognized as antiviral signaling platforms that mediate IFN expression (Dixit *et al.*, 2010; Odendall *et al.*, 2014). Subsequently, it was shown that multiple viruses employ different strategies to deplete peroxisomes during infection, likely as a means to suppress IFN induction (reviewed in (Wong *et al.*, 2018). Examples include flaviviruses like ZIKV, DENV, WNV and HCV as well as coronaviruses such as SARS-CoV-2 and porcine epidemic diarrhea virus (PEDV) (Knoblach *et al.*, 2021; Lupberger *et al.*, 2019; Wong *et al.*, 2019; You *et al.*, 2015; Zhang *et al.*, 2018). Consistent with my data, a study by

another laboratory reported loss of peroxisomes during ZIKV infection (Coyaud et al., 2018). This included reduction in PMP70 protein levels and lower peroxisome density in ZIKV-infected cells. In Chapter 3 and in Wong et al., 2019, I showed that over-expression of PEX11B induced peroxisome proliferation which in turn enhanced the IFN response thus inhibiting ZIKV replication. The data further consolidate the role of peroxisomes in restricting viral infections.

While much of the published data are consistent with respect to what happens to peroxisomes during viral infection, two studies propose contrasting views on the roles of peroxisomes during ZIKV infection (Coyaud *et al.*, 2018; Farelo et al., 2022), specifically that ZIKV requires peroxisomes to establish infection. They show that the replication of ZIKV in fibroblast lines derived from patients with peroxisomal biogenesis disorders is lower than in fibroblasts from control patients. However, the effects of the genetic background of different host donors on ZIKV replication were not taken into consideration. This is important as our lab showed that the permissiveness of human fetal astrocytes to ZIKV varied significantly depending upon the individual donor (Limonta et al., 2018) indicating that differences within the host genetic background can affect viral infection. Furthermore, no significant differences in the production of ZIKV between infected normal and peroxisome-deficient cells were observed until 96 h.p.i. and even then, the differences in titers were only less than one log. (Coyaud *et al.*, 2018). Therefore, these data alone are not evidence to support the conclusion that ZIKV depends on peroxisomes to establish infection.

Instead of using cells derived from patients with peroxisome biogenesis disorders, we used CRISPR to create a line of A549 cells devoid of peroxisomes due to a lack of PEX19, which is essential for formation of peroxisomes (**Appendix 1A**). PEX19 knockout (KO) cells were infected with ZIKV for 48 hours, and the media and cell lysates were collected for plaque assay and qRT-PCR analyses respectively. Data in **Appendix 1B** show that replication of ZIKV was not affected

in peroxisome-deficient cells, indicating the virus does not require peroxisomes to establish infection. The similar viral titers and viral RNA levels between PEX19 KO cells and WT cells are likely owing to the unaffected cellular antiviral immune response in the absence of peroxisomes, as the expression of interferon signaling genes (ISGs), including *IFN β* and *IFN λ* , does not reduce as reported in (Bender *et al.*, 2015; Odendall *et al.*, 2014). It is possible that the abundance of MAVS is comparable in cells with or without peroxisomes and mitochondrial MAVS might compensate for peroxisomal MAVS in cells lacking peroxisomes. In contrast to ZIKV, replication of the herpesvirus family member HCMV was reduced by more than 50% in PEX19 KO fibroblasts (Jean Beltran *et al.*, 2018). Moreover, peroxisome proliferation is promoted during HCMV infection, likely in order to increase synthesis of plasmalogen, which is enriched in the viral membranes.

Similar to flaviviruses, infection with the alphacoronavirus PEDV and the betacoronavirus SARS-CoV-2 result in loss of peroxisomes (Knoblach *et al.*, 2021; Zhang *et al.*, 2018). Expression of PEDV NSP1 alone was shown to deplete peroxisomes, possibly by inhibiting the translation of mRNAs encoding peroxisomal proteins (Shen *et al.*, 2018). The reduction of peroxisome numbers in NSP1 expressing cells is also consistent with the finding that NSP1 overexpression inhibits induction of *IFN λ* (Zhang *et al.*, 2018). Interestingly, SARS-CoV-2 infection appears to affect the integrity of peroxisomes (Farelo *et al.*, 2022; Knoblach *et al.*, 2021; Wong *et al.*, 2019; You *et al.*, 2015). Specifically, peroxisomal matrix proteins are mislocalized to the cytosol, possibly as a result of the interaction between the viral protein ORF14 and PEX14, a component of the docking complex that is required for matrix protein import. The compromised integrity of peroxisomes observed in SARS-CoV-2 infected cells may in turn impair the ability of these organelles to support an antiviral defense against this virus, which is extremely sensitive to IFN.

5.3 Elimination of peroxisomes by ZIKV capsid protein

Coyaud *et al.* also attempted to determine the viral determinant(s) of ZIKV responsible for the depletion of peroxisomes (Coyaud *et al.*, 2018). They used a BioID/IP-MS ZIKV-host interactome to identify interactions between host and ZIKV proteins. More than 3,000 interactions were identified, including showing that ZIKV NS2A binds to PEX3 as well as PEX19, both of which are critical peroxisome biosynthesis factors. The authors suggested that ZIKV NS2A interacts with PEX19 to impair peroxisome biogenesis but did not describe the possible mechanisms. Furthermore, peroxisome density was only reduced by ~8% in cells over-expressing ZIKV NS2A as revealed by confocal microscopy. No other approaches were used to validate interactions between viral proteins and peroxisome proteins identified in the interactome screen. For example, the interaction between ZIKV NS2A and PEX19 was not confirmed by co-immunoprecipitation or another independent assay. The authors also reported that GFP-NS2A localizes to peroxisomes as determined by colocalization with PMP70. In contrast, subsequent studies showed that HA-NS2A and flag-NS2A localized to the ER but not to peroxisomes (Alzhanova *et al.*, 2021; Zhang *et al.*, 2019). The discrepancy in the localization of ZIKV NS2A may stem from the differences in the size of the tag proteins. The protein size of GFP is ~28kDa, which is slightly larger than ZIKV NS2A and ~28 times larger than HA and flag proteins (Einhauer and Jungbauer, 2001; Prasher *et al.*, 1992; Wilson *et al.*, 1984; Zhang *et al.*, 2019). This may in turn interfere with the folding of NS2A.

Consistent with my data, other studies have reported that flavivirus capsid proteins interact with PEX19 (Farelo *et al.*, 2022; Scaturro *et al.*, 2018; You *et al.*, 2015). The most recent study by Farelo *et al.* showed that lower numbers of peroxisomes were observed in ZIKV capsid-expressing cells. Together, these results suggest that ZIKV capsid protein is a major viral

determinant in reducing peroxisome numbers in cells, likely in large part by targeting PEX19 for downregulation. Given that peroxisomes are important for the antiviral response (Dixit *et al.*, 2010; Odendall *et al.*, 2014), targeting of peroxisomes by flavivirus capsid proteins ZIKV infection is yet another means by which these viruses impair the IFN pathway. Consistent with this notion, qRT-PCR data show that expression of ZIKV capsid inhibits expression of IFN β and IFN λ in response to poly(I:C) (**Appendix 2**).

Future experiments will focus on understanding the mechanisms by which flavivirus capsid proteins reduce PEX19 protein levels. Results in **Appendix 3** show that ZIKV infection does not reduce PEX19 mRNA levels and because the capsid protein does not possess enzymatic activity, it cannot directly degrade PEX19. Therefore, other cellular factors must be involved in this process. Multiple flavivirus proteins are known to interact with host proteins in order to antagonize IFN induction and signaling pathways. For example, DENV NS5 protein binds to the E3 ubiquitin ligase UBR4 and promotes the interaction between UBR4 and STAT2 to mediate the degradation of STAT2, thereby suppressing IFN signaling (Morrison *et al.*, 2013). Possible host proteins mediating the loss of PEX19 include E3 ubiquitin ligase HUWE1, which was identified as interacting ZIKV capsid protein during an interactome analysis conducted by our collaborator, Dr. Lori Frappier (U of Toronto). It is possible that ZIKV capsid protein interacts with the ubiquitin ligase to target PEX19 for proteasomal degradation, resulting in impaired peroxisome biogenesis during infection. To investigate if HUWE1 mediates the loss of PEX19, cells were transfected with siRNAs targeting HUWE1 for 24 hours and then ZIKV infection for another 48 hours. Cell lysates were collected for Western blot analysis or RNA extraction for qRT-PCR analysis. Results show that levels of ZIKV viral RNA were not affected in cells transfected with HUWE1-specific siRNAs (**Appendix 4A**) nor were PEX19 protein levels affected (**Appendix**

4B). Unfortunately, knockdown of *HUWE1* RNA was not very efficient (**Appendix 4C**) and therefore, optimizing the knockdown efficiency is needed to better examine the potential role of *HUWE1* on capsid-dependent reduction of *PEX19*. Use of CRISPR/Cas9 to disrupt *HUWE1* may be the best approach.

In addition to *HUWE1*, *ZIKV* capsid was reported to interact with VAMP-associated proteins *VAPA* and *VAPB* (Hua *et al.*, 2017), which are ER-resident proteins that interact with peroxisomal membrane protein acyl-CoA binding domain containing 5 (*ACBD5*). The *VAP-ACBD5* interaction acts as a tether for peroxisomes to the ER. Loss of *VAPA* and *VAPB* by siRNA-mediated knockdown results in the reduction of peroxisome surface area in cells (Hua *et al.*, 2017). It is possible that *ZIKV* capsid protein interacts with *VAPA* and/or *VAPB* to cause loss of peroxisomes, resulting in the reduction of peroxisomal protein levels including *PEX19*. To this end, I transfected the cells with shRNA plasmid targeting *VAPA* for 24 hours, after which I infected the cells with *ZIKV* for another 48 hours. Cell lysates were collected for Western blot analysis or processed for RNA extraction for qRT-PCR analysis. Results show that transduction of lentivirus expressing shRNA targeting *VAPA* did not reduce *ZIKV* viral RNA level (**Appendix 5A**). In addition, *PEX19* protein levels in cells silencing with *VAPA* are comparable to the control during *ZIKV* infection (**Appendix 5B**). Optimizing the knockdown efficiency is needed as the qRT-PCR result shows that *VAPA* mRNA level unexpectedly increases in cells transduced with lentiviruses expressing shRNA targeting *VAPA* (**Appendix 5C**). Finally, validation of the interactions between capsid and host proteins which were identified in the interactome by assays including co-immunoprecipitation is important for subsequent functional analyses of the capsid-mediated loss of peroxisomes in cells.

5.4 Potentials use of Wnt/ β -catenin inhibitors in treating COVID-19

IFN β and IFN λ have been investigated for efficacy as treatments for hospitalized patients with mild to moderate COVID-19 (Feld *et al.*, 2021; Hung *et al.*, 2020; Monk *et al.*, 2020). Patients who received IFN β or IFN λ alone by injection or inhalation, or in combination with other drugs showed lower viral load in comparison to patients who did not receive IFN. However, a phase III study which evaluated the effect of Remdesivir alone or in combination with subcutaneously administered IFN β in treating hospitalized patients with COVID-19 pneumonia showed contrasting results (Kalil *et al.*, 2021). Specifically, IFN β in combination with Remdesivir was no more effective than Remdesivir alone in reducing duration of symptoms and time to recovery. It is worth noting that the study focused on more severely ill patients with radiographic infiltrates who required supplemental oxygen. Therefore, the potential benefits of IFN β or even IFN λ in patients with early-stage or mild COVID-19 was not clear.

Besides the administration of recombinant IFNs, host-directed antivirals which induce IFN expression have also been explored to treat COVID-19. One study reported prophylactic and therapeutic intranasal administration of a diamidobenzimidazole STING agonist, diABZI-4, in SARS-CoV-2 infected transgenic mice expressing human ACE2 (hACE2) (Humphries *et al.*, 2021). Results of the study showed that the antiviral effects of diABZI-4 were IFN-dependent, indicating that the induction of IFN response restricts SARS-CoV-2 infection in mice. RNA samples extracted from lungs of diABZI-4 treated hACE2 mice revealed that the drug up-regulated expression of an array of inflammatory cytokines even in the absence of viral infection. This is not surprising given that IFNs have been shown to induce an inflammatory response in lung tissues without viral infections (reviewed in (Makris *et al.*, 2017)). As such, it is possible that

agents which directly stimulate IFN expression in the absence of viral infections may constitutively induce or even exacerbate inflammation.

The antiviral effects of the Wnt/ β -catenin inhibitors described in Chapter 4 are likely the result of increased peroxisome proliferation and concomitant enhanced IFN β and IFN λ expression. Importantly, none of the inhibitors up-regulate IFN expression in the absence of viral infection, suggesting that the pro-inflammatory side-effects of IFNs may be avoided when the drugs are administered for prophylactic use to people such as the essential workers during future pandemics. Among the 10 inhibitors reported, 3 of them also show strong antiviral activities when they were added after infection was established suggesting that some Wnt/ β -catenin inhibitors could also be used as therapeutics for outpatients with mild COVID-19. Advantages of this type of host-directed antivirals include reducing the reliance on injection or inhalation of recombinant IFNs and increasing the genetic barrier of the virus to escape the immune response.

Future experiments include whether the Wnt/ β -catenin inhibitors exhibit efficacy against SARS-CoV-2 replication *in vivo*. Drugs which are efficacious in treating COVID-19 in the animals may become potential candidates for possible clinical trials in the future, which will aim at evaluating the efficacies of Wnt/ β -catenin inhibitors in treating patients in early-stage COVID-19. Outcomes of the clinical studies will provide insights into the possible adverse effects, the appropriate dose and means of delivery for the use of the inhibitors as therapeutics in humans. Prophylaxis trials on Wnt/ β -catenin inhibitors are also worth exploring since the currently authorized direct-acting antivirals for COVID-19 are therapeutics only. On the other hand, the investigations on the potential complications of this peroxisome-based therapy on HCMV infected patients are also needed as it was reported that HCMV infection induces peroxisome proliferation

in cells to increase plasmalogen levels for the synthesis of viral membrane (Jean Beltran *et al.*, 2018).

5.5 Induction of peroxisome proliferation by inhibiting Wnt/ β -catenin signaling pathway

HIV infection activates Wnt/ β -catenin signaling pathway which results in the loss of peroxisomes (Xu *et al.*, 2020). Intriguingly, contrasting effects on this pathway and peroxisome biogenesis are observed during HCMV infection. It was reported that HCMV infection downregulates Wnt/ β -catenin signaling pathway by promoting loss of β -catenin protein (Angelova *et al.*, 2012), while inducing peroxisome proliferation to promote the synthesis of plasmalogen, which is enriched in HCMV viral membranes (Jean Beltran *et al.*, 2018). In chapter 4, I further addressed the link between Wnt/ β -catenin signaling pathway and peroxisome biogenesis by discovering a previously unrecognized role of Wnt/ β -catenin signaling pathway inhibitors in inducing peroxisome proliferation. In this section, I will discuss the possible underlying mechanisms by which Wnt/ β -catenin signaling pathway stimulates peroxisome proliferation.

Over-expression of PEX11B has been shown in multiple studies to induce peroxisome proliferation in human cells (Odendall *et al.*, 2014; Schrader *et al.*, 1998b; Wong *et al.*, 2019). Peroxisome proliferation can also be stimulated by fatty acids and hypolipidemic fibrates, which bind to the nuclear hormone receptor peroxisome proliferator-activated receptor alpha (PPAR α). Binding of agonists to PPAR α and its partner retinoid X receptor (RXR) results in the formation of PPAR/RXR heterodimers which then bind to peroxisome proliferator response elements (PPREs) in peroxisomal genes to initiate gene expression and therefore drive peroxisome proliferation (Forman *et al.*, 1997; Krey *et al.*, 1997). Multiple reports have documented crosstalk between the Wnt/ β -catenin signaling pathway and peroxisome proliferator-activated receptor

gamma (PPAR γ) (reviewed in (Vallée et al., 2018)). Connections between Wnt/ β -catenin signaling pathway and PPAR α agonists are reported in a human hepatocarcinoma cell line and a human retinal pigment epithelial cell line (Mandala et al., 2020; Thomas et al., 2015). However, the effects of the PPAR α agonists on peroxisome biogenesis in the human cell lines were not investigated in the studies.

Recently, a novel PPAR-independent pathway that induces peroxisome proliferation was described. The study reported a small worm phenotype/Mothers Against Decapentaplegic homolog 2/3 (SMAD2/3) transcription factor binding site in the promoter region of PEX11B (Azadi et al., 2020). Consistent with a previous study (Schrader et al., 1998a), Azadi et al demonstrated induction of peroxisome proliferation by TGF β in a SMAD2/3 dependent manner in a human hepatoblastoma cell line. Other peroxisome genes containing putative SMAD2/3 binding sites include Fis, PEX13 and PEX14, further indicating a role for SMAD2/3 and possibly TGF β signaling in peroxisome proliferation.

In contrast, there is evidence to suggest that SMAD2/3 is an inducer of the Wnt/ β -catenin signaling pathway. It interacts with and stabilizes β -catenin resulting in expression of Wnt-target genes when the pathway is stimulated by Wnt ligands (Zhang et al., 2010). This would seem to be at odds with a report from the Hobman lab showing that activation of Wnt/ β -catenin signaling pathway impairs peroxisome biogenesis, including PEX11B protein expression (Xu *et al.*, 2020). It is tempting to speculate that SMAD2/3 interaction with β -catenin alters in response to Wnt/ β -catenin signaling. Upon the activation of the Wnt/ β -catenin signaling pathway, SMAD2/3 may preferentially bind with β -catenin, whereas it may interact with PEX11B promoter region when Wnt/ β -catenin signaling is inhibited. The elucidation on the promoter regions of important biogenesis factors including PEX11B, and the possible interaction of Wnt/ β -catenin signaling

pathway with SMAD2/3 may reveal more potential pathways in inducing peroxisome proliferation.

The Hobman lab previously reported that overexpression of HIV vpu protein causes loss of peroxisomes by upregulating host miRNAs (miR-500a-5p, miR-34c-3p, and miR-381-3p) which target peroxisome biogenesis factors (PEX2, PEX7, and PEX13), a process which is dependent on the activated Wnt/ β -catenin signaling pathway (Xu *et al.*, 2020). The results indicate that peroxisome gene expression is downregulated by enhancing the expression of a subset of host miRNAs upon the activation of Wnt/ β -catenin signaling pathway. Conversely, Wnt/ β -catenin inhibitors may reduce or block expression of miRNAs targeting peroxisome biogenesis factors, and consequently drive peroxisome proliferation. Since the miRNA expression profile is cell-type specific, examinations on the changes on the expression of host miRNAs in response to the treatment of Wnt/ β -catenin inhibitors in different cell types will shed more light on the roles of Wnt/ β -catenin signaling pathway in peroxisome biogenesis.

5.6 IFN-independent antiviral effects of Wnt/ β -catenin signaling pathway inhibitors

Androgen signaling was recently reported to regulate ACE2 and TMPRSS2 levels in human lung cells (Samuel *et al.*, 2020). The study showed that drugs that inhibit androgen receptor (AR) or RNAi-mediated knockdown of AR downregulated the expression of ACE2 and TMPRSS2 in human primary lung epithelial cells. The antiandrogenic drugs not only reduced ACE2 levels in human lung organoid cultures, but when added prior to infection with SARS-CoV-2, reduced viral titers by 50% to 70%. The Wnt/ β -catenin signaling pathway is known to intersect with AR signaling. The Wnt/ β -catenin pathway inhibitor iCRT-3 was shown to reduce interaction of β -catenin with AR and inhibit AR target gene expression including *AR* and *CDK1* (Lee *et al.*, 2013). Another Wnt/ β -catenin inhibitor CWP232291 was shown to downregulate AR and reduce

TMPRSS2 RNA levels (Pak et al., 2019). In line with this, our qRT-PCR results in **Appendix 6** also show that stimulation of Wnt agonists upregulates the expression of AR. Furthermore, SARS-CoV-2 infection induces the expression of AR along with an array of Wnt target genes such as TCF1, TCF4, and c-myc. It seems that SARS-CoV-2 infection activates Wnt/ β -catenin signaling pathway, which results in the up-regulation of Wnt target genes including AR, likely to induce the expression of ACE2 and /or TMPRSS2 to promote viral entry.

Results described in Chapter 4 indicate that Wnt/ β -catenin signaling pathway inhibitors block the replication of SARS-CoV-2, largely in part by enhancing peroxisome proliferation and consequently IFN induction. Wnt/ β -catenin inhibitors may also limit SARS-CoV-2 infection by downregulating expression of AR which in turn, results in lower levels of ACE2 and/or TMPRSS2. This IFN-independent antiviral effects of Wnt/ β -catenin inhibitors are not mutually exclusive to the mechanism that I proposed in Chapter 4, but rather, may play a complementary role in limiting SARS-CoV-2 infection: one blocking the viral entry while the other one boosts the IFN response.

5.7 Peroxisome-independent antiviral effects of Wnt/ β -catenin signaling pathway inhibitors

Consistent with my data in Chapter 4, a study reported that siRNA mediated knockdown of β -catenin increased IFN expression in response to Sendai virus in human cells ((Baril *et al.*, 2013)). In Chapter 4, I proposed plausible antiviral effects of the inhibitors by presenting evidence that Wnt/ β -catenin inhibitors potentiated the IFN response by inducing peroxisome proliferation. Barli *et al.* elucidated the mechanisms in which Wnt/ β -catenin signaling pathway impaired IFN induction by showing that β -catenin interacts with IRF3 in Sendai virus infected HEK 293T cells ((Baril *et al.*, 2013)), suggesting a possible role of Wnt/ β -catenin signaling pathway in the inhibition of the antiviral innate immune response through regulation of IRF3. Conversely,

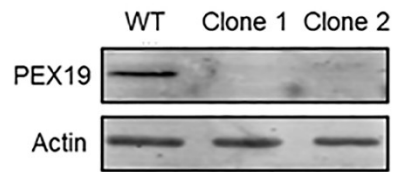
inhibition of Wnt/ β -catenin signaling pathway may result in the removal of the inhibitory effects on IRF3, inducing the expression of IFN β . This possible antiviral effect of Wnt/ β -catenin inhibitors does not exclude the possibility of the antiviral effects of peroxisome proliferation that I proposed in Chapter 4. In fact, both mechanisms may play their roles in parallel in inducing IFN response, which consequently result in the inhibition of viral replication.

5.8 Concluding remarks

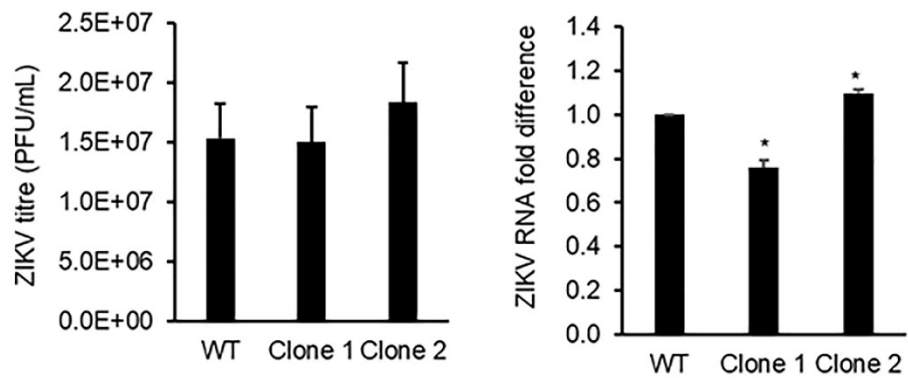
In the past two decades, rapidly evolving emerging and re-emerging viruses have caused diseases that disrupt society and the healthcare systems. It is important to better understand various cellular pathways involved in the diseases. Peroxisomes are targeted by RNA viruses for elimination because of their antiviral properties. Manipulation of cellular pathways to induce peroxisome proliferation provides an approach to induce host immune response, and consequently restrict viral infections. By inducing peroxisome proliferation, Wnt/ β -catenin inhibitors can be used as host-directed antivirals for COVID-19, and they provide treatments which do not require injection or inhalation of IFNs, further reducing the burden of the healthcare systems around the globe. Wnt/ β -catenin inhibitors may be prospective candidates for delivering the peroxisome-based therapy not only for COVID-19, but also possibly for respiratory diseases caused by newly emerging coronaviruses in the future. The discovery of the role of Wnt/ β -catenin signaling pathways inhibitors in inducing peroxisome proliferation opens up a novel avenue for researchers to repurpose existing drugs that modulate peroxisome biogenesis to inhibit viral replication.

Appendices

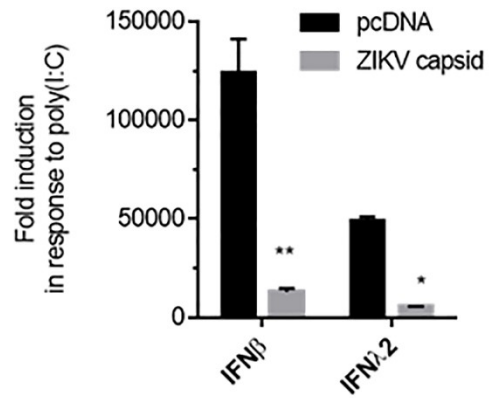
A.



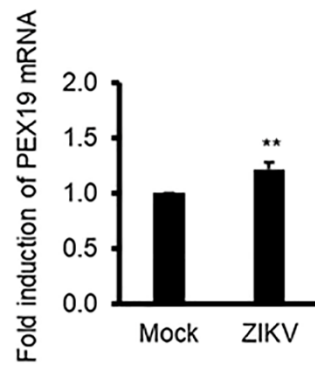
B.



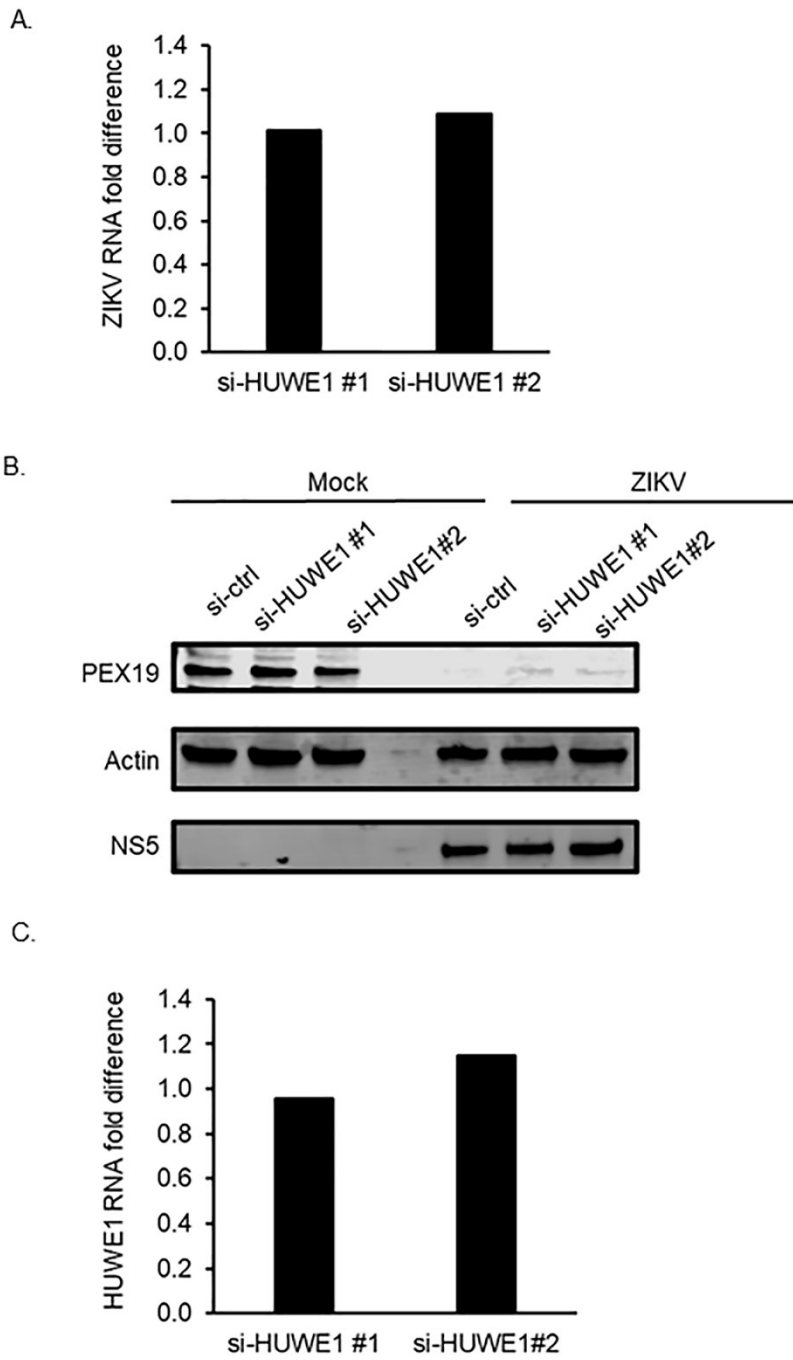
Appx. 1 ZIKV replication is not affected in A549 cells devoid of peroxisomes.
N=3



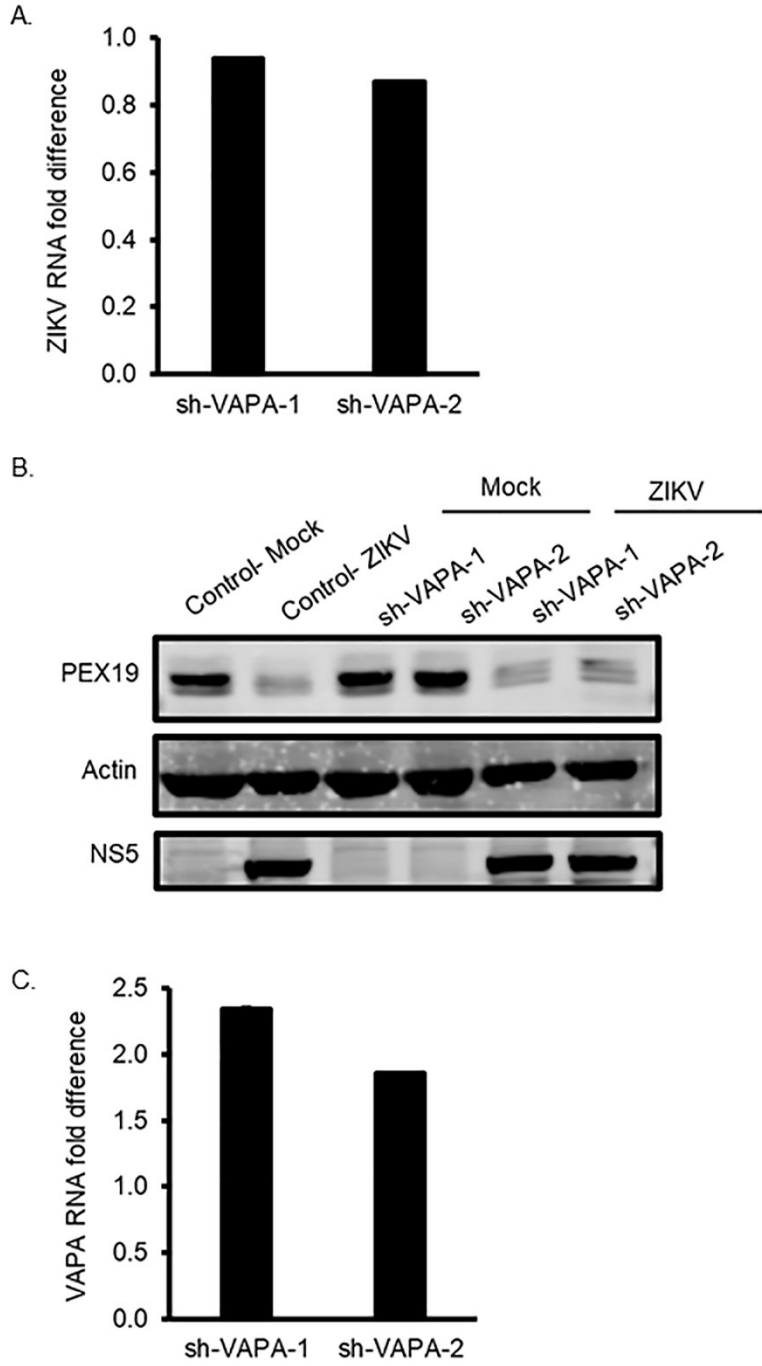
Appx.2 Expression of ZIKV capsid protein suppresses the induction of the expression of *IFNβ* and *IFNλ2* in response to poly(I:C) in A549 cells. N=3



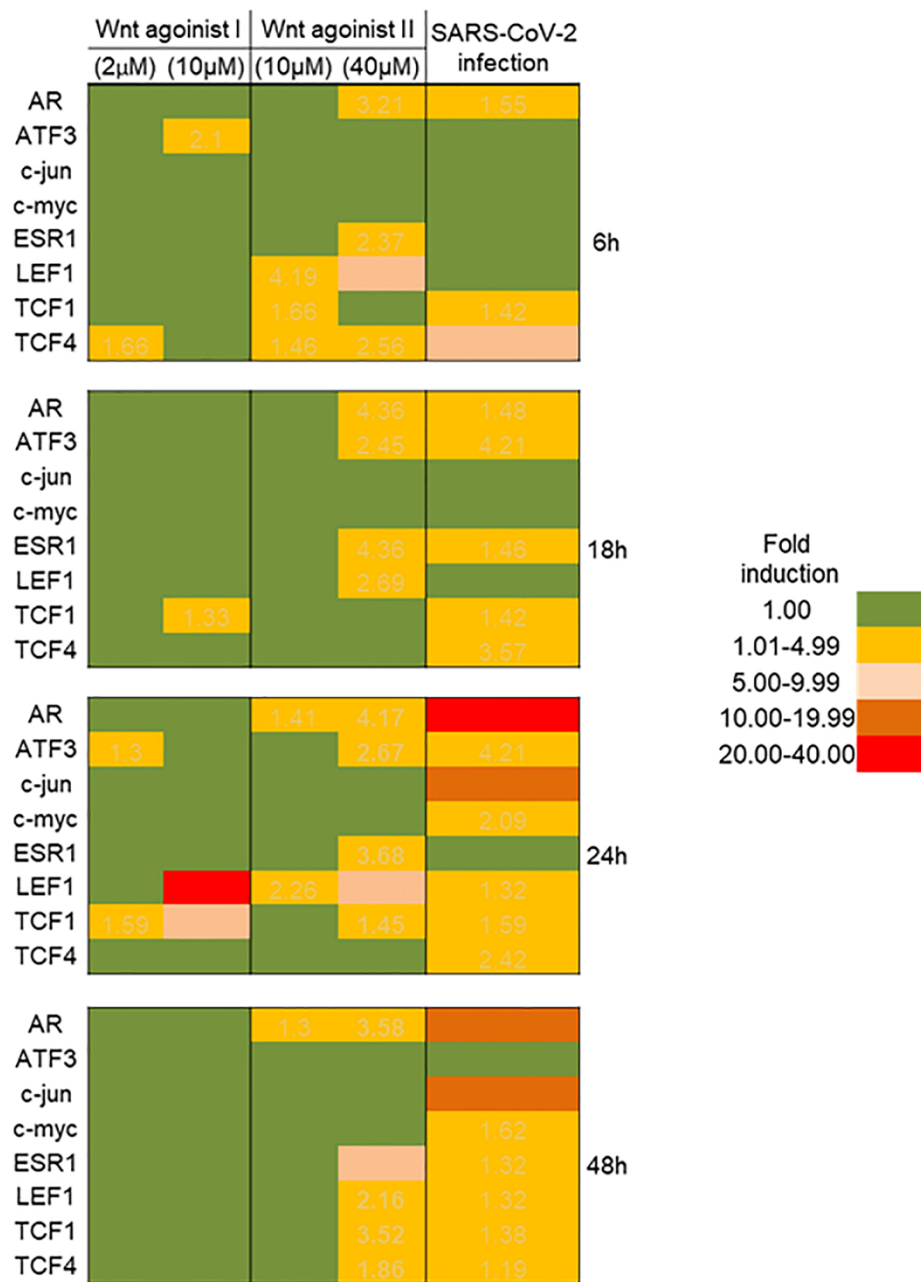
Appx. 3 PEX19 mRNA level slightly increases in ZIKV infected U251 cells. N=3



Appx. 4. Effects of siRNA mediated knockdown of HUWE1 on ZIKV replication in A549 cells. N=2



Appx. 5. Effects of shRNA mediated knockdown of VAPA on ZIKV replication in A549 cells. N=1



Appx.6 Fold induction of Wnt target genes by Wnt agonists and SARS-CoV-2 infection at the indicated time points post-infection or post treatment. Wnt agonist I (CAS 853220-52-7) and Wnt agonist II (SKL2001) were used. AR: androgen receptor. ATF3: activating transcription factor 3. ESR1: estrogen Receptor 1. LEF1: lymphoid enhancer-binding factor-1. TCF1: transcription factor T cell factor 1. TCF4: transcription factor T cell factor 4. N=3

References

- Abbink, P., Larocca, R.A., De La Barrera, R.A., Bricault, C.A., Moseley, E.T., Boyd, M., Kirilova, M., Li, Z., Ng'ang'a, D., Nanayakkara, O., et al. (2016). Protective efficacy of multiple vaccine platforms against Zika virus challenge in rhesus monkeys. *Science* 353, 1129-1132. 10.1126/science.aah6157.
- Abe, I., and Fujiki, Y. (1998). cDNA cloning and characterization of a constitutively expressed isoform of the human peroxin Pex11p. *Biochem Biophys Res Commun* 252, 529-533. 10.1006/bbrc.1998.9684.
- Aktepe, T.E., and Mackenzie, J.M. (2018). Shaping the flavivirus replication complex: It is curvaceous! *Cell Microbiol* 20, e12884. 10.1111/cmi.12884.
- Aliota, M.T., Caine, E.A., Walker, E.C., Larkin, K.E., Camacho, E., and Osorio, J.E. (2016). Characterization of Lethal Zika Virus Infection in AG129 Mice. *PLoS Negl Trop Dis* 10, e0004682. 10.1371/journal.pntd.0004682.
- Alzhanova, D., Corcoran, K., Bailey, A.G., Long, K., Taft-Benz, S., Graham, R.L., Broussard, G.S., Heise, M., Neumann, G., Halfmann, P., et al. (2021). Novel modulators of p53-signaling encoded by unknown genes of emerging viruses. *PLoS Pathog* 17, e1009033. 10.1371/journal.ppat.1009033.
- Amberg, S.M., and Rice, C.M. (1999). Mutagenesis of the NS2B-NS3-mediated cleavage site in the flavivirus capsid protein demonstrates a requirement for coordinated processing. *J Virol* 73, 8083-8094. 10.1128/JVI.73.10.8083-8094.1999.
- Angelini, M.M., Akhlaghpour, M., Neuman, B.W., and Buchmeier, M.J. (2013). Severe acute respiratory syndrome coronavirus nonstructural proteins 3, 4, and 6 induce double-membrane vesicles. *mBio* 4. 10.1128/mBio.00524-13.
- Angelova, M., Zvezdaryk, K., Ferris, M., Shan, B., Morris, C.A., and Sullivan, D.E. (2012). Human cytomegalovirus infection dysregulates the canonical Wnt/ β -catenin signaling pathway. *PLoS Pathog* 8, e1002959. 10.1371/journal.ppat.1002959.
- Aranovich, A., Hua, R., Rutenberg, A.D., and Kim, P.K. (2014). PEX16 contributes to peroxisome maintenance by constantly trafficking PEX3 via the ER. *J Cell Sci* 127, 3675-3686. 10.1242/jcs.146282.
- Azadi, A.S., Carmichael, R.E., Kovacs, W.J., Koster, J., Kors, S., Waterham, H.R., and Schrader, M. (2020). A Functional SMAD2/3 Binding Site in the PEX11 β Promoter Identifies a Role for TGF β in Peroxisome Proliferation in Humans. *Frontiers in cell and developmental biology* 8, 1184.
- Baril, M., Es-Saad, S., Chatel-Chaix, L., Fink, K., Pham, T., Raymond, V.A., Audette, K., Guenier, A.S., Duchaine, J., Servant, M., et al. (2013). Genome-wide RNAi screen reveals a new role of a WNT/CTNBN1 signaling pathway as negative regulator of virus-induced innate immune responses. *PLoS Pathog* 9, e1003416. 10.1371/journal.ppat.1003416.

Baum, A., Sachidanandam, R., and García-Sastre, A. (2010). Preference of RIG-I for short viral RNA molecules in infected cells revealed by next-generation sequencing. *Proc Natl Acad Sci U S A* *107*, 16303-16308. 10.1073/pnas.1005077107.

Bayer, A., Lennemann, N.J., Ouyang, Y., Bramley, J.C., Morosky, S., Marques, E.T., Cherry, S., Sadovsky, Y., and Coyne, C.B. (2016). Type III Interferons Produced by Human Placental Trophoblasts Confer Protection against Zika Virus Infection. *Cell Host Microbe* *19*, 705-712. 10.1016/j.chom.2016.03.008.

Bender, S., Reuter, A., Eberle, F., Einhorn, E., Binder, M., and Bartenschlager, R. (2015). Activation of Type I and III Interferon Response by Mitochondrial and Peroxisomal MAVS and Inhibition by Hepatitis C Virus. *PLoS Pathog* *11*, e1005264. 10.1371/journal.ppat.1005264.

Blanco-Melo, D., Nilsson-Payant, B.E., Liu, W.C., Uhl, S., Hoagland, D., Møller, R., Jordan, T.X., Oishi, K., Panis, M., Sachs, D., et al. (2020). Imbalanced Host Response to SARS-CoV-2 Drives Development of COVID-19. *Cell* *181*, 1036-1045.e1039. 10.1016/j.cell.2020.04.026.

Boehmer, T.K., Kompaniyets, L., Lavery, A.M., Hsu, J., Ko, J.Y., Yusuf, H., Romano, S.D., Gundlapalli, A.V., Oster, M.E., and Harris, A.M. (2021). Association Between COVID-19 and Myocarditis Using Hospital-Based Administrative Data - United States, March 2020-January 2021. *MMWR Morb Mortal Wkly Rep* *70*, 1228-1232. 10.15585/mmwr.mm7035e5.

Bonekamp, N.A., Völkl, A., Fahimi, H.D., and Schrader, M. (2009). Reactive oxygen species and peroxisomes: struggling for balance. *Biofactors* *35*, 346-355. 10.1002/biof.48.

Brasil, P., Pereira, J.P., Moreira, M.E., Ribeiro Nogueira, R.M., Damasceno, L., Wakimoto, M., Rabello, R.S., Valderramos, S.G., Halai, U.A., Salles, T.S., et al. (2016). Zika Virus Infection in Pregnant Women in Rio de Janeiro. *N Engl J Med* *375*, 2321-2334. 10.1056/NEJMoa1602412.

Busnadiego, I., Fernbach, S., Pohl, M.O., Karakus, U., Huber, M., Trkola, A., Stertz, S., and Hale, B.G. (2020). Antiviral Activity of Type I, II, and III Interferons Counterbalances ACE2 Inducibility and Restricts SARS-CoV-2. *mBio* *11*. 10.1128/mBio.01928-20.

Caine, E.A., Scheaffer, S.M., Arora, N., Zaitsev, K., Artyomov, M.N., Coyne, C.B., Moley, K.H., and Diamond, M.S. (2019). Interferon lambda protects the female reproductive tract against Zika virus infection. *Nat Commun* *10*, 280. 10.1038/s41467-018-07993-2.

Calvet, G., Aguiar, R.S., Melo, A.S.O., Sampaio, S.A., de Filippis, I., Fabri, A., Araujo, E.S.M., de Sequeira, P.C., de Mendonça, M.C.L., de Oliveira, L., et al. (2016). Detection and sequencing of Zika virus from amniotic fluid of fetuses with microcephaly in Brazil: a case study. *Lancet Infect Dis* *16*, 653-660. 10.1016/S1473-3099(16)00095-5.

Cantell, K., Hirvonen, S., Kauppinen, H.L., and Myllylä, G. (1981). Production of interferon in human leukocytes from normal donors with the use of Sendai virus. *Methods Enzymol* *78*, 29-38. 10.1016/0076-6879(81)78094-7.

Cao-Lormeau, V.M., Blake, A., Mons, S., Lastère, S., Roche, C., Vanhomwegen, J., Dub, T., Baudouin, L., Teissier, A., Larre, P., et al. (2016). Guillain-Barré Syndrome outbreak associated

with Zika virus infection in French Polynesia: a case-control study. *Lancet* 387, 1531-1539. 10.1016/S0140-6736(16)00562-6.

Cao-Lormeau, V.M., Roche, C., Teissier, A., Robin, E., Berry, A.L., Mallet, H.P., Sall, A.A., and Musso, D. (2014). Zika virus, French polynesia, South pacific, 2013. *Emerg Infect Dis* 20, 1085-1086. 10.3201/eid2006.140138.

Cevik, M., Bamford, C.G.G., and Ho, A. (2020). COVID-19 pandemic-a focused review for clinicians. *Clin Microbiol Infect* 26, 842-847. 10.1016/j.cmi.2020.04.023.

Cha, P.H., Cho, Y.H., Lee, S.K., Lee, J., Jeong, W.J., Moon, B.S., Yun, J.H., Yang, J.S., Choi, S., Yoon, J., et al. (2016). Small-molecule binding of the axin RGS domain promotes β -catenin and Ras degradation. *Nat Chem Biol* 12, 593-600. 10.1038/nchembio.2103.

Chan, J.F., Yuan, S., Kok, K.H., To, K.K., Chu, H., Yang, J., Xing, F., Liu, J., Yip, C.C., Poon, R.W., et al. (2020). A familial cluster of pneumonia associated with the 2019 novel coronavirus indicating person-to-person transmission: a study of a family cluster. *Lancet* 395, 514-523. 10.1016/S0140-6736(20)30154-9.

Chen, Y., Maguire, T., Hileman, R.E., Fromm, J.R., Esko, J.D., Linhardt, R.J., and Marks, R.M. (1997). Dengue virus infectivity depends on envelope protein binding to target cell heparan sulfate. *Nat Med* 3, 866-871. 10.1038/nm0897-866.

Chen, Y., Pieuchot, L., Loh, R.A., Yang, J., Kari, T.M., Wong, J.Y., and Jedd, G. (2014). Hydrophobic handoff for direct delivery of peroxisome tail-anchored proteins. *Nat Commun* 5, 5790. 10.1038/ncomms6790.

Chen, Y.T., Shao, S.C., Hsu, C.K., Wu, I.W., Hung, M.J., and Chen, Y.C. (2020). Incidence of acute kidney injury in COVID-19 infection: a systematic review and meta-analysis. *Crit Care* 24, 346. 10.1186/s13054-020-03009-y.

Chu, H., Chan, J.F., Yuen, T.T., Shuai, H., Yuan, S., Wang, Y., Hu, B., Yip, C.C., Tsang, J.O., Huang, X., et al. (2020). Comparative tropism, replication kinetics, and cell damage profiling of SARS-CoV-2 and SARS-CoV with implications for clinical manifestations, transmissibility, and laboratory studies of COVID-19: an observational study. *Lancet Microbe* 1, e14-e23. 10.1016/S2666-5247(20)30004-5.

Cimini, E., Castilletti, C., Sacchi, A., Casetti, R., Bordoni, V., Romanelli, A., Turchi, F., Martini, F., Tumino, N., Nicastri, E., et al. (2017). Human Zika infection induces a reduction of IFN- γ producing CD4 T-cells and a parallel expansion of effector V δ 2 T-cells. *Sci Rep* 7, 6313. 10.1038/s41598-017-06536-x.

Corry, J., Arora, N., Good, C.A., Sadovsky, Y., and Coyne, C.B. (2017). Organotypic models of type III interferon-mediated protection from Zika virus infections at the maternal-fetal interface. *Proc Natl Acad Sci U S A* 114, 9433-9438. 10.1073/pnas.1707513114.

Coyaud, E., Ranadheera, C., Cheng, D., Gonçalves, J., Dyakov, B.J.A., Laurent, E.M.N., St-Germain, J., Pelletier, L., Gingras, A.C., Brumell, J.H., et al. (2018). Global Interactomics

Uncovers Extensive Organellar Targeting by Zika Virus. *Mol Cell Proteomics* 17, 2242-2255. 10.1074/mcp.TIR118.000800.

Dalskov, L., Narita, R., Andersen, L.L., Jensen, N., Assil, S., Kristensen, K.H., Mikkelsen, J.G., Fujita, T., Mogensen, T.H., Paludan, S.R., and Hartmann, R. (2020). Characterization of distinct molecular interactions responsible for IRF3 and IRF7 phosphorylation and subsequent dimerization. *Nucleic Acids Res* 48, 11421-11433. 10.1093/nar/gkaa873.

Daugherty, S.E., Guo, Y., Heath, K., Dasmariñas, M.C., Jubilo, K.G., Samranvedhya, J., Lipsitch, M., and Cohen, K. (2021). Risk of clinical sequelae after the acute phase of SARS-CoV-2 infection: retrospective cohort study. *BMJ* 373, n1098. 10.1136/bmj.n1098.

de Araújo, T.V.B., Rodrigues, L.C., de Alencar Ximenes, R.A., de Barros Miranda-Filho, D., Montarroyos, U.R., de Melo, A.P.L., Valongueiro, S., de Albuquerque, M.F.P.M., Souza, W.V., Braga, C., et al. (2016). Association between Zika virus infection and microcephaly in Brazil, January to May, 2016: preliminary report of a case-control study. *Lancet Infect Dis* 16, 1356-1363. 10.1016/S1473-3099(16)30318-8.

Decout, A., Katz, J.D., Venkatraman, S., and Ablasser, A. (2021). The cGAS-STING pathway as a therapeutic target in inflammatory diseases. *Nat Rev Immunol* 21, 548-569. 10.1038/s41577-021-00524-z.

Delille, H.K., Dodt, G., and Schrader, M. (2011). Pex11p β -mediated maturation of peroxisomes. *Commun Integr Biol* 4, 51-54. 10.4161/cib.4.1.13647.

Deng, S.Q., and Peng, H.J. (2020). Characteristics of and Public Health Responses to the Coronavirus Disease 2019 Outbreak in China. *J Clin Med* 9. 10.3390/jcm9020575.

Deosaran, E., Larsen, K.B., Hua, R., Sargent, G., Wang, Y., Kim, S., Lamark, T., Jauregui, M., Law, K., Lippincott-Schwartz, J., et al. (2013). NBR1 acts as an autophagy receptor for peroxisomes. *J Cell Sci* 126, 939-952. 10.1242/jcs.114819.

Deshmukh, V., Seo, T., O'Green, A.L., Ibanez, M., Hofilena, B., Kc, S., Stewart, J., Dellamary, L., Chiu, K., Ghias, A., et al. (2020). SM04755, a small-molecule inhibitor of the Wnt pathway, as a potential topical treatment for tendinopathy. *J Orthop Res*. 10.1002/jor.24898.

Desmyter, J., Melnick, J.L., and Rawls, W.E. (1968). Defectiveness of interferon production and of rubella virus interference in a line of African green monkey kidney cells (Vero). *J Virol* 2, 955-961.

Dick, G.W., KITCHEN, S.F., and HADDOW, A.J. (1952). Zika virus. I. Isolations and serological specificity. *Trans R Soc Trop Med Hyg* 46, 509-520.

Ding, J., Aldo, P., Roberts, C.M., Stabach, P., Liu, H., You, Y., Qiu, X., Jeong, J., Maxwell, A., Lindenbach, B., et al. (2021). Placenta-derived interferon-stimulated gene 20 controls ZIKA virus infection. *EMBO Rep* 22, e52450. 10.15252/embr.202152450.

Dixit, E., Boulant, S., Zhang, Y., Lee, A.S., Odendall, C., Shum, B., Hacohen, N., Chen, Z.J., Whelan, S.P., Fransen, M., et al. (2010). Peroxisomes are signaling platforms for antiviral innate immunity. *Cell* 141, 668-681. 10.1016/j.cell.2010.04.018.

Dong, Y., Dai, T., Wang, B., Zhang, L., Zeng, L.H., Huang, J., Yan, H., and Zhou, F. (2021). The way of SARS-CoV-2 vaccine development: success and challenges. *Signal Transduct Target Ther* 6, 387. 10.1038/s41392-021-00796-w.

Driggers, R.W., Ho, C.Y., Korhonen, E.M., Kuivanen, S., Jääskeläinen, A.J., Smura, T., Rosenberg, A., Hill, D.A., DeBiasi, R.L., Vezina, G., et al. (2016). Zika Virus Infection with Prolonged Maternal Viremia and Fetal Brain Abnormalities. *N Engl J Med* 374, 2142-2151. 10.1056/NEJMoA1601824.

Duffy, M.R., Chen, T.H., Hancock, W.T., Powers, A.M., Kool, J.L., Lanciotti, R.S., Pretrick, M., Marfel, M., Holzbauer, S., Dubray, C., et al. (2009). Zika virus outbreak on Yap Island, Federated States of Micronesia. *N Engl J Med* 360, 2536-2543. 10.1056/NEJMoA0805715.

Einhauer, A., and Jungbauer, A. (2001). The FLAG peptide, a versatile fusion tag for the purification of recombinant proteins. *J Biochem Biophys Methods* 49, 455-465. 10.1016/s0165-022x(01)00213-5.

Fang, Y., Morrell, J.C., Jones, J.M., and Gould, S.J. (2004). PEX3 functions as a PEX19 docking factor in the import of class I peroxisomal membrane proteins. *J Cell Biol* 164, 863-875. 10.1083/jcb.200311131.

Farelo, M.A., Korrou-Karava, D., Brooks, K.F., Russell, T.A., Maringer, K., and Mayerhofer, P.U. (2022). Dengue and Zika Virus Capsid Proteins Contain a Common PEX19-Binding Motif. *Viruses* 14. 10.3390/v14020253.

Faria, N.R., Azevedo, R.D.S.D., Kraemer, M.U.G., Souza, R., Cunha, M.S., Hill, S.C., Thézé, J., Bonsall, M.B., Bowden, T.A., Rissanan, I., et al. (2016). Zika virus in the Americas: Early epidemiological and genetic findings. *Science* 352, 345-349. 10.1126/science.aaf5036.

Fauci, A.S., and Morens, D.M. (2016). Zika Virus in the Americas--Yet Another Arbovirus Threat. *N Engl J Med* 374, 601-604. 10.1056/NEJMp1600297.

Feld, J.J., Kandel, C., Biondi, M.J., Kozak, R.A., Zahoor, M.A., Lemieux, C., Borgia, S.M., Boggild, A.K., Powis, J., McCready, J., et al. (2021). Peginterferon lambda for the treatment of outpatients with COVID-19: a phase 2, placebo-controlled randomised trial. *Lancet Respir Med* 9, 498-510. 10.1016/S2213-2600(20)30566-X.

Ferreira, A.R., Magalhães, A.C., Camões, F., Gouveia, A., Vieira, M., Kagan, J.C., and Ribeiro, D. (2016). Hepatitis C virus NS3-4A inhibits the peroxisomal MAVS-dependent antiviral signalling response. *J Cell Mol Med* 20, 750-757. 10.1111/jcmm.12801.

Figueiredo, C.M., Neris, R.L.D.S., Gavino-Leopoldino, D., da Silva, M.O.L., Almeida, J.S., Dos-Santos, J.S., Figueiredo, C.P., Bellio, M., Bozza, M.T., and Assunção-Miranda, I. (2019). Mayaro Virus Replication Restriction and Induction of Muscular Inflammation in Mice Are Dependent on

Age, Type-I Interferon Response, and Adaptive Immunity. *Front Microbiol* *10*, 2246. 10.3389/fmicb.2019.02246.

Forman, B.M., Chen, J., and Evans, R.M. (1997). Hypolipidemic drugs, polyunsaturated fatty acids, and eicosanoids are ligands for peroxisome proliferator-activated receptors alpha and delta. *Proc Natl Acad Sci U S A* *94*, 4312-4317. 10.1073/pnas.94.9.4312.

Foy, B.D., Kobylinski, K.C., Chilson Foy, J.L., Blitvich, B.J., Travassos da Rosa, A., Haddow, A.D., Lanciotti, R.S., and Tesh, R.B. (2011). Probable non-vector-borne transmission of Zika virus, Colorado, USA. *Emerg Infect Dis* *17*, 880-882. 10.3201/eid1705.101939.

Fransen, M., Nordgren, M., Wang, B., and Apanasets, O. (2012). Role of peroxisomes in ROS/RNS-metabolism: implications for human disease. *Biochim Biophys Acta* *1822*, 1363-1373. 10.1016/j.bbadis.2011.12.001.

Fransen, M., Vastiau, I., Brees, C., Brys, V., Mannaerts, G.P., and Van Veldhoven, P.P. (2005). Analysis of human Pex19p's domain structure by pentapeptide scanning mutagenesis. *J Mol Biol* *346*, 1275-1286. 10.1016/j.jmb.2005.01.013.

Fu, Y.Z., Wang, S.Y., Zheng, Z.Q., Yi Huang, Li, W.W., Xu, Z.S., and Wang, Y.Y. (2021). SARS-CoV-2 membrane glycoprotein M antagonizes the MAVS-mediated innate antiviral response. *Cell Mol Immunol* *18*, 613-620. 10.1038/s41423-020-00571-x.

Fujiki, Y., Rachubinski, R.A., and Lazarow, P.B. (1984). Synthesis of a major integral membrane polypeptide of rat liver peroxisomes on free polysomes. *Proc Natl Acad Sci U S A* *81*, 7127-7131. 10.1073/pnas.81.22.7127.

Gandre-Babbe, S., and van der Blik, A.M. (2008). The novel tail-anchored membrane protein Mff controls mitochondrial and peroxisomal fission in mammalian cells. *Mol Biol Cell* *19*, 2402-2412. 10.1091/mbc.e07-12-1287.

Garcia-Beltran, W.F., Lam, E.C., St Denis, K., Nitido, A.D., Garcia, Z.H., Hauser, B.M., Feldman, J., Pavlovic, M.N., Gregory, D.J., Poznansky, M.C., et al. (2021). Multiple SARS-CoV-2 variants escape neutralization by vaccine-induced humoral immunity. *Cell* *184*, 2523. 10.1016/j.cell.2021.04.006.

Gatto, G.J., Geisbrecht, B.V., Gould, S.J., and Berg, J.M. (2000). Peroxisomal targeting signal-1 recognition by the TPR domains of human PEX5. *Nat Struct Biol* *7*, 1091-1095. 10.1038/81930.

Gaudinski, M.R., Houser, K.V., Morabito, K.M., Hu, Z., Yamshchikov, G., Rothwell, R.S., Berkowitz, N., Mendoza, F., Saunders, J.G., Novik, L., et al. (2018). Safety, tolerability, and immunogenicity of two Zika virus DNA vaccine candidates in healthy adults: randomised, open-label, phase 1 clinical trials. *Lancet* *391*, 552-562. 10.1016/S0140-6736(17)33105-7.

Ghinai, I., McPherson, T.D., Hunter, J.C., Kirking, H.L., Christiansen, D., Joshi, K., Rubin, R., Morales-Estrada, S., Black, S.R., Pacilli, M., et al. (2020). First known person-to-person transmission of severe acute respiratory syndrome coronavirus 2 (SARS-CoV-2) in the USA. *Lancet* *395*, 1137-1144. 10.1016/S0140-6736(20)30607-3.

- Ghosh, S., Dellibovi-Ragheb, T.A., Kerviel, A., Pak, E., Qiu, Q., Fisher, M., Takvorian, P.M., Bleck, C., Hsu, V.W., Fehr, A.R., et al. (2020). β -Coronaviruses Use Lysosomes for Egress Instead of the Biosynthetic Secretory Pathway. *Cell* *183*, 1520-1535.e1514. 10.1016/j.cell.2020.10.039.
- Giacomelli, A., Pezzati, L., Conti, F., Bernacchia, D., Siano, M., Oreni, L., Rusconi, S., Gervasoni, C., Ridolfo, A.L., Rizzardini, G., et al. (2020). Self-reported Olfactory and Taste Disorders in Patients With Severe Acute Respiratory Coronavirus 2 Infection: A Cross-sectional Study. *Clin Infect Dis* *71*, 889-890. 10.1093/cid/ciaa330.
- Gobillot, T.A., Humes, D., Sharma, A., Kikawa, C., and Overbaugh, J. (2020). The Robust Restriction of Zika Virus by Type-I Interferon in A549 Cells Varies by Viral Lineage and Is Not Determined by IFITM3. *Viruses* *12*. 10.3390/v12050503.
- Gonsalves, F.C., Klein, K., Carson, B.B., Katz, S., Ekas, L.A., Evans, S., Nagourney, R., Cardozo, T., Brown, A.M., and DasGupta, R. (2011). An RNAi-based chemical genetic screen identifies three small-molecule inhibitors of the Wnt/wingless signaling pathway. *Proc Natl Acad Sci U S A* *108*, 5954-5963. 10.1073/pnas.1017496108.
- Goubau, D., Deddouche, S., and Reis e Sousa, C. (2013). Cytosolic sensing of viruses. *Immunity* *38*, 855-869. 10.1016/j.immuni.2013.05.007.
- Gould, S.J., Keller, G.A., Hosken, N., Wilkinson, J., and Subramani, S. (1989). A conserved tripeptide sorts proteins to peroxisomes. *J Cell Biol* *108*, 1657-1664.
- Gralinski, L.E., and Menachery, V.D. (2020). Return of the Coronavirus: 2019-nCoV. *Viruses* *12*. 10.3390/v12020135.
- Grant, A., Ponia, S.S., Tripathi, S., Balasubramaniam, V., Miorin, L., Sourisseau, M., Schwarz, M.C., Sánchez-Seco, M.P., Evans, M.J., Best, S.M., and García-Sastre, A. (2016). Zika Virus Targets Human STAT2 to Inhibit Type I Interferon Signaling. *Cell Host Microbe* *19*, 882-890. 10.1016/j.chom.2016.05.009.
- Green, D.S., Young, H.A., and Valencia, J.C. (2017). Current prospects of type II interferon γ signaling and autoimmunity. *J Biol Chem* *292*, 13925-13933. 10.1074/jbc.R116.774745.
- Grou, C.P., Carvalho, A.F., Pinto, M.P., Wiese, S., Piechura, H., Meyer, H.E., Warscheid, B., Sá-Miranda, C., and Azevedo, J.E. (2008). Members of the E2D (UbcH5) family mediate the ubiquitination of the conserved cysteine of Pex5p, the peroxisomal import receptor. *J Biol Chem* *283*, 14190-14197. 10.1074/jbc.M800402200.
- Hackstadt, T., Chiramel, A.I., Hoyt, F.H., Williamson, B.N., Dooley, C.A., Beare, P.A., de Wit, E., Best, S.M., and Fischer, E.R. (2021). Disruption of the Golgi Apparatus and Contribution of the Endoplasmic Reticulum to the SARS-CoV-2 Replication Complex. *Viruses* *13*. 10.3390/v13091798.

Haddow, A.D., Schuh, A.J., Yasuda, C.Y., Kasper, M.R., Heang, V., Huy, R., Guzman, H., Tesh, R.B., and Weaver, S.C. (2012). Genetic characterization of Zika virus strains: geographic expansion of the Asian lineage. *PLoS Negl Trop Dis* 6, e1477. 10.1371/journal.pntd.0001477.

Hadjadj, J., Yatim, N., Barnabei, L., Corneau, A., Boussier, J., Smith, N., Péré, H., Charbit, B., Bondet, V., Chenevier-Gobeaux, C., et al. (2020). Impaired type I interferon activity and inflammatory responses in severe COVID-19 patients. *Science* 369, 718-724. 10.1126/science.abc6027.

Hamner, L., Dubbel, P., Capron, I., Ross, A., Jordan, A., Lee, J., Lynn, J., Ball, A., Narwal, S., Russell, S., et al. (2020). High SARS-CoV-2 Attack Rate Following Exposure at a Choir Practice - Skagit County, Washington, March 2020. *MMWR Morb Mortal Wkly Rep* 69, 606-610. 10.15585/mmwr.mm6919e6.

Hartenian, E., Nandakumar, D., Lari, A., Ly, M., Tucker, J.M., and Glaunsinger, B.A. (2020). The molecular virology of coronaviruses. *J Biol Chem* 295, 12910-12934. 10.1074/jbc.REV120.013930.

Hartmann, G. (2017). Nucleic Acid Immunity. *Adv Immunol* 133, 121-169. 10.1016/bs.ai.2016.11.001.

Hasan, S.S., Sevana, M., Kuhn, R.J., and Rossmann, M.G. (2018). Structural biology of Zika virus and other flaviviruses. *Nat Struct Mol Biol* 25, 13-20. 10.1038/s41594-017-0010-8.

Helbig, K.J., Carr, J.M., Calvert, J.K., Wati, S., Clarke, J.N., Eyre, N.S., Narayana, S.K., Fiches, G.N., McCartney, E.M., and Beard, M.R. (2013). Viperin is induced following dengue virus type-2 (DENV-2) infection and has anti-viral actions requiring the C-terminal end of viperin. *PLoS Negl Trop Dis* 7, e2178. 10.1371/journal.pntd.0002178.

Helbig, K.J., Eyre, N.S., Yip, E., Narayana, S., Li, K., Fiches, G., McCartney, E.M., Jangra, R.K., Lemon, S.M., and Beard, M.R. (2011). The antiviral protein viperin inhibits hepatitis C virus replication via interaction with nonstructural protein 5A. *Hepatology* 54, 1506-1517. 10.1002/hep.24542.

Helms, J., Tacquard, C., Severac, F., Leonard-Lorant, I., Ohana, M., Delabranche, X., Merdji, H., Clere-Jehl, R., Schenck, M., Fagot Gandet, F., et al. (2020). High risk of thrombosis in patients with severe SARS-CoV-2 infection: a multicenter prospective cohort study. *Intensive Care Med* 46, 1089-1098. 10.1007/s00134-020-06062-x.

Hoagland, D.A., Møller, R., Uhl, S.A., Oishi, K., Frere, J., Golynger, I., Horiuchi, S., Panis, M., Blanco-Melo, D., Sachs, D., et al. (2021). Leveraging the antiviral type I interferon system as a first line of defense against SARS-CoV-2 pathogenicity. *Immunity* 54, 557-570.e555. 10.1016/j.immuni.2021.01.017.

Hoffmann, M., Kleine-Weber, H., Schroeder, S., Krüger, N., Herrler, T., Erichsen, S., Schiergens, T.S., Herrler, G., Wu, N.H., Nitsche, A., et al. (2020). SARS-CoV-2 Cell Entry Depends on ACE2 and TMPRSS2 and Is Blocked by a Clinically Proven Protease Inhibitor. *Cell* 181, 271-280.e278. 10.1016/j.cell.2020.02.052.

Hornung, V., Ellegast, J., Kim, S., Brzózka, K., Jung, A., Kato, H., Poeck, H., Akira, S., Conzelmann, K.K., Schlee, M., et al. (2006). 5'-Triphosphate RNA is the ligand for RIG-I. *Science* 314, 994-997. 10.1126/science.1132505.

Hou, F., Sun, L., Zheng, H., Skaug, B., Jiang, Q.X., and Chen, Z.J. (2011). MAVS forms functional prion-like aggregates to activate and propagate antiviral innate immune response. *Cell* 146, 448-461. 10.1016/j.cell.2011.06.041.

Hou, Y.J., Okuda, K., Edwards, C.E., Martinez, D.R., Asakura, T., Dinno, K.H., Kato, T., Lee, R.E., Yount, B.L., Mascenik, T.M., et al. (2020). SARS-CoV-2 Reverse Genetics Reveals a Variable Infection Gradient in the Respiratory Tract. *Cell* 182, 429-446.e414. 10.1016/j.cell.2020.05.042.

Hu, Y., Dong, X., He, Z., Wu, Y., Zhang, S., Lin, J., Yang, Y., Chen, J., An, S., Yin, Y., et al. (2019). Zika virus antagonizes interferon response in patients and disrupts RIG-I-MAVS interaction through its CARD-TM domains. *Cell Biosci* 9, 46. 10.1186/s13578-019-0308-9.

Hua, R., Cheng, D., Coyaud, É., Freeman, S., Di Pietro, E., Wang, Y., Vissa, A., Yip, C.M., Fairn, G.D., Braverman, N., et al. (2017). VAPs and ACBD5 tether peroxisomes to the ER for peroxisome maintenance and lipid homeostasis. *J Cell Biol* 216, 367-377. 10.1083/jcb.201608128.

Hua, R., Gidda, S.K., Aranovich, A., Mullen, R.T., and Kim, P.K. (2015). Multiple Domains in PEX16 Mediate Its Trafficking and Recruitment of Peroxisomal Proteins to the ER. *Traffic* 16, 832-852. 10.1111/tra.12292.

Huang, S.M., Mishina, Y.M., Liu, S., Cheung, A., Stegmeier, F., Michaud, G.A., Charlat, O., Wiellette, E., Zhang, Y., Wiessner, S., et al. (2009). Tankyrase inhibition stabilizes axin and antagonizes Wnt signalling. *Nature* 461, 614-620. 10.1038/nature08356.

Humphries, F., Shmuel-Galia, L., Jiang, Z., Wilson, R., Landis, P., Ng, S.-L., Parsi, K.M., Maehr, R., Cruz, J., Morales, A., et al. (2021). A diamidobenzimidazole STING agonist protects against SARS-CoV-2 infection. *Science Immunology* 6, eabi9002. doi:10.1126/sciimmunol.abi9002.

Hung, I.F.-N., Lung, K.-C., Tso, E.Y.-K., Liu, R., Chung, T.W.-H., Chu, M.-Y., Ng, Y.-Y., Lo, J., Chan, J., and Tam, A.R. (2020). Triple combination of interferon beta-1b, lopinavir-ritonavir, and ribavirin in the treatment of patients admitted to hospital with COVID-19: an open-label, randomised, phase 2 trial. *The Lancet* 395, 1695-1704.

Imanaka, T., Shiina, Y., Takano, T., Hashimoto, T., and Osumi, T. (1996). Insertion of the 70-kDa peroxisomal membrane protein into peroxisomal membranes in vivo and in vitro. *J Biol Chem* 271, 3706-3713. 10.1074/jbc.271.7.3706.

Jackson, C.B., Farzan, M., Chen, B., and Choe, H. (2022). Mechanisms of SARS-CoV-2 entry into cells. *Nat Rev Mol Cell Biol* 23, 3-20. 10.1038/s41580-021-00418-x.

Jagger, B.W., Miner, J.J., Cao, B., Arora, N., Smith, A.M., Kovacs, A., Mysorekar, I.U., Coyne, C.B., and Diamond, M.S. (2017). Gestational Stage and IFN- λ Signaling Regulate ZIKV Infection In Utero. *Cell Host Microbe* 22, 366-376.e363. 10.1016/j.chom.2017.08.012.

Jean Beltran, P.M., Cook, K.C., Hashimoto, Y., Galitzine, C., Murray, L.A., Vitek, O., and Cristea, I.M. (2018). Infection-Induced Peroxisome Biogenesis Is a Metabolic Strategy for Herpesvirus Replication. *Cell Host Microbe* 24, 526-541.e527. 10.1016/j.chom.2018.09.002.

Jiang, F., Ramanathan, A., Miller, M.T., Tang, G.Q., Gale, M., Patel, S.S., and Marcotrigiano, J. (2011). Structural basis of RNA recognition and activation by innate immune receptor RIG-I. *Nature* 479, 423-427. 10.1038/nature10537.

Jones, J.M., Morrell, J.C., and Gould, S.J. (2004). PEX19 is a predominantly cytosolic chaperone and import receptor for class 1 peroxisomal membrane proteins. *J Cell Biol* 164, 57-67. 10.1083/jcb.200304111.

Kalil, A.C., Mehta, A.K., Patterson, T.F., Erdmann, N., Gomez, C.A., Jain, M.K., Wolfe, C.R., Ruiz-Palacios, G.M., Kline, S., Regalado Pineda, J., et al. (2021). Efficacy of interferon beta-1a plus remdesivir compared with remdesivir alone in hospitalised adults with COVID-19: a double-blind, randomised, placebo-controlled, phase 3 trial. *Lancet Respir Med* 9, 1365-1376. 10.1016/S2213-2600(21)00384-2.

Kamerkar, S.C., Kraus, F., Sharpe, A.J., Pucadyil, T.J., and Ryan, M.T. (2018). Dynamin-related protein 1 has membrane constricting and severing abilities sufficient for mitochondrial and peroxisomal fission. *Nat Commun* 9, 5239. 10.1038/s41467-018-07543-w.

Kato, H., Takahashi, K., and Fujita, T. (2011). RIG-I-like receptors: cytoplasmic sensors for non-self RNA. *Immunol Rev* 243, 91-98. 10.1111/j.1600-065X.2011.01052.x.

Kawai, T., Takahashi, K., Sato, S., Coban, C., Kumar, H., Kato, H., Ishii, K.J., Takeuchi, O., and Akira, S. (2005). IPS-1, an adaptor triggering RIG-I- and Mda5-mediated type I interferon induction. *Nat Immunol* 6, 981-988. 10.1038/ni1243.

Kawasaki, T., and Kawai, T. (2014). Toll-like receptor signaling pathways. *Front Immunol* 5, 461. 10.3389/fimmu.2014.00461.

Kim, P.K., Hailey, D.W., Mullen, R.T., and Lippincott-Schwartz, J. (2008). Ubiquitin signals autophagic degradation of cytosolic proteins and peroxisomes. *Proc Natl Acad Sci U S A* 105, 20567-20574. 10.1073/pnas.0810611105.

Kim, P.K., and Hettema, E.H. (2015). Multiple pathways for protein transport to peroxisomes. *J Mol Biol* 427, 1176-1190. 10.1016/j.jmb.2015.02.005.

Kim, P.K., Mullen, R.T., Schumann, U., and Lippincott-Schwartz, J. (2006). The origin and maintenance of mammalian peroxisomes involves a de novo PEX16-dependent pathway from the ER. *J Cell Biol* 173, 521-532. 10.1083/jcb.200601036.

Kimelman, D., and Xu, W. (2006). beta-catenin destruction complex: insights and questions from a structural perspective. *Oncogene* 25, 7482-7491. 10.1038/sj.onc.1210055.

Klein, S., Cortese, M., Winter, S.L., Wachsmuth-Melm, M., Neufeldt, C.J., Cerikan, B., Stanifer, M.L., Boulant, S., Bartenschlager, R., and Chlanda, P. (2020). SARS-CoV-2 structure and

replication characterized by in situ cryo-electron tomography. *Nat Commun* 11, 5885. 10.1038/s41467-020-19619-7.

Klok, F.A., Kruij, M.J.H.A., van der Meer, N.J.M., Arbous, M.S., Gommers, D.A.M.P., Kant, K.M., Kaptein, F.H.J., van Paassen, J., Stals, M.A.M., Huisman, M.V., and Endeman, H. (2020). Incidence of thrombotic complications in critically ill ICU patients with COVID-19. *Thromb Res* 191, 145-147. 10.1016/j.thromres.2020.04.013.

Knoblach, B., Ishida, R., Hobman, T.C., and Rachubinski, R.A. (2021). Peroxisomes exhibit compromised structure and matrix protein content in SARS-CoV-2-infected cells. *Mol Biol Cell* 32, 1273-1282. 10.1091/mbc.E21-02-0074.

Knoblach, B., Sun, X., Coquelle, N., Fagarasanu, A., Poirier, R.L., and Rachubinski, R.A. (2013). An ER-peroxisome tether exerts peroxisome population control in yeast. *EMBO J* 32, 2439-2453. 10.1038/emboj.2013.170.

Kobayashi, S., Tanaka, A., and Fujiki, Y. (2007). Fis1, DLP1, and Pex11p coordinately regulate peroxisome morphogenesis. *Exp Cell Res* 313, 1675-1686. 10.1016/j.yexcr.2007.02.028.

Koch, A., Yoon, Y., Bonekamp, N.A., McNiven, M.A., and Schrader, M. (2005). A role for Fis1 in both mitochondrial and peroxisomal fission in mammalian cells. *Mol Biol Cell* 16, 5077-5086. 10.1091/mbc.e05-02-0159.

Koch, J., and Brocard, C. (2012). PEX11 proteins attract Mff and human Fis1 to coordinate peroxisomal fission. *J Cell Sci* 125, 3813-3826. 10.1242/jcs.102178.

Konno, Y., Kimura, I., Uriu, K., Fukushi, M., Irie, T., Koyanagi, Y., Sauter, D., Gifford, R.J., Nakagawa, S., Sato, K., and Consortium, U.-C. (2020). SARS-CoV-2 ORF3b Is a Potent Interferon Antagonist Whose Activity Is Increased by a Naturally Occurring Elongation Variant. *Cell Rep* 32, 108185. 10.1016/j.celrep.2020.108185.

Kotenko, S.V., and Durbin, J.E. (2017). Contribution of type III interferons to antiviral immunity: location, location, location. *J Biol Chem* 292, 7295-7303. 10.1074/jbc.R117.777102.

Kotenko, S.V., Rivera, A., Parker, D., and Durbin, J.E. (2019). Type III IFNs: Beyond antiviral protection. *Semin Immunol* 43, 101303. 10.1016/j.smim.2019.101303.

Krey, G., Braissant, O., L'Horset, F., Kalkhoven, E., Perroud, M., Parker, M.G., and Wahli, W. (1997). Fatty acids, eicosanoids, and hypolipidemic agents identified as ligands of peroxisome proliferator-activated receptors by coactivator-dependent receptor ligand assay. *Mol Endocrinol* 11, 779-791. 10.1210/mend.11.6.0007.

Kumar, A., Hou, S., Airo, A.M., Limonta, D., Mancinelli, V., Branton, W., Power, C., and Hobman, T.C. (2016). Zika virus inhibits type-I interferon production and downstream signaling. *EMBO Rep* 17, 1766-1775. 10.15252/embr.201642627.

Kumar, A., Ishida, R., Strilets, T., Cole, J., Lopez-Orozco, J., Fayad, N., Felix-Lopez, A., Elaish, M., Evseev, D., Magor, K.E., et al. (2021). SARS-CoV-2 Nonstructural Protein 1 Inhibits the

- Interferon Response by Causing Depletion of Key Host Signaling Factors. *J Virol* *95*, e0026621. 10.1128/JVI.00266-21.
- Kumar, D., Kumar, A., Bhardwaj, T., and Giri, R. (2020). Zika virus NS4A N-Terminal region (1-48) acts as a cofactor for inducing NTPase activity of NS3 helicase but not NS3 protease. *Arch Biochem Biophys* *695*, 108631. 10.1016/j.abb.2020.108631.
- Lanyon-Hogg, T., Warriner, S.L., and Baker, A. (2010). Getting a camel through the eye of a needle: the import of folded proteins by peroxisomes. *Biol Cell* *102*, 245-263. 10.1042/BC20090159.
- Lazarow, P.B., and Fujiki, Y. (1985). Biogenesis of peroxisomes. *Annu Rev Cell Biol* *1*, 489-530. 10.1146/annurev.cb.01.110185.002421.
- Lazear, H.M., Govero, J., Smith, A.M., Platt, D.J., Fernandez, E., Miner, J.J., and Diamond, M.S. (2016). A Mouse Model of Zika Virus Pathogenesis. *Cell Host Microbe* *19*, 720-730. 10.1016/j.chom.2016.03.010.
- Lazear, H.M., Nice, T.J., and Diamond, M.S. (2015). Interferon- λ : Immune Functions at Barrier Surfaces and Beyond. *Immunity* *43*, 15-28. 10.1016/j.immuni.2015.07.001.
- Lazear, H.M., Schoggins, J.W., and Diamond, M.S. (2019). Shared and Distinct Functions of Type I and Type III Interferons. *Immunity* *50*, 907-923. 10.1016/j.immuni.2019.03.025.
- Lee, E., Madar, A., David, G., Garabedian, M.J., Dasgupta, R., and Logan, S.K. (2013). Inhibition of androgen receptor and β -catenin activity in prostate cancer. *Proc Natl Acad Sci U S A* *110*, 15710-15715. 10.1073/pnas.1218168110.
- Lee, I.T., Nakayama, T., Wu, C.T., Goltsev, Y., Jiang, S., Gall, P.A., Liao, C.K., Shih, L.C., Schürch, C.M., McIlwain, D.R., et al. (2020). ACE2 localizes to the respiratory cilia and is not increased by ACE inhibitors or ARBs. *Nat Commun* *11*, 5453. 10.1038/s41467-020-19145-6.
- Lei, X., Dong, X., Ma, R., Wang, W., Xiao, X., Tian, Z., Wang, C., Wang, Y., Li, L., Ren, L., et al. (2020). Activation and evasion of type I interferon responses by SARS-CoV-2. *Nat Commun* *11*, 3810. 10.1038/s41467-020-17665-9.
- Li, X., and Gould, S.J. (2002). PEX11 promotes peroxisome division independently of peroxisome metabolism. *J Cell Biol* *156*, 643-651. 10.1083/jcb.200112028.
- Limonta, D., Jovel, J., Kumar, A., Airo, A., Hou, S., Saito, L., Branton, W., Ka-Shu Wong, G., Mason, A., and Power, C. (2018). Human Fetal Astrocytes Infected with Zika Virus Exhibit Delayed Apoptosis and Resistance to Interferon: Implications for Persistence. *Viruses* *10*, 646.
- Lindenbach, B.D., and Charles, M. (2007). Rice, Flaviviridae: the Viruses and their Replication. by DM Knipe, PM Howley, DE Griffin, RA Lamb, MA Martin, B. Roizmen, SE Straus (Lippincott Williams and Wilkins, Philadelphia, 2007), 1101-1152.

- Liu, J., Pan, S., Hsieh, M.H., Ng, N., Sun, F., Wang, T., Kasibhatla, S., Schuller, A.G., Li, A.G., Cheng, D., et al. (2013). Targeting Wnt-driven cancer through the inhibition of Porcupine by LGK974. *Proc Natl Acad Sci U S A* *110*, 20224-20229. 10.1073/pnas.1314239110.
- Liu, S., Cai, X., Wu, J., Cong, Q., Chen, X., Li, T., Du, F., Ren, J., Wu, Y.T., Grishin, N.V., and Chen, Z.J. (2015). Phosphorylation of innate immune adaptor proteins MAVS, STING, and TRIF induces IRF3 activation. *Science* *347*, aaa2630. 10.1126/science.aaa2630.
- Liu, S.T., Sharon-Friling, R., Ivanova, P., Milne, S.B., Myers, D.S., Rabinowitz, J.D., Brown, H.A., and Shenk, T. (2011). Synaptic vesicle-like lipidome of human cytomegalovirus virions reveals a role for SNARE machinery in virion egress. *Proc Natl Acad Sci U S A* *108*, 12869-12874. 10.1073/pnas.1109796108.
- Livak, K.J., and Schmittgen, T.D. (2001). Analysis of relative gene expression data using real-time quantitative PCR and the 2(-Delta Delta C(T)) Method. *Methods* *25*, 402-408. 10.1006/meth.2001.1262.
- Llitjos, J.F., Leclerc, M., Chochois, C., Monsallier, J.M., Ramakers, M., Auvray, M., and Merouani, K. (2020). High incidence of venous thromboembolic events in anticoagulated severe COVID-19 patients. *J Thromb Haemost* *18*, 1743-1746. 10.1111/jth.14869.
- Lokugamage, K.G., Hage, A., de Vries, M., Valero-Jimenez, A.M., Schindewolf, C., Dittmann, M., Rajsbaum, R., and Menachery, V.D. (2020). Type I Interferon Susceptibility Distinguishes SARS-CoV-2 from SARS-CoV. *J Virol* *94*. 10.1128/JVI.01410-20.
- Lundberg, R., Melén, K., Westenius, V., Jiang, M., Österlund, P., Khan, H., Vapalahti, O., Julkunen, I., and Kakkola, L. (2019). Zika Virus Non-Structural Protein NS5 Inhibits the RIG-I Pathway and Interferon Lambda 1 Promoter Activation by Targeting IKK Epsilon. *Viruses* *11*. 10.3390/v11111024.
- Lupberger, J., Croonenborghs, T., Roca Suarez, A.A., Van Renne, N., Jühling, F., Oudot, M.A., Virzi, A., Bandiera, S., Jamey, C., Meszaros, G., et al. (2019). Combined Analysis of Metabolomes, Proteomes, and Transcriptomes of Hepatitis C Virus-Infected Cells and Liver to Identify Pathways Associated With Disease Development. *Gastroenterology* *157*, 537-551.e539. 10.1053/j.gastro.2019.04.003.
- MacDonald, B.T., Tamai, K., and He, X. (2009). Wnt/beta-catenin signaling: components, mechanisms, and diseases. *Dev Cell* *17*, 9-26. 10.1016/j.devcel.2009.06.016.
- Macnamara, F.N. (1954). Zika virus: a report on three cases of human infection during an epidemic of jaundice in Nigeria. *Trans R Soc Trop Med Hyg* *48*, 139-145. 10.1016/0035-9203(54)90006-1.
- Madan, B., Ke, Z., Harmston, N., Ho, S.Y., Frois, A.O., Alam, J., Jeyaraj, D.A., Pendharkar, V., Ghosh, K., Virshup, I.H., et al. (2016). Wnt addiction of genetically defined cancers reversed by PORCN inhibition. *Oncogene* *35*, 2197-2207. 10.1038/onc.2015.280.

- Mahmoudi, T., Li, V.S., Ng, S.S., Taouatas, N., Vries, R.G., Mohammed, S., Heck, A.J., and Clevers, H. (2009). The kinase TNIK is an essential activator of Wnt target genes. *EMBO J* 28, 3329-3340. 10.1038/emboj.2009.285.
- Makris, S., Paulsen, M., and Johansson, C. (2017). Type I Interferons as Regulators of Lung Inflammation. *Front Immunol* 8, 259. 10.3389/fimmu.2017.00259.
- Malone, B., Urakova, N., Snijder, E.J., and Campbell, E.A. (2022). Structures and functions of coronavirus replication–transcription complexes and their relevance for SARS-CoV-2 drug design. *Nature Reviews Molecular Cell Biology* 23, 21-39.
- Mandala, A., Armstrong, A., Girresch, B., Zhu, J., Chilakala, A., Chavalmane, S., Chaudhary, K., Biswas, P., Ogilvie, J., and Gnana-Prakasam, J.P. (2020). Fenofibrate prevents iron induced activation of canonical Wnt/ β -catenin and oxidative stress signaling in the retina. *NPJ Aging Mech Dis* 6, 12. 10.1038/s41514-020-00050-7.
- Mantlo, E., Bukreyeva, N., Maruyama, J., Paessler, S., and Huang, C. (2020). Antiviral activities of type I interferons to SARS-CoV-2 infection. *Antiviral Res* 179, 104811. 10.1016/j.antiviral.2020.104811.
- Mao, R., Qiu, Y., He, J.S., Tan, J.Y., Li, X.H., Liang, J., Shen, J., Zhu, L.R., Chen, Y., Iacucci, M., et al. (2020). Manifestations and prognosis of gastrointestinal and liver involvement in patients with COVID-19: a systematic review and meta-analysis. *Lancet Gastroenterol Hepatol* 5, 667-678. 10.1016/S2468-1253(20)30126-6.
- Marcato, V., Luron, L., Laqueuvre, L.M., Simon, D., Mansuroglu, Z., Flamand, M., Panthier, J.J., Soues, S., Massaad, C., and Bonnefoy, E. (2016). beta-Catenin Upregulates the Constitutive and Virus-Induced Transcriptional Capacity of the Interferon Beta Promoter through T-Cell Factor Binding Sites. *Mol Cell Biol* 36, 13-29. 10.1128/mcb.00641-15.
- Martin-Sancho, L., Lewinski, M.K., Pache, L., Stoneham, C.A., Yin, X., Becker, M.E., Pratt, D., Churas, C., Rosenthal, S.B., Liu, S., et al. (2021). Functional landscape of SARS-CoV-2 cellular restriction. *Mol Cell* 81, 2656-2668.e2658. 10.1016/j.molcel.2021.04.008.
- Mast, F.D., Jamakhandi, A., Saleem, R.A., Dilworth, D.J., Rogers, R.S., Rachubinski, R.A., and Aitchison, J.D. (2016). Peroxisins Pex30 and Pex29 Dynamically Associate with Reticulons to Regulate Peroxisome Biogenesis from the Endoplasmic Reticulum. *J Biol Chem* 291, 15408-15427. 10.1074/jbc.M116.728154.
- Masuda, M., Uno, Y., Ohbayashi, N., Ohata, H., Mimata, A., Kukimoto-Niino, M., Moriyama, H., Kashimoto, S., Inoue, T., Goto, N., et al. (2016). TNIK inhibition abrogates colorectal cancer stemness. *Nat Commun* 7, 12586. 10.1038/ncomms12586.
- Mazeaud, C., Freppel, W., and Chatel-Chaix, L. (2018). The Multiples Fates of the Flavivirus RNA Genome During Pathogenesis. *Front Genet* 9, 595. 10.3389/fgene.2018.00595.
- McBride, R., van Zyl, M., and Fielding, B.C. (2014). The coronavirus nucleocapsid is a multifunctional protein. *Viruses* 6, 2991-3018. 10.3390/v6082991.

- McGonigle, S., Chen, Z., Wu, J., Chang, P., Kolber-Simonds, D., Ackermann, K., Twine, N.C., Shie, J.L., Miu, J.T., Huang, K.C., et al. (2015). E7449: A dual inhibitor of PARP1/2 and tankyrase1/2 inhibits growth of DNA repair deficient tumors and antagonizes Wnt signaling. *Oncotarget* 6, 41307-41323. 10.18632/oncotarget.5846.
- McNab, F., Mayer-Barber, K., Sher, A., Wack, A., and O'Garra, A. (2015). Type I interferons in infectious disease. *Nat Rev Immunol* 15, 87-103. 10.1038/nri3787.
- Meertens, L., Carnec, X., Lecoin, M.P., Ramdasi, R., Guivel-Benhassine, F., Lew, E., Lemke, G., Schwartz, O., and Amara, A. (2012). The TIM and TAM families of phosphatidylserine receptors mediate dengue virus entry. *Cell Host Microbe* 12, 544-557. 10.1016/j.chom.2012.08.009.
- Miorin, L., Kehrer, T., Sanchez-Aparicio, M.T., Zhang, K., Cohen, P., Patel, R.S., Cupic, A., Makio, T., Mei, M., Moreno, E., et al. (2020). SARS-CoV-2 Orf6 hijacks Nup98 to block STAT nuclear import and antagonize interferon signaling. *Proc Natl Acad Sci U S A* 117, 28344-28354. 10.1073/pnas.2016650117.
- Monk, P.D., Marsden, R.J., Tear, V.J., Brookes, J., Batten, T.N., Mankowski, M., Gabbay, F.J., Davies, D.E., Holgate, S.T., Ho, L.P., et al. (2020). Safety and efficacy of inhaled nebulised interferon beta-1a (SNG001) for treatment of SARS-CoV-2 infection: a randomised, double-blind, placebo-controlled, phase 2 trial. *Lancet Respir Med*. 10.1016/s2213-2600(20)30511-7.
- Morrison, J., Laurent-Rolle, M., Maestre, A.M., Rajsbaum, R., Pisanelli, G., Simon, V., Mulder, L.C., Fernandez-Sesma, A., and García-Sastre, A. (2013). Dengue virus co-opts UBR4 to degrade STAT2 and antagonize type I interferon signaling. *PLoS Pathog* 9, e1003265. 10.1371/journal.ppat.1003265.
- Mu, J., Fang, Y., Yang, Q., Shu, T., Wang, A., Huang, M., Jin, L., Deng, F., Qiu, Y., and Zhou, X. (2020). SARS-CoV-2 N protein antagonizes type I interferon signaling by suppressing phosphorylation and nuclear translocation of STAT1 and STAT2. *Cell Discov* 6, 65. 10.1038/s41421-020-00208-3.
- Musso, D., Roche, C., Robin, E., Nhan, T., Teissier, A., and Cao-Lormeau, V.M. (2015). Potential sexual transmission of Zika virus. *Emerg Infect Dis* 21, 359-361. 10.3201/eid2102.141363.
- Nagy, A., and Alhatlani, B. (2021). An overview of current COVID-19 vaccine platforms. *Comput Struct Biotechnol J* 19, 2508-2517. 10.1016/j.csbj.2021.04.061.
- Neuman, B.W., Kiss, G., Kunding, A.H., Bhella, D., Baksh, M.F., Connelly, S., Droese, B., Klaus, J.P., Makino, S., Sawicki, S.G., et al. (2011). A structural analysis of M protein in coronavirus assembly and morphology. *J Struct Biol* 174, 11-22. 10.1016/j.jsb.2010.11.021.
- O'Brien, T.R., Prokunina-Olsson, L., and Donnelly, R.P. (2014). IFN- λ 4: the paradoxical new member of the interferon lambda family. *J Interferon Cytokine Res* 34, 829-838. 10.1089/jir.2013.0136.

Odendall, C., Dixit, E., Stavru, F., Bierne, H., Franz, K.M., Durbin, A.F., Boulant, S., Gehrke, L., Cossart, P., and Kagan, J.C. (2014). Diverse intracellular pathogens activate type III interferon expression from peroxisomes. *Nat Immunol* 15, 717-726. 10.1038/ni.2915.

Oliveira Melo, A.S., Malinger, G., Ximenes, R., Szejnfeld, P.O., Alves Sampaio, S., and Bispo de Filippis, A.M. (2016). Zika virus intrauterine infection causes fetal brain abnormality and microcephaly: tip of the iceberg? *Ultrasound Obstet Gynecol* 47, 6-7. 10.1002/uog.15831.

Osuchowski, M.F., Winkler, M.S., Skirecki, T., Cajander, S., Shankar-Hari, M., Lachmann, G., Monneret, G., Venet, F., Bauer, M., Brunkhorst, F.M., et al. (2021). The COVID-19 puzzle: deciphering pathophysiology and phenotypes of a new disease entity. *Lancet Respir Med* 9, 622-642. 10.1016/S2213-2600(21)00218-6.

Overby, A.K., Popov, V.L., Niedrig, M., and Weber, F. (2010). Tick-borne encephalitis virus delays interferon induction and hides its double-stranded RNA in intracellular membrane vesicles. *J Virol* 84, 8470-8483. 10.1128/JVI.00176-10.

Owczarek, K., Chykunova, Y., Jassoy, C., Maksym, B., Rajfur, Z., and Pyrc, K. (2019). Zika virus: mapping and reprogramming the entry. *Cell Commun Signal* 17, 41. 10.1186/s12964-019-0349-z.

Owen, D.R., Allerton, C.M.N., Anderson, A.S., Aschenbrenner, L., Avery, M., Berritt, S., Boras, B., Cardin, R.D., Carlo, A., Coffman, K.J., et al. (2021). An oral SARS-CoV-2 Mpro inhibitor clinical candidate for the treatment of COVID-19. *Science* 374, 1586-1593. 10.1126/science.abl4784.

PAHO (2018). Zika Cumulative Cases.

Pak, S., Park, S., Kim, Y., Park, J.H., Park, C.H., Lee, K.J., Kim, C.S., and Ahn, H. (2019). The small molecule WNT/ β -catenin inhibitor CWP232291 blocks the growth of castration-resistant prostate cancer by activating the endoplasmic reticulum stress pathway. *J Exp Clin Cancer Res* 38, 342. 10.1186/s13046-019-1342-5.

Panayiotou, C., Lindqvist, R., Kurhade, C., Vonderstein, K., Pasto, J., Edlund, K., Upadhyay, A.S., and Överby, A.K. (2018). Viperin Restricts Zika Virus and Tick-Borne Encephalitis Virus Replication by Targeting NS3 for Proteasomal Degradation. *J Virol* 92. 10.1128/JVI.02054-17.

Pardi, N., Hogan, M.J., Pelc, R.S., Muramatsu, H., Andersen, H., DeMaso, C.R., Dowd, K.A., Sutherland, L.L., Scarce, R.M., Parks, R., et al. (2017). Zika virus protection by a single low-dose nucleoside-modified mRNA vaccination. *Nature* 543, 248-251. 10.1038/nature21428.

Parra, B., Lizarazo, J., Jiménez-Arango, J.A., Zea-Vera, A.F., González-Manrique, G., Vargas, J., Angarita, J.A., Zuñiga, G., Lopez-Gonzalez, R., Beltran, C.L., et al. (2016). Guillain-Barré Syndrome Associated with Zika Virus Infection in Colombia. *N Engl J Med* 375, 1513-1523. 10.1056/NEJMoal605564.

Perlman, S., and Netland, J. (2009). Coronaviruses post-SARS: update on replication and pathogenesis. *Nat Rev Microbiol* 7, 439-450. 10.1038/nrmicro2147.

- Pestka, S., Krause, C.D., and Walter, M.R. (2004). Interferons, interferon-like cytokines, and their receptors. *Immunol Rev* 202, 8-32. 10.1111/j.0105-2896.2004.00204.x.
- Petriv, O.I., Tang, L., Titorenko, V.I., and Rachubinski, R.A. (2004). A new definition for the consensus sequence of the peroxisome targeting signal type 2. *J Mol Biol* 341, 119-134. 10.1016/j.jmb.2004.05.064.
- Pfaender, S., Mar, K.B., Michailidis, E., Kratzel, A., Boys, I.N., V'kovski, P., Fan, W., Kelly, J.N., Hirt, D., Ebert, N., et al. (2020). LY6E impairs coronavirus fusion and confers immune control of viral disease. *Nat Microbiol* 5, 1330-1339. 10.1038/s41564-020-0769-y.
- Pierson, T.C., and Diamond, M.S. (2020). The continued threat of emerging flaviviruses. *Nat Microbiol* 5, 796-812. 10.1038/s41564-020-0714-0.
- Prasher, D.C., Eckenrode, V.K., Ward, W.W., Prendergast, F.G., and Cormier, M.J. (1992). Primary structure of the *Aequorea victoria* green-fluorescent protein. *Gene* 111, 229-233. 10.1016/0378-1119(92)90691-h.
- Proffitt, K.D., Madan, B., Ke, Z., Pendharkar, V., Ding, L., Lee, M.A., Hannoush, R.N., and Virshup, D.M. (2013). Pharmacological inhibition of the Wnt acyltransferase PORCN prevents growth of WNT-driven mammary cancer. *Cancer Res* 73, 502-507. 10.1158/0008-5472.CAN-12-2258.
- Prokunina-Olsson, L., Muchmore, B., Tang, W., Pfeiffer, R.M., Park, H., Dickensheets, H., Hergott, D., Porter-Gill, P., Mumy, A., Kohaar, I., et al. (2013). A variant upstream of IFNL3 (IL28B) creating a new interferon gene IFNL4 is associated with impaired clearance of hepatitis C virus. *Nat Genet* 45, 164-171. 10.1038/ng.2521.
- Quicke, K.M., Bowen, J.R., Johnson, E.L., McDonald, C.E., Ma, H., O'Neal, J.T., Rajakumar, A., Wrammert, J., Rimawi, B.H., Pulendran, B., et al. (2016). Zika Virus Infects Human Placental Macrophages. *Cell Host Microbe* 20, 83-90. 10.1016/j.chom.2016.05.015.
- Rathore, S.S., Rojas, G.A., Sondhi, M., Pothuru, S., Pydi, R., Kancherla, N., Singh, R., Ahmed, N.K., Shah, J., Tousif, S., et al. (2021). Myocarditis associated with Covid-19 disease: A systematic review of published case reports and case series. *Int J Clin Pract* 75, e14470. 10.1111/ijcp.14470.
- Renauld, J.C. (2003). Class II cytokine receptors and their ligands: key antiviral and inflammatory modulators. *Nat Rev Immunol* 3, 667-676. 10.1038/nri1153.
- Richard, A.S., Shim, B.S., Kwon, Y.C., Zhang, R., Otsuka, Y., Schmitt, K., Berri, F., Diamond, M.S., and Choe, H. (2017). AXL-dependent infection of human fetal endothelial cells distinguishes Zika virus from other pathogenic flaviviruses. *Proc Natl Acad Sci U S A* 114, 2024-2029. 10.1073/pnas.1620558114.
- Rodrigues, T.A., Alencastre, I.S., Francisco, T., Brites, P., Fransen, M., Grou, C.P., and Azevedo, J.E. (2014). A PEX7-centered perspective on the peroxisomal targeting signal type 2-mediated protein import pathway. *Mol Cell Biol* 34, 2917-2928. 10.1128/MCB.01727-13.

- Roos, R.P. (2016). Zika Virus-A Public Health Emergency of International Concern. *JAMA Neurol* 73, 1395-1396. 10.1001/jamaneurol.2016.3677.
- Rubin, E.J., Greene, M.F., and Baden, L.R. (2016). Zika Virus and Microcephaly. *N Engl J Med* 374, 984-985. 10.1056/NEJMe1601862.
- Samuel, R.M., Majd, H., Richter, M.N., Ghazizadeh, Z., Zekavat, S.M., Navickas, A., Ramirez, J.T., Asgharian, H., Simoneau, C.R., Bonser, L.R., et al. (2020). Androgen Signaling Regulates SARS-CoV-2 Receptor Levels and Is Associated with Severe COVID-19 Symptoms in Men. *Cell Stem Cell* 27, 876-889.e812. 10.1016/j.stem.2020.11.009.
- Sargent, G., van Zutphen, T., Shatseva, T., Zhang, L., Di Giovanni, V., Bandsma, R., and Kim, P.K. (2016). PEX2 is the E3 ubiquitin ligase required for pexophagy during starvation. *J Cell Biol* 214, 677-690. 10.1083/jcb.201511034.
- Saxena, S.K., Elahi, A., Gadugu, S., and Prasad, A.K. (2016). Zika virus outbreak: an overview of the experimental therapeutics and treatment. *Virusdisease* 27, 111-115. 10.1007/s13337-016-0307-y.
- Sbrana, M.F., Fornazieri, M.A., Bruni-Cardoso, A., Avelino-Silva, V.I., Schechtman, D., Voegels, R.L., Malnic, B., Glezer, I., and de Rezende Pinna, F. (2021). Olfactory Dysfunction in Frontline Health Care Professionals During COVID-19 Pandemic in Brazil. *Front Physiol* 12, 622987. 10.3389/fphys.2021.622987.
- Scaturro, P., Stukalov, A., Haas, D.A., Cortese, M., Draganova, K., Płaszczyc, A., Bartenschlager, R., Götz, M., and Pichlmair, A. (2018). An orthogonal proteomic survey uncovers novel Zika virus host factors. *Nature* 561, 253-257. 10.1038/s41586-018-0484-5.
- Schneider, W.M., Chevillotte, M.D., and Rice, C.M. (2014). Interferon-stimulated genes: a complex web of host defenses. *Annu Rev Immunol* 32, 513-545. 10.1146/annurev-immunol-032713-120231.
- Schoenborn, J.R., and Wilson, C.B. (2007). Regulation of interferon-gamma during innate and adaptive immune responses. *Adv Immunol* 96, 41-101. 10.1016/S0065-2776(07)96002-2.
- Schrader, M., Bonekamp, N.A., and Islinger, M. (2012). Fission and proliferation of peroxisomes. *Biochim Biophys Acta* 1822, 1343-1357. 10.1016/j.bbadis.2011.12.014.
- Schrader, M., Krieglstein, K., and Fahimi, H.D. (1998a). Tubular peroxisomes in HepG2 cells: selective induction by growth factors and arachidonic acid. *Eur J Cell Biol* 75, 87-96. 10.1016/s0171-9335(98)80051-4.
- Schrader, M., Reuber, B.E., Morrell, J.C., Jimenez-Sanchez, G., Obie, C., Stroh, T.A., Valle, D., Schroer, T.A., and Gould, S.J. (1998b). Expression of PEX11beta mediates peroxisome proliferation in the absence of extracellular stimuli. *J Biol Chem* 273, 29607-29614.

- Seth, R.B., Sun, L., Ea, C.K., and Chen, Z.J. (2005). Identification and characterization of MAVS, a mitochondrial antiviral signaling protein that activates NF-kappaB and IRF 3. *Cell* 122, 669-682. 10.1016/j.cell.2005.08.012.
- Shang, Z., Song, H., Shi, Y., Qi, J., and Gao, G.F. (2018). Crystal Structure of the Capsid Protein from Zika Virus. *J Mol Biol* 430, 948-962. 10.1016/j.jmb.2018.02.006.
- Shen, Z., Ye, G., Deng, F., Wang, G., Cui, M., Fang, L., Xiao, S., Fu, Z.F., and Peng, G. (2018). Structural Basis for the Inhibition of Host Gene Expression by Porcine Epidemic Diarrhea Virus nsp1. *J Virol* 92. 10.1128/JVI.01896-17.
- Shepard, D.S., Halasa, Y.A., Tyagi, B.K., Adhish, S.V., Nandan, D., Karthiga, K.S., Chellaswamy, V., Gaba, M., Arora, N.K., and Group, I.S. (2014). Economic and disease burden of dengue illness in India. *Am J Trop Med Hyg* 91, 1235-1242. 10.4269/ajtmh.14-0002.
- Sheridan, M.A., Yunusov, D., Balaraman, V., Alexenko, A.P., Yabe, S., Verjovski-Almeida, S., Schust, D.J., Franz, A.W., Sadovsky, Y., Ezashi, T., and Roberts, R.M. (2017). Vulnerability of primitive human placental trophoblast to Zika virus. *Proc Natl Acad Sci U S A* 114, E1587-E1596. 10.1073/pnas.1616097114.
- Shin, D., Mukherjee, R., Grewe, D., Bojkova, D., Baek, K., Bhattacharya, A., Schulz, L., Widera, M., Mehdipour, A.R., Tascher, G., et al. (2020). Papain-like protease regulates SARS-CoV-2 viral spread and innate immunity. *Nature* 587, 657-662. 10.1038/s41586-020-2601-5.
- Sikka, V., Chattu, V.K., Popli, R.K., Galwankar, S.C., Kelkar, D., Sawicki, S.G., Stawicki, S.P., and Papadimos, T.J. (2016). The Emergence of Zika Virus as a Global Health Security Threat: A Review and a Consensus Statement of the INDUSEM Joint working Group (JWG). *J Glob Infect Dis* 8, 3-15. 10.4103/0974-777X.176140.
- Stadler, K., Allison, S.L., Schalich, J., and Heinz, F.X. (1997). Proteolytic activation of tick-borne encephalitis virus by furin. *J Virol* 71, 8475-8481. 10.1128/JVI.71.11.8475-8481.1997.
- Stanifer, M.L., Kee, C., Cortese, M., Zumaran, C.M., Triana, S., Mukenhirn, M., Kraeusslich, H.G., Alexandrov, T., Bartenschlager, R., and Boulant, S. (2020). Critical Role of Type III Interferon in Controlling SARS-CoV-2 Infection in Human Intestinal Epithelial Cells. *Cell Rep* 32, 107863. 10.1016/j.celrep.2020.107863.
- Stertz, S., Reichelt, M., Spiegel, M., Kuri, T., Martínez-Sobrido, L., García-Sastre, A., Weber, F., and Kochs, G. (2007). The intracellular sites of early replication and budding of SARS-coronavirus. *Virology* 361, 304-315. 10.1016/j.virol.2006.11.027.
- Stiasny, K., Fritz, R., Pangerl, K., and Heinz, F.X. (2011). Molecular mechanisms of flavivirus membrane fusion. *Amino Acids* 41, 1159-1163. 10.1007/s00726-009-0370-4.
- Strange, D.P., Jiyarom, B., Sadri-Ardekani, H., Cazares, L.H., Kenny, T.A., Ward, M.D., and Verma, S. (2021). Paracrine IFN Response Limits ZIKV Infection in Human Sertoli Cells. *Front Microbiol* 12, 667146. 10.3389/fmicb.2021.667146.

Sui, L., Zhao, Y., Wang, W., Wu, P., Wang, Z., Yu, Y., Hou, Z., Tan, G., and Liu, Q. (2021). SARS-CoV-2 Membrane Protein Inhibits Type I Interferon Production Through Ubiquitin-Mediated Degradation of TBK1. *Front Immunol* *12*, 662989. 10.3389/fimmu.2021.662989.

Sychev, Z.E., Hu, A., DiMaio, T.A., Gitter, A., Camp, N.D., Noble, W.S., Wolf-Yadlin, A., and Lagunoff, M. (2017). Integrated systems biology analysis of KSHV latent infection reveals viral induction and reliance on peroxisome mediated lipid metabolism. *PLoS Pathog* *13*, e1006256. 10.1371/journal.ppat.1006256.

Szretter, K.J., Brien, J.D., Thackray, L.B., Virgin, H.W., Cresswell, P., and Diamond, M.S. (2011). The interferon-inducible gene viperin restricts West Nile virus pathogenesis. *J Virol* *85*, 11557-11566. 10.1128/JVI.05519-11.

Takeuchi, O., and Akira, S. (2010). Pattern recognition receptors and inflammation. *Cell* *140*, 805-820. 10.1016/j.cell.2010.01.022.

Tam, B.Y., Chiu, K., Chung, H., Bossard, C., Nguyen, J.D., Creger, E., Eastman, B.W., Mak, C.C., Ibanez, M., Ghias, A., et al. (2020). The CLK inhibitor SM08502 induces anti-tumor activity and reduces Wnt pathway gene expression in gastrointestinal cancer models. *Cancer Lett* *473*, 186-197. 10.1016/j.canlet.2019.09.009.

Tam, Y.Y., Fagarasanu, A., Fagarasanu, M., and Rachubinski, R.A. (2005). Pex3p initiates the formation of a preperoxisomal compartment from a subdomain of the endoplasmic reticulum in *Saccharomyces cerevisiae*. *J Biol Chem* *280*, 34933-34939. 10.1074/jbc.M506208200.

Tan, T.Y., Fibriansah, G., Kostyuchenko, V.A., Ng, T.S., Lim, X.X., Zhang, S., Lim, X.N., Wang, J., Shi, J., Morais, M.C., et al. (2020). Capsid protein structure in Zika virus reveals the flavivirus assembly process. *Nat Commun* *11*, 895. 10.1038/s41467-020-14647-9.

Tanaka, A., Okumoto, K., and Fujiki, Y. (2003). cDNA cloning and characterization of the third isoform of human peroxin Pex11p. *Biochem Biophys Res Commun* *300*, 819-823. 10.1016/s0006-291x(02)02936-4.

Thomas, M., Bayha, C., Vetter, S., Hofmann, U., Schwarz, M., Zanger, U.M., and Braeuning, A. (2015). Activating and Inhibitory Functions of WNT/ β -Catenin in the Induction of Cytochromes P450 by Nuclear Receptors in HepaRG Cells. *Mol Pharmacol* *87*, 1013-1020. 10.1124/mol.114.097402.

Thoms, M., Buschauer, R., Ameismeier, M., Koepke, L., Denk, T., Hirschenberger, M., Kratzat, H., Hayn, M., Mackens-Kiani, T., Cheng, J., et al. (2020). Structural basis for translational shutdown and immune evasion by the Nsp1 protein of SARS-CoV-2. *Science* *369*, 1249-1255. 10.1126/science.abc8665.

Thorne, C.A., Hanson, A.J., Schneider, J., Tahinci, E., Orton, D., Cselenyi, C.S., Jernigan, K.K., Meyers, K.C., Hang, B.I., Waterson, A.G., et al. (2010). Small-molecule inhibition of Wnt signaling through activation of casein kinase 1 α . *Nat Chem Biol* *6*, 829-836. 10.1038/nchembio.453.

Townsley, F.M., Cliffe, A., and Bienz, M. (2004). Pygopus and Legless target Armadillo/beta-catenin to the nucleus to enable its transcriptional co-activator function. *Nat Cell Biol* 6, 626-633. 10.1038/ncb1141.

Upadhyay, A.K., Cyr, M., Longenecker, K., Tripathi, R., Sun, C., and Kempf, D.J. (2017). Crystal structure of full-length Zika virus NS5 protein reveals a conformation similar to Japanese encephalitis virus NS5. *Acta Crystallogr F Struct Biol Commun* 73, 116-122. 10.1107/S2053230X17001601.

Urbanowski, M.D., and Hobman, T.C. (2013). The West Nile virus capsid protein blocks apoptosis through a phosphatidylinositol 3-kinase-dependent mechanism. *J Virol* 87, 872-881. 10.1128/JVI.02030-12.

V'kovski, P., Kratzel, A., Steiner, S., Stalder, H., and Thiel, V. (2021). Coronavirus biology and replication: implications for SARS-CoV-2. *Nat Rev Microbiol* 19, 155-170. 10.1038/s41579-020-00468-6.

Vallée, A., Lecarpentier, Y., Guillevin, R., and Vallée, J.N. (2018). Opposite Interplay Between the Canonical WNT/ β -Catenin Pathway and PPAR Gamma: A Potential Therapeutic Target in Gliomas. *Neurosci Bull* 34, 573-588. 10.1007/s12264-018-0219-5.

van den Bosch, H., Schutgens, R.B., Wanders, R.J., and Tager, J.M. (1992). Biochemistry of peroxisomes. *Annu Rev Biochem* 61, 157-197. 10.1146/annurev.bi.61.070192.001105.

Van der Hoek, K.H., Eyre, N.S., Shue, B., Khantisitthiporn, O., Glab-Ampi, K., Carr, J.M., Gartner, M.J., Jolly, L.A., Thomas, P.Q., Adikusuma, F., et al. (2017). Viperin is an important host restriction factor in control of Zika virus infection. *Sci Rep* 7, 4475. 10.1038/s41598-017-04138-1.

van der Zand, A., Gent, J., Braakman, I., and Tabak, H.F. (2012). Biochemically distinct vesicles from the endoplasmic reticulum fuse to form peroxisomes. *Cell* 149, 397-409. 10.1016/j.cell.2012.01.054.

Van Veldhoven, P.P. (2010). Biochemistry and genetics of inherited disorders of peroxisomal fatty acid metabolism. *J Lipid Res* 51, 2863-2895. 10.1194/jlr.R005959.

Viruses, C.S.G.o.t.I.C.o.T.o. (2020). The species Severe acute respiratory syndrome-related coronavirus: classifying 2019-nCoV and naming it SARS-CoV-2. *Nat Microbiol* 5, 536-544. 10.1038/s41564-020-0695-z.

Wahl, A., Gralinski, L.E., Johnson, C.E., Yao, W., Kovarova, M., Dinnon, K.H., Liu, H., Madden, V.J., Krzystek, H.M., De, C., et al. (2021). SARS-CoV-2 infection is effectively treated and prevented by EIDD-2801. *Nature* 591, 451-457. 10.1038/s41586-021-03312-w.

Wang, H., Garcia, C.A., Rehani, K., Cekic, C., Alard, P., Kinane, D.F., Mitchell, T., and Martin, M. (2008). IFN-beta production by TLR4-stimulated innate immune cells is negatively regulated by GSK3-beta. *J Immunol* 181, 6797-6802. 10.4049/jimmunol.181.10.6797.

Welsch, S., Miller, S., Romero-Brey, I., Merz, A., Bleck, C.K., Walther, P., Fuller, S.D., Antony, C., Krijnse-Locker, J., and Bartenschlager, R. (2009). Composition and three-dimensional architecture of the dengue virus replication and assembly sites. *Cell Host Microbe* 5, 365-375. 10.1016/j.chom.2009.03.007.

WHO (2014). Infection prevention and control of epidemic- and pandemic-prone acute respiratory infections in health care.

WHO (2020). *Coronavirus disease (COVID-2019) situation reports*. <https://www.who.int/emergencies/diseases/novel-coronavirus-2019/situation-reports>.

WHO (2022a). Coronavirus (COVID-19) Dashboard.

WHO (2022b). COVID-19 vaccine tracker and landscape.

Wilamowski, M., Hammel, M., Leite, W., Zhang, Q., Kim, Y., Weiss, K.L., Jedrzejczak, R., Rosenberg, D.J., Fan, Y., Wower, J., et al. (2021). Transient and stabilized complexes of Nsp7, Nsp8, and Nsp12 in SARS-CoV-2 replication. *Biophys J* 120, 3152-3165. 10.1016/j.bpj.2021.06.006.

Wilson, I.A., Niman, H.L., Houghten, R.A., Cherenson, A.R., Connolly, M.L., and Lerner, R.A. (1984). The structure of an antigenic determinant in a protein. *Cell* 37, 767-778. 10.1016/0092-8674(84)90412-4.

Wolff, G., Limpens, R.W.A.L., Zevenhoven-Dobbe, J.C., Laugks, U., Zheng, S., de Jong, A.W.M., Koning, R.I., Agard, D.A., Grünewald, K., Koster, A.J., et al. (2020). A molecular pore spans the double membrane of the coronavirus replication organelle. *Science* 369, 1395-1398. 10.1126/science.abd3629.

Wong, C.P., Xu, Z., Hou, S., Limonta, D., Kumar, A., Power, C., and Hobman, T.C. (2019). Interplay between Zika Virus and Peroxisomes during Infection. *Cells* 8, 725.

Wong, C.P., Xu, Z., Power, C., and Hobman, T.C. (2018). Targeted Elimination of Peroxisomes During Viral Infection: Lessons from HIV and Other Viruses. *DNA Cell Biol* 37, 417-421. 10.1089/dna.2018.4153.

Wu, B., Peisley, A., Richards, C., Yao, H., Zeng, X., Lin, C., Chu, F., Walz, T., and Hur, S. (2013). Structural basis for dsRNA recognition, filament formation, and antiviral signal activation by MDA5. *Cell* 152, 276-289. 10.1016/j.cell.2012.11.048.

Wu, F., Zhao, S., Yu, B., Chen, Y.M., Wang, W., Song, Z.G., Hu, Y., Tao, Z.W., Tian, J.H., Pei, Y.Y., et al. (2020a). A new coronavirus associated with human respiratory disease in China. *Nature* 579, 265-269. 10.1038/s41586-020-2008-3.

Wu, Y., Liu, Q., Zhou, J., Xie, W., Chen, C., Wang, Z., Yang, H., and Cui, J. (2017). Zika virus evades interferon-mediated antiviral response through the co-operation of multiple nonstructural proteins. *Cell Discov* 3, 17006. 10.1038/celldisc.2017.6.

Wu, Y., Yang, X., Yao, Z., Dong, X., Zhang, D., Hu, Y., Zhang, S., Lin, J., Chen, J., An, S., et al. (2020b). C19orf66 interrupts Zika virus replication by inducing lysosomal degradation of viral NS3. *PLoS Negl Trop Dis* *14*, e0008083. 10.1371/journal.pntd.0008083.

Xia, H., Luo, H., Shan, C., Muruato, A.E., Nunes, B.T.D., Medeiros, D.B.A., Zou, J., Xie, X., Giraldo, M.I., Vasconcelos, P.F.C., et al. (2018). An evolutionary NS1 mutation enhances Zika virus evasion of host interferon induction. *Nat Commun* *9*, 414. 10.1038/s41467-017-02816-2.

Xu, L.G., Wang, Y.Y., Han, K.J., Li, L.Y., Zhai, Z., and Shu, H.B. (2005). VISA is an adapter protein required for virus-triggered IFN-beta signaling. *Mol Cell* *19*, 727-740. 10.1016/j.molcel.2005.08.014.

Xu, S., Ci, Y., Wang, L., Yang, Y., Zhang, L., Xu, C., Qin, C., and Shi, L. (2019). Zika virus NS3 is a canonical RNA helicase stimulated by NS5 RNA polymerase. *Nucleic Acids Res* *47*, 8693-8707. 10.1093/nar/gkz650.

Xu, Z., Asahchop, E.L., Branton, W.G., Gelman, B.B., Power, C., and Hobman, T.C. (2017). MicroRNAs upregulated during HIV infection target peroxisome biogenesis factors: Implications for virus biology, disease mechanisms and neuropathology. *PLoS Pathog* *13*, e1006360. 10.1371/journal.ppat.1006360.

Xu, Z., Lodge, R., Power, C., Cohen, E.A., and Hobman, T.C. (2020). The HIV-1 Accessory Protein Vpu Downregulates Peroxisome Biogenesis. *mBio* *11*. 10.1128/mBio.03395-19.

Yockey, L.J., Varela, L., Rakib, T., Khoury-Hanold, W., Fink, S.L., Stutz, B., Szigeti-Buck, K., Van den Pol, A., Lindenbach, B.D., Horvath, T.L., and Iwasaki, A. (2016). Vaginal Exposure to Zika Virus during Pregnancy Leads to Fetal Brain Infection. *Cell* *166*, 1247-1256.e1244. 10.1016/j.cell.2016.08.004.

You, J., Hou, S., Malik-Soni, N., Xu, Z., Kumar, A., Rachubinski, R.A., Frappier, L., and Hobman, T.C. (2015). Flavivirus Infection Impairs Peroxisome Biogenesis and Early Antiviral Signaling. *J Virol* *89*, 12349-12361. 10.1128/JVI.01365-15.

You, L., Zhang, C., Yarravarapu, N., Morlock, L., Wang, X., Zhang, L., Williams, N.S., Lum, L., and Chen, C. (2016). Development of a triazole class of highly potent Porcn inhibitors. *Bioorg Med Chem Lett* *26*, 5891-5895. 10.1016/j.bmcl.2016.11.012.

Yu, I.M., Holdaway, H.A., Chipman, P.R., Kuhn, R.J., Rossmann, M.G., and Chen, J. (2009). Association of the pr peptides with dengue virus at acidic pH blocks membrane fusion. *J Virol* *83*, 12101-12107. 10.1128/JVI.01637-09.

Zang, R., Case, J.B., Yutuc, E., Ma, X., Shen, S., Gomez Castro, M.F., Liu, Z., Zeng, Q., Zhao, H., Son, J., et al. (2020). Cholesterol 25-hydroxylase suppresses SARS-CoV-2 replication by blocking membrane fusion. *Proc Natl Acad Sci U S A* *117*, 32105-32113. 10.1073/pnas.2012197117.

- Zhang, M., Wang, M., Tan, X., Li, T.F., Zhang, Y.E., and Chen, D. (2010). Smad3 prevents beta-catenin degradation and facilitates beta-catenin nuclear translocation in chondrocytes. *J Biol Chem* 285, 8703-8710. 10.1074/jbc.M109.093526.
- Zhang, Q., Ke, H., Blikslager, A., Fujita, T., and Yoo, D. (2018). Type III interferon restriction by porcine epidemic diarrhea virus and the role of viral protein nsp1 in IRF1 signaling. *Journal of virology* 92, e01677-01617.
- Zhang, X., Xie, X., Xia, H., Zou, J., Huang, L., Popov, V.L., Chen, X., and Shi, P.Y. (2019). Zika Virus NS2A-Mediated Virion Assembly. *mBio* 10. 10.1128/mBio.02375-19.
- Zheng, Y., Zhuang, M.W., Han, L., Zhang, J., Nan, M.L., Zhan, P., Kang, D., Liu, X., Gao, C., and Wang, P.H. (2020). Severe acute respiratory syndrome coronavirus 2 (SARS-CoV-2) membrane (M) protein inhibits type I and III interferon production by targeting RIG-I/MDA-5 signaling. *Signal Transduct Target Ther* 5, 299. 10.1038/s41392-020-00438-7.
- Zhou, P., Yang, X.L., Wang, X.G., Hu, B., Zhang, L., Zhang, W., Si, H.R., Zhu, Y., Li, B., Huang, C.L., et al. (2020). A pneumonia outbreak associated with a new coronavirus of probable bat origin. *Nature* 579, 270-273. 10.1038/s41586-020-2012-7.
- Zhou, S., Hill, C.S., Sarkar, S., Tse, L.V., Woodburn, B.M.D., Schinazi, R.F., Sheahan, T.P., Baric, R.S., Heise, M.T., and Swanstrom, R. (2021). β -d-N4-hydroxycytidine Inhibits SARS-CoV-2 Through Lethal Mutagenesis But Is Also Mutagenic To Mammalian Cells. *J Infect Dis* 224, 415-419. 10.1093/infdis/jiab247.
- Zhu, N., Zhang, D., Wang, W., Li, X., Yang, B., Song, J., Zhao, X., Huang, B., Shi, W., Lu, R., et al. (2020). A Novel Coronavirus from Patients with Pneumonia in China, 2019. *N Engl J Med* 382, 727-733. 10.1056/NEJMoa2001017.
- Züst, R., Cervantes-Barragan, L., Habjan, M., Maier, R., Neuman, B.W., Ziebuhr, J., Szretter, K.J., Baker, S.C., Barchet, W., Diamond, M.S., et al. (2011). Ribose 2'-O-methylation provides a molecular signature for the distinction of self and non-self mRNA dependent on the RNA sensor Mda5. *Nat Immunol* 12, 137-143. 10.1038/ni.1979.